Proyecto Fin de Carrera
Ingeniería Aeronáutica

Open-hole tensile strength and size effect of CFR polymers: an anisotropic approach

Autor: Ignacio Roldán Fernández

Tutores: Vladislav Mantič Leščišin y José Cañas Delgado

Dep. de Mecánica de Medios Continuos y Teoría de Estructuras

Escuela Técnica Superior de Ingeniería
Universidad de Sevilla

Sevilla, 2017

Proyecto Fin de Carrera
Ingeniería Aeronáutica

Open-hole tensile strength and size effect of CFR polymers: an anisotropic approach

Autor:
Ignacio Roldán Fernández

Tutores:
Vladislav Mantič Leščišin
Catedrático de Universidad

José Cañas Delgado
Catedrático de Universidad

Dep. de Mecánica de Medios Continuos y Teoría de Estructuras
Escuela Técnica Superior de Ingeniería
Universidad de Sevilla

Sevilla, 2017

Proyecto Fin de Carrera:

Open-hole tensile strength and size effect of CFR polymers: an anisotropic approach

Autor: Ignacio Roldán Fernández

Tutores: Vladislav Mantič Leščišin

José Cañas Delgado

El tribunal nombrado para juzgar el Proyecto arriba indicado, compuesto por los siguientes miembros:

Presidente:

Vocales:

Secretario:

Acuerdan otorgarle la calificación de:

Sevilla, 2017

El Secretario del Tribunal

A mis padres, por su paciencia y cariño infinitos.

Agradecimientos

Este Proyecto Fin de Carrera no habría sido posible sin la colaboración de mis tutores, Vladislav Mantič y José Cañas, que me han guiado y corregido pacientemente a lo largo de todos estos meses. Asimismo, el Departamento de Mecánica de Medios Contínuos y Tª de Estructuras de la Universidad de Sevilla, a través del Laboratorio de Elasticidad y Resistencia de Materiales, ha proporcionado generosamente los materiales y los recursos necesarios para la realización de la parte experimental de este trabajo. Es a ellos a los que debo mi primer y muy profundo agradecimiento.

Pero tengo muchas más cosas que agradecer, y que, si no fuera por estas palabras, quedarían ocultas en mi memoria. Hablo de la paciencia (palabra que repetiré mucho) y el apoyo moral de todos mis seres queridos, empezando por mis padres, Ignacio y Lupe, a los que dedico el resultado de este año y medio de esfuerzos. A ellos les debo la vida, y no se me ocurre mejor agradecimiento por todos los sacrificios que han hecho para que llegue hasta aquí que este fruto del trabajo de los años pasados.

No solo mis padres han servido de apoyo en esta etapa final de mi vida estudiantil. Hay muchos otros nombres propios que merecen mi eterno agradecimiento: Miguel, Antonio, Isabel, José Ramón y todas esas personas que han pasado por el LERM, tanto por su ayuda para enseñarme cómo funciona todo por allí como por hacer los largos y monótonos días de fabricación mucho más amenos. Jorge, Miguel y Fernando, por ese apoyo durante los años de clases sobre los que he podido construir este proyecto. Nacho, Balta, Matthew, Niko y tanta otra gente con la que he convivido estos años pasados y que me han dado energías para afrontar los momentos de baja fuerza de voluntad. Fran, María, Lola y Nico, por esa amistad duradera que también da energías.

Por último, pero no menos importante, tengo que agradecer su paciencia al resto de mi familia: a mi hermano Ricardo, a mi tío Angel Luis, cuya inteligencia y cultura me inspiraron a elegir esta carrera, y a todos los demás familiares que han estado esperando pacientemente este momento.

Este último párrafo va dedicado a esas personas especiales en mi vida que engloban un poco de todos los mencionados arriba, y a los que he querido dedicar un espacio aparte por haber estado a mi lado muy cercanamente en los últimos tiempos: Paco, por ser mi primo y mi hermano; José, por ser ese otro primo adoptado e imprescindible en nuestra mini-familia; y Sofie, por todo.

Ignacio Roldán Fernández

Sevilla, 2017

Resumen

La distribución de tensiones exacta y anisótropa de un laminado con una abertura circular bajo carga de tensión uniaxial de la teoría de Lekhnitskii es comparada a la aproximación ortótropa de Tan para distintos criterios de fallo. Las predicciones de estos métodos son validadas mediante los resultados de una extensiva campaña experimental. Esta campaña usa un preimpregnado unidireccional de resina epoxy reforzada con fibra de carbono para la fabricación de laminados ortótropos con secuencias de apilado $[0]_6$, $[90]_6$ y $[0/90]_2$. La solución de Lekhnitskii parece proporcionar una mejor predicción que la aproximación de Tan en la mayoría de los laminados ensayados. Esto podría deberse a que la primera es una mejor representación de la distribución real para el caso ortótropo. Las mejoras son insignificantes para laminados cuasi isótropos de la bibliografía, pero el método propuesto resulta en un enfoque más general para la mayoría de problemas.

Abstract

The exact, anisotropic stress distribution of a laminate with a circular opening under uniaxial tension from Lekhnitskii's theory is compared to Tan's orthotropic approximation for several failure criteria. The predictions of these methods are compared to an extensive experimental campaign for validation. The campaign makes use of a carbon-fiber-reinforced epoxy unidirectional prepeg to manufacture orthotropic laminates of lay-ups $[0]_6$, $[90]_6$ and $[0/90]_{2s}$. Lekhnitskii's solution seems to provide a better prediction than Tan's approximation in most cases for the tested laminates. This might to be due to the former being a better depiction of the real stress distribution for the orthotropic case. The improvements are negligible for quasi-isotropic laminates from the literature, but the proposed method provides a more general approach to most problems.

Index

List of symbols

$\sigma_y^{\infty}(x,0)$	Stress distribution along the x axis in the infinite case.
$\sigma_y(x,0)$	Stress distribution along the x axis in the finite case (see Figure 2-1).
σ_n	Average stress along the net section of the specimen.
σ_g	Average stress along the gross section of the specimen. Also used for the stress applied at the infinity of the plate.
R	Radius of the specimen's hole.
W	Total width of the specimen.
$2R/W$	Diameter-to-width ratio of the specimen.
γ	Adimensional geometric variable x (adimensionalized by R)
K_T^{∞}	Stress concentration factor referred to σ_g for the infinite plate.
K_T	Stress concentration factor referred to σ_g for the finite plate.
K_{Tn}	Stress concentration factor referred to σ_n for the finite plate.
F_w	Finite-width correction factor.
μ_1, μ_2	Complex parameters that are the principal roots of equation (2.6).

1 INTRODUCTION: BIBLIOGRAPHIC REVIEW

If I have seen further it is by standing
on the shoulders of Giants.

- Sir Isaac Newton-

Humans have used structural composite materials for a very long time, starting from natural ones such as wood and plywood, through man-made substances like concrete, to the latest fiber-reinforced plastics composites. A common characteristic of the usage of these materials is that, at first, their precise resistance mechanisms were not known, so they were tested via trial-and-error, followed by an approximate description of this resistance based on experience, and eventually a detailed scientific explanation was obtained.

For the past six decades, carbon- and glass-reinforced plastics have been in the second stage of this evolution: since they started to be used mainly in the military and aeronautical fields, physicists and engineers have not been able to develop a simple, complete theoretical framework that explains the real-life failure of composite structures, in contrast to other materials. Despite that, many experimental formulas have been introduced and used by designers to take advantage of the already known high resistance-to-weight ratios of these materials. This project aims to be just one more sand grain of this mountain of empirical hypotheses on which a simple, accurate, and final theory will be built in the future.

1.1 Composite material laminates failure mechanisms

One of the reasons that hinders the development of such a theory is the number of failure processes that can occur in a composite material structure because of their complexity and manufacturing methods [1]. The list would be too extensive if it pretended to include all types of composite materials configurations; these will be narrowed down progressively to the one studied here.

The first reduction consists of considering long-fibers-reinforced polymers in laminates, still a wide but very used category. Its most typical micromechanical failure modes are fiber rupture, fiber buckling, fiber-matrix separation or *debonding*, matrix cracking, and delamination, which can occur simultaneously [1]–[9].

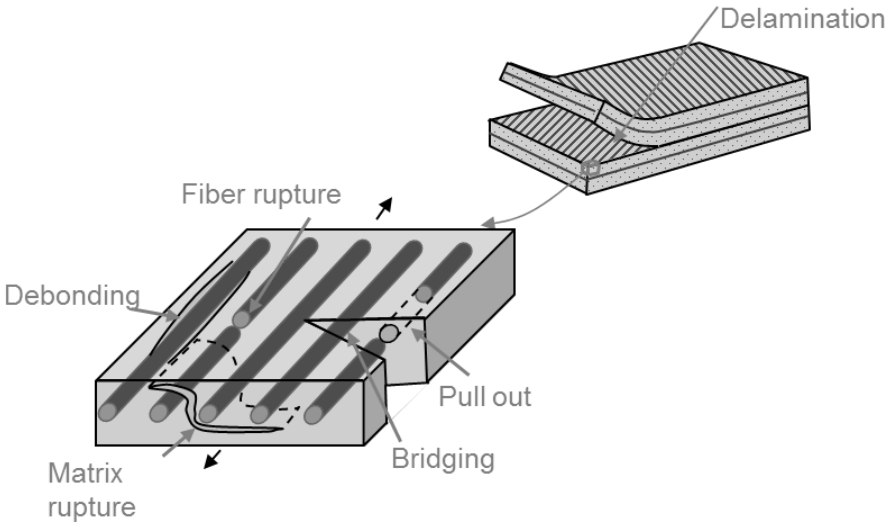

Figure 1-1. Composite laminates failure mechanisms [9]

1.2 Damage initiation and growth

As with other well-known materials, failure in composite laminates is considered micromechanically as a two-step process: first, a damage appears or exists somewhere inside the material, and then, under a certain tensional state, this defect grows along a certain path until it reaches a size that causes the structural failure at the macroscopic level [1], [10]–[12].

The difference with composite laminates is the complexity introduced by the heterogeneity found both micro and macroscopically. For this reason, many methodologies exist that try to predict the stresses that initiate damage and that make it evolve.

The models that calculate the appearance of damage consist of two main subgroups: stress damage criteria and Fracture Mechanics models. The first ones usually consider the lamina as the basic element, and make use of properties defined experimentally. They are also classified according to the number of failure modes they can predict: Uncoupled Damage Criteria (maximum stress and maximum strain [1], [4], [13], [14]), Coupled Damage Criteria (Tsai-Hill [15], Tsai-Wu [16], Hoffman [17]), and multiple-modes failure criteria (Hashin [18], Chang-Chang [19], Hou [20], Puck [21]). The Fracture Mechanics approach is focused mainly on brittle materials and assume an existing defect or crack that grows under certain conditions. It has been applied successfully to delamination and debonding problems [5], and the energetic criteria derived from it are preferable to stress-based ones due to the former involving invariant material properties [2], [22], [23].

But the appearance of damage does not always involve a structural failure of the element. It is useful to model the degradation of properties that these defects induce in the laminate and to study its evolution up to the total failure. The Damage Progression models do this either in combination with the ones mentioned above or independently from them [5]; Fracture Mechanics is somewhere in between both. There are two branches of Damage Progression: Continuum Damage Mechanics (CDM) and Discrete Damage Mechanics (DDM).

CDM models try to predict all the different failure modes that appear microscopically by their effect on the mesoscopic level of the material [24]. On this scale, the lamina is taken as the Representative Volume Element (RVE) that allows it to be considered as a homogeneous material and, thus, to describe its properties by use of continuous functions. The problems they present is the difficulty of obtaining needed properties experimentally [2], [25], and the introduction of many degradation parameters. On the other hand, DDM models study damage behavior at the microstructural level, where the state variable is the number of cracks per unit length. This is an advantage over CDM, because there is no need to define additional parameters, and they do not depend on the mesh size when numerically implemented. However, available solutions are limited to symmetric laminates under plane loads [2], [26]–[31], [32].

1.3 The effect of holes

Holes and cracks are necessary elements in composite material structures. As with other innovative fields, aeronautics is the sector that has contributed the most to theory- and experience-based research in composites, and, scary as it may sound, airplanes are full of holes: bolts, rivets, manholes… all needed and all problematic.

Every discontinuity introduces stress/strain concentrations and possible crack appearances [33], [34]. The shape of the hole affects this stress concentration: linear cracks are the worst type of discontinuity while circular notches induce lesser gradients. The former are avoidable in most design cases, but the latter are indispensable and make the prediction of composites strength a lot more difficult, even under simple load states [8], [35].

Usually, the stress localization induced by the discontinuity is evaluated through a Stress Concentration Factor (SCF) K_T [19], [33], [34], [36]–[42]. It relates the maximum tensile stress in the proximity of the hole[1], $\sigma_{y,max}$, to a reference one, normally the stress applied at the infinity of the laminate, σ_∞, if considered as an infinite plate, or along its gross section, σ_g, if it is a real, finite problem. In this case, the SCF is defined in equation (1.1):

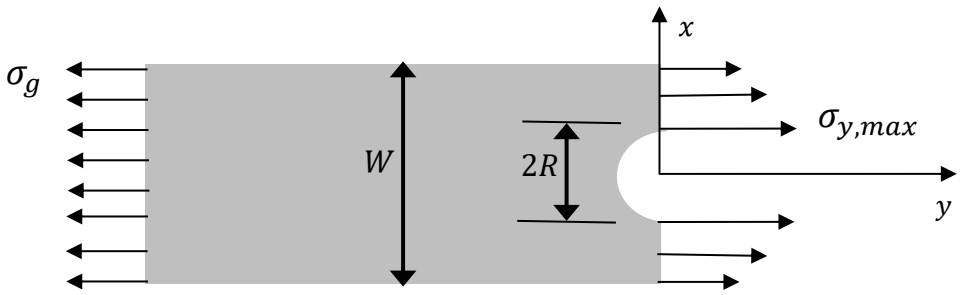

Figure 1-2. Geometry and problem's variables definitions.

$$K_T = \frac{\sigma_{y,max}}{\sigma_g} . \tag{1.1}$$

Many authors have analyzed this problem and the relation of the SCF with different elastic properties, loads and geometries, including the finite plate [36]–[43].

The failure stress of a notched laminate depends on several variables such as: material properties, specimen's size, hole diameter, thickness, laminae orientation, machining quality and the width-to-diameter ratio [34], [44], [45]. Of these, the most important ones are the following two:

- Influence of geometry: The laminate's size effect, or aspect ratio, $2R/W$, is a determining factor in predicting its stiffness. For thin laminates, an increase in this ratio entails a decrease in its strength. On the other hand, for thick laminates where delamination is the typical failure mode, the relationship is the inverse [10]–[12], [34], [44], [46]–[48]. Another interesting conclusion is what is called the "size effect paradox": a stronger reduction in the nominal strength the bigger the hole diameter; it is paradoxical because size effects on the adimensional K_t are not to be expected. These effects have been studied by Waddoups [49], Whitney and Nuismer [50], [51], and more recently by Camanho et al. [46], Erçin et al. [47], and many others [34], [52].
- Influence of laminate thickness: In general, increasing the laminate thickness raises the tensile strength, but it also modifies the mode of failure of the laminate. There are two ways of increasing thickness: ply-level scaling, which consists in augmenting the number of laminae in a group of them with the same fiber orientation, and sublaminate-level scaling, where the number of repeating sublaminates (composed of different-direction laminae) is raised. There are some studies [53], [54], that show a decrease in strength for a sublaminate-level scaling compared to a ply-level one, even though they both contain the same number of laminae with the same orientation.

[1] Sometimes, the SCF is studied along the whole width of the plate; if no reference is made to a geometric parameter such as x, it should be understood that the SCF is applied at $x = R$, i.e., the edge of the hole.

2 THEORETICAL BASIS

If mathematical equations can't make progress in understanding complex phenomena in the natural world, how might we make progress?

- Stephen Wolfram -

Several failure criteria are mathematically described in this chapter. The first section introduces the concept of stress concentration factors and finite-width correction factors that will be used in the rest of the models described later. The equations in this chapter will then be used in the next one for comparison to the experimental results of a campaign designed for this thesis.

The reader is referred to the table of symbols on page *xvii* due to the number of variables and notations used in this chapter. The present author has written the mathematical expressions with both similarity to the symbols used in the literature and consistency in mind.

2.1 Notch sensitivity (maximum stress)

The following description of two possible failure modes that can be encountered in the open-hole tensile test is based on a simple maximum tension approach applied at the extreme of the hole. Let us define the geometry of the problem as the one in Figure 2-1, with σ_g being the load applied at the extremes of the specimen during the test, and equal to the gross-section stress; sometimes it is referred to as σ_∞, notation avoided here to prevent confusion with the infinite plate case. The distribution of stresses normal to x along the line $y = 0$, $\sigma_y(x, 0)$, can be expressed per two mutually exclusive failure modes, described in the following subsections.

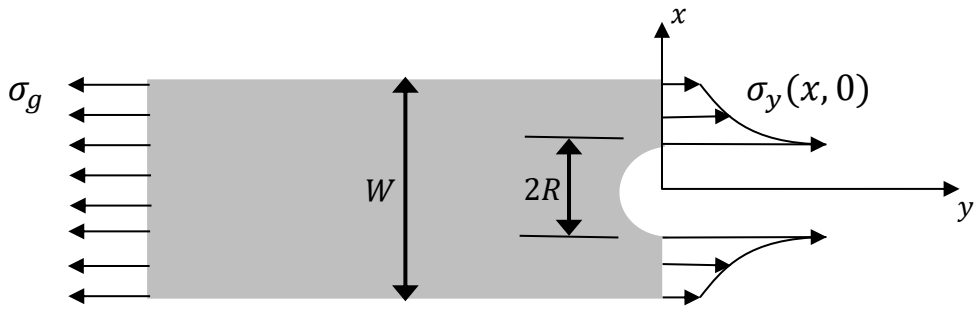

Figure 2-1. Geometry and problem's variables definitions.

2.1.1 Notch-insensitive failure

This model assumes that the hole has no influence in the aforementioned stress distribution, so that it is constant along the x axis and equal to the nominal stress σ_n, defined in equation (2.1). This implies an instant regularization of the tensions from the proximity of the hole, as seen in Figure 2-2, and a simple stress balance that yields equation (2.2):

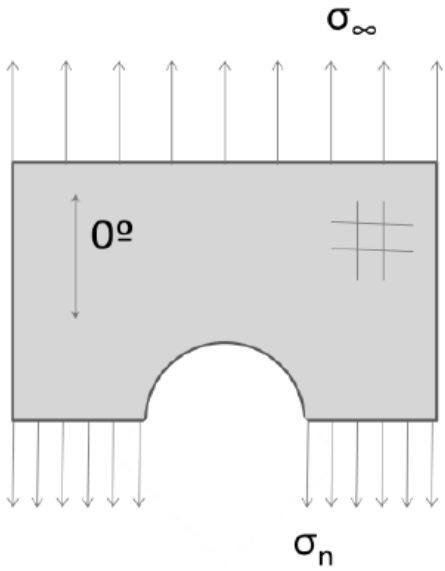

Figure 2-2. Notch-insensitive model [55].

$$\sigma_y(x,0) = \sigma_n \,, \tag{2.1}$$

$$\sigma_n = \frac{W}{W-2R}\sigma_g \;\Leftrightarrow\; \sigma_g = \left(1-\frac{2R}{W}\right)\sigma_n \,. \tag{2.2}$$

Under the maximum stress criterion at the hole edge, the failure with respect to the adimensional net-section stress at fracture is given by (2.3), where X_T is the unnotched laminate's tensile strength. Introducing it in (2.2) and defining the adimensional gross-section stress, the expression of the latter is given in (2.4);

$$\bar{\sigma}_y(R,0) = \bar{\sigma}_n = X_T \;\Rightarrow\; \hat{\bar{\sigma}}_n = \frac{\bar{\sigma}_n}{X_T} = 1 \,, \tag{2.3}$$

$$\hat{\bar{\sigma}}_g = \frac{\bar{\sigma}_g}{X_T} = 1-\frac{2R}{W} \,. \tag{2.4}$$

The notation here makes use of two types of accents: a bar $\bar{\square}$ to indicate the stresses when failure occurs, and a hat $\hat{\square}$ for adimensionality. Thus, equation (2.4) represents the value of the adimensional gross-section stress at failure with respect to the parameter $2R/W$, which is simply a straight line with a slope value of -1; in the case of equation (2.3), it is a horizontal line. This, of course, is not the real stress value at failure in most cases, but it approximates well to certain experimental results, as will be seen in section 3.3.

2.1.2 Notch-sensitive failure

2.1.2.1 The infinite plate case

There are several proposals for the stress distribution $\sigma_y(x,0)$ around a notch, which depend on the geometry of the notch itself, the lay-up tested, or the loading conditions; here the formulas used are based on the infinite plate solution, which will be described in this section. For simplicity in the notation, the stress applied at the infinity of the hole, σ_∞, will be identified with the gross-sectional stress of the finite plate, σ_g. Lekhnitskii [56] found an exact analytical solution for an infinite, anisotropic plate with an elliptical opening under tension; his analysis is based on a complex variable method. Its expression, as given by Tan [57], and particularized for the circular hole, is in (2.5):

$$\sigma_y^\infty(\gamma,0)=\sigma_g+\sigma_g\,\mathrm{Re}\left\{\frac{1}{\mu_1-\mu_2}\left[\frac{-\mu_2(1-i\mu_1)}{\sqrt{\gamma^2-1-\mu_1^2}\left(\gamma+\sqrt{\gamma^2-1-\mu_1^2}\right)}+\frac{\mu_1(1-i\mu_2)}{\sqrt{\gamma^2-1-\mu_2^2}\left(\gamma+\sqrt{\gamma^2-1-\mu_2^2}\right)}\right]\right\}, \tag{2.5}$$

where $\gamma=\frac{x}{R}$, μ_1 and μ_2 are the principal roots of the characteristic equation

$$a_{22}\mu^4-2a_{26}\mu^3+(2a_{12}+a_{66})\mu^2-2a_{16}\mu+a_{11}=0\,, \tag{2.6}$$

and a_{ij} with $i,j=\{1,2,6\}$ are the compliances of the laminate, being 1 parallel and 2 perpendicular to the loading direction; the axes chosen in Figure 2-1 result in $1\equiv y$, $2\equiv x$, but the numerical notation will be kept for clarity.

For an orthotropic laminate, $a_{16}=a_{26}=0$, and the solutions can be expressed in the compact form (2.7), as

$$\mu_1=\frac{i}{2}\left(\sqrt{\frac{E_{11}}{G_{12}}-2\nu_{12}+2\sqrt{\frac{E_{11}}{E_{22}}}}+\sqrt{\frac{E_{11}}{G_{12}}-2\nu_{12}-2\sqrt{\frac{E_{11}}{E_{22}}}}\right),$$
$$\mu_2=\frac{i}{2}\left(\sqrt{\frac{E_{11}}{G_{12}}-2\nu_{12}+2\sqrt{\frac{E_{11}}{E_{22}}}}-\sqrt{\frac{E_{11}}{G_{12}}-2\nu_{12}-2\sqrt{\frac{E_{11}}{E_{22}}}}\right), \tag{2.7}$$

where E_{ii}, G_{ij} are the longitudinal and tangential elastic moduli, respectively, and ν_{ij} is the Poisson's ratio; These solutions usually have only imaginary part,

$$\alpha=\mathrm{Im}(\mu_1)\,,\qquad \beta=\mathrm{Im}(\mu_2)\,. \tag{2.8}$$

Since $\alpha,\beta\in\mathbb{R}$, it must be checked for each orthotropic laminate that the terms inside the roots in (2.7) are non-negative; this means that $\sqrt{E_{11}/E_{22}}\le E_{11}/2G_{12}-\nu_{12}$, and it can happen that this inequality does not hold for

some orthotropic laminates not loaded along their orthotropy axes. If the inequality holds, introducing (2.6) in terms of α, β in (2.5) yields (2.9)

$$\sigma_y^{\infty}(\gamma,0)|_{orth.} = \sigma_g + \frac{\sigma_g}{\alpha-\beta}\left[\frac{-\beta(1+\alpha)}{\sqrt{\gamma^2-1+\alpha^2}\left(\gamma+\sqrt{\gamma^2-1+\alpha^2}\right)} + \frac{\alpha(1+\beta)}{\sqrt{\gamma^2-1+\beta^2}\left(\gamma+\sqrt{\gamma^2-1+\beta^2}\right)}\right], \tag{2.9}$$

From these stress distributions, it is possible to obtain the stress concentration factor (SCF), defined in (2.10), dividing them by the applied stress and making $x = R \Rightarrow \gamma = 1$; the general, anisotropic case is given in (2.11) and the particularization for orthotropic materials is (2.12):

$$K_T^{\infty} = \frac{\sigma_y^{\infty}(x=R,0)}{\sigma_g} = \hat{\sigma}_y^{\infty}(\gamma=1,0)\,, \tag{2.10}$$

$$K_T^{\infty}|_{anis.} = 1 + \mathrm{Re}\left[\frac{i(\mu_1+\mu_2)}{\mu_1\mu_2}\right], \tag{2.11}$$

$$K_T^{\infty}|_{orth.} = 1 + \frac{\alpha+\beta}{\alpha\beta}\,. \tag{2.12}$$

Equation (2.11) recovers the usual form in terms of the engineering properties, (2.13), when the values of μ_1 and μ_2 from (2.7) are substituted, and remembering that $\nu_{ij}/E_{ii} = \nu_{ji}/E_{jj}$:

$$K_T^{\infty} = \sqrt{2\left(\sqrt{\frac{E_{22}}{E_{11}}} - \nu_{21}\right) + \frac{E_{22}}{G_{12}}}\,. \tag{2.13}$$

2.1.2.2 Finite-width correction factors

The transformation from the infinite- to the finite-plate case developed in this section is based on Tan's introduction of a finite-width correction factor (FWCF). This whole theory lies on the following

HYPOTHESIS:

The normal stress profile along the net section of a finite plate under uniaxial tension (Figure 2-1) is proportional by a finite-width correction factor, F_w, to that of an infinite plate under the same loading[2]*:*

$$F_w \sigma_y^{\infty}(x,0) = \sigma_y(x,0)\,. \tag{2.14}$$

Note the use of the superscript $\square^{\infty}$ to indicate the infinite case. This FWCF is defined in [57] as the quotient

[2] According to Tan, this assumption is examined using a typical finite-element solution in [51].

between the SCF's at the opening edge for the finite and the infinite situations, (2.15)

$$F_w = \frac{K_T}{K_T^\infty} \,, \tag{2.15}$$

where K_T^∞ has been defined in (2.10) and K_T is, analogously

$$K_T = \frac{\sigma_y(x = R, 0)}{\sigma_g} \,. \tag{2.16}$$

It is important to notice that the formal definitions of the stress concentration factors in (2.10) and (2.16) use the gross-sectional stress σ_g as the reference value. Instead of it, the net-sectional stress σ_n can be used by simply substituting equation (2.2) in (2.16); the notation of the SCF is changed to K_{Tn} to reflect the different reference;

$$K_{Tn} = \frac{\sigma_y(x = R, 0)}{\sigma_n} = \left(1 - \frac{2R}{W}\right) K_T \,. \tag{2.17}$$

It could be argued that the equilibrium equation (2.2) is obtained in the notch-insensitive case and should not be used for the definition in (2.17). In this model, σ_n is not the constant value of the profile $\sigma_y(x, 0)$, but rather its average across the net section, so that

$$\sigma_n \coloneqq \frac{2}{W - 2R} \int_R^{W/2} \sigma_y(x, 0) \, \mathrm{d}x \,. \tag{2.18}$$

Equation (2.18) can be then seen as the general case, and for the notch-insensitive model, where the profile is assumed as constant, $\sigma_y(x, 0) = C$, application of (2.18) results in $C = \sigma_n$, which is equal to (2.2) again.

Tan obtains the expression of the FWCF by combining (2.2), (2.18) and the hypothesis (2.14), and integrating along x from the edge of the opening to the half width of the plate; adimensionalizing x with R, the resulting expression for the circular hole is:

$$RF_w \int_1^{\frac{W}{2R}} \sigma_y^\infty(\gamma, 0) \, \mathrm{d}\gamma = R \int_1^{\frac{W}{2R}} \sigma_y(\gamma, 0) \, \mathrm{d}\gamma = \frac{W}{2} \sigma_g \,. \tag{2.19}$$

Substituting now $\sigma_y^\infty(\gamma, 0)$ from (2.5), integrating, and reordering yields the reciprocal of the FWCF for anisotropic materials:

$$(F_w)^{-1} = 1 - \frac{2R}{W} + \mathrm{Re}\left\langle \frac{1}{\mu_1 - \mu_2}\left\{ \frac{\mu_2}{1+i\mu_1}\left[1-(1+i\mu_1)\frac{2R}{W} - \sqrt{1-(1+\mu_1^2)\left(\frac{2R}{W}\right)^2}\right]\right.\right.$$
$$\left.\left. - \frac{\mu_1}{1+i\mu_2}\left[1-(1+i\mu_2)\frac{2R}{W} - \sqrt{1-(1+\mu_2^2)\left(\frac{2R}{W}\right)^2}\right]\right\}\right\rangle . \quad (2.20)$$

For the purely orthotropic case described before, i.e., an orthotropic material loaded along its orthotropy axes, using (2.8) results in the exact orthotropic FWC factor:

$$(F_w|_{orth.})^{-1} = 1 - \frac{2R}{W} + \frac{1}{\alpha - \beta}\left\{ \frac{\beta}{1-\alpha}\left[1-(1-\alpha)\frac{2R}{W} - \sqrt{1-(1-\alpha^2)\left(\frac{2R}{W}\right)^2}\right]\right.$$
$$\left. - \frac{\alpha}{1-\beta}\left[1-(1-\beta)\frac{2R}{W} - \sqrt{1-(1-\beta^2)\left(\frac{2R}{W}\right)^2}\right]\right\} . \quad (2.21)$$

2.1.2.3 Tan's orthotropic approximations

Tan proposed in [38] an approximate stress distribution for the infinite plate based on Lekhnitskii's solution, (2.5), particularized for the isotropic case, $\mu_1 = \mu_2 = i$, which is equal to Timoshenko's stress function [58]:

$$\tilde{\sigma}_y^{\infty}(\gamma, 0) = \frac{\sigma_g}{2}\{2 + \gamma^{-2} + 3\gamma^{-4}\} . \quad (2.22)$$

This expression is a polynomial of the first two even powers of $1/\gamma = R/x$, so he added two more terms and the appropriate boundary conditions to obtain the corresponding coefficients. Theoretically, more terms can be assumed for better accuracy, with their respective boundary conditions. The expression of this approximate distribution for an orthotropic, infinite plate with a circular opening under a tension σ_g directed along one of its principal axes, is:

$$\tilde{\sigma}_y^{\infty}(\gamma, 0) = \frac{\sigma_g}{2}\{2 + \gamma^{-2} + 3\gamma^{-4} - (K_T^{\infty} - 3)[5\gamma^{-6} - 7\gamma^{-8}]\} . \quad (2.23)$$

The tilde $\tilde{\square}$ will indicate from now on that the value under it is derived from the above approximation. Integrating this equation in (2.19) and reordering gives the approximate orthotropic FWC factor:

$$\tilde{F}_w|_{orth.} = \frac{\tilde{K}_T|_{orth.}}{K_T^{\infty}} = 2\left\{2 - \left(\frac{2R}{W}\right)^2 - \left(\frac{2R}{W}\right)^4 + (K_T^{\infty} - 3)\left(\frac{2R}{W}\right)^6\left[1 - \left(\frac{2R}{W}\right)^2\right]\right\}^{-1} . \quad (2.24)$$

The exact[3] isotropic finite-width correction factor can be obtained from (2.24) by making $K_T^\infty = 3$, which gives:

$$F_w|_{isot.} = \frac{K_T|_{isot.}}{K_T^\infty} = \frac{2}{2 - \left(\frac{2R}{W}\right)^2 - \left(\frac{2R}{W}\right)^4} . \tag{2.25}$$

Tan states that the finite-width SCF's obtained from (2.24) and (2.25) are more accurate for elliptical openings with a ratio $a_e/b_e \geq 4$, being a_e the dimesion of the axis perpendicular to the loading direction and b_e the dimension of the parallel one, according to the photoelastic experiments of Durelli et al.[59]. For this reason, a magnification factor M is developed to improve the previous theory when $a_e/b_e < 4$. This factor is obtained by considering Heywood's formula, (2.26), which is very good for isotropic plates with circular openings, and equating it to (2.25) but where the diameter-to-width ratios are factored by M; solving for this factor results in (2.27):

$$F_w|_{Heyw.} = \frac{K_T|_{Heyw.}}{K_T^\infty} = \frac{2 + \left(1 - \frac{2R}{W}\right)^3}{3\left(1 - \frac{2R}{W}\right)} . \tag{2.26}$$

$$M^2 = \frac{\sqrt{1 - 8\left[\frac{3\left(1 - \frac{2R}{W}\right)}{2 + \left(1 - \frac{2R}{W}\right)^3} - 1\right]} - 1}{2(2R/W)^2} . \tag{2.27}$$

Then this magnification factor is applied to the previously obtained FWCF's, (2.21) and (2.24)[4], by substituting every $2R/W$ ratio by this same ratio times M. This correction will be designated by the superscript *, and when used it will also omit the reference to orthotropy for clarity; in the approximate case, (2.29), the equation from which M is obtained is used to simplify its expression.

$$F_w^* = \left\langle 1 - \left(\frac{2R}{W}M\right) + \frac{1}{\alpha - \beta}\left\{\frac{\beta}{1-\alpha}\left[1 - (1-\alpha)\left(\frac{2R}{W}M\right) - \sqrt{1 - (1-\alpha^2)\left(\frac{2R}{W}M\right)^2}\right]\right.\right.$$
$$\left.\left. - \frac{\alpha}{1-\beta}\left[1 - (1-\beta)\left(\frac{2R}{W}M\right) - \sqrt{1 - (1-\beta^2)\left(\frac{2R}{W}M\right)^2}\right]\right\}\right\rangle^{-1} , \tag{2.28}$$

$$\tilde{F}_w^* = \left\{\frac{3(1-2R/W)}{2 + (1-2R/W)^3} + \frac{1}{2}(K_T^\infty - 3)\left(\frac{2R}{W}M\right)^6\left[1 - \left(\frac{2R}{W}M\right)^2\right]\right\}^{-1} . \tag{2.29}$$

A discussion on the suitability of these finite-width correction factors and the stress concentration factors derived from them will be done in section 2.1.3 after applying the failure criterion.

[3] This expression is not referred to as "approximate" because it derives from the exact isotropic stress distribution.
[4] The magnification factor will not be applied to the anisotropic FWCF to avoid too complicated expressions.

2.1.2.4 Application of the maximum stress criterion

Following the same procedure as in the notch-insensitive case, (2.3), the failure criterion applied is that of the maximum stress at the edge of the hole, that is, FCR:

$$\bar{\sigma}_y(R,0) = X_T \,. \tag{2.30}$$

Considering the definition of the SCF in (2.16), the criterion for the adimensional gross-sectional stress can be reformulated as (2.31), analogous to (2.4):

$$\hat{\bar{\sigma}}_g = \frac{\bar{\sigma}_g}{X_T} = \frac{1}{K_T} \,. \tag{2.31}$$

Remembering the definition of the SCF in (2.15), (2.31) can be reformulated in terms of the finite-width correction factor:

$$\hat{\bar{\sigma}}_g = \frac{1}{K_T^{\infty} F_w} \,. \tag{2.32}$$

To use the net-section stress as the refence value, either (2.2) or (2.17) can be used:

$$\hat{\bar{\sigma}}_n = \frac{1}{K_T^{\infty}\left(1-\frac{2R}{W}\right) F_w} \,. \tag{2.33}$$

It is worth noting that the failure criterion is always the same (maximum stress at the edge of the opening), but what changes is the expression of the FWC factor F_w implemented in it; for this reason, and for clarity, the notation of the various FWCF's will not be carried to the adimensional stress, but rather will be expressed in the second term through the finite-width correction factor itself. Substituting the different expressions of this factor calculated in sections 2.1.2.2 and 2.1.2.3, the following equations are obtained.

Adimensional gross-section stress expressions

Using the exact anisotropic FWC factor derived from Lekhnitskii's solution:

$$\hat{\bar{\sigma}}_g = \frac{1}{K_T^{\infty} F_w} = \frac{1-\frac{2R}{W}}{K_T^{\infty}} + \mathrm{Re}\left\langle \frac{\frac{1}{K_T^{\infty}}}{\mu_1-\mu_2}\left\{ \frac{\mu_2}{1+i\mu_1}\left[1-(1+i\mu_1)\frac{2R}{W}-\sqrt{1-(1+\mu_1^2)\left(\frac{2R}{W}\right)^2}\right] \right.\right.$$
$$\left.\left. -\frac{\mu_1}{1+i\mu_2}\left[1-(1+i\mu_2)\frac{2R}{W}-\sqrt{1-(1+\mu_2^2)\left(\frac{2R}{W}\right)^2}\right]\right\}\right\rangle \,; \tag{2.34}$$

for the purely orthotropic case, using the expressions of α, β reduces (2.34) to

$$\hat{\bar{\sigma}}_g = \frac{1}{K_T^{\infty} F_w|_{orth.}} = \frac{1-\frac{2R}{W}}{K_T^{\infty}} + \frac{1}{K_T^{\infty}(\alpha-\beta)}\left\{\frac{\beta}{1-\alpha}\left[1-(1-\alpha)\frac{2R}{W}-\sqrt{1-(1-\alpha^2)\left(\frac{2R}{W}\right)^2}\right]\right.$$
$$\left.-\frac{\alpha}{1-\beta}\left[1-(1-\beta)\frac{2R}{W}-\sqrt{1-(1-\beta^2)\left(\frac{2R}{W}\right)^2}\right]\right\}. \quad (2.35)$$

With the FWC factor calculated using Tan's orthotropic approximation:

$$\hat{\bar{\sigma}}_g = \frac{1}{K_T^{\infty} \tilde{F}_w|_{orth.}} = \frac{1}{2K_T^{\infty}}\left\{2-\left(\frac{2R}{W}\right)^2-\left(\frac{2R}{W}\right)^4+(K_T^{\infty}-3)\left(\frac{2R}{W}\right)^6\left[1-\left(\frac{2R}{W}\right)^2\right]\right\}, \quad (2.36)$$

and particularized for the isotropic case:

$$\hat{\bar{\sigma}}_g = \frac{1}{K_T^{\infty} F_w|_{isot.}} = \frac{2-\left(\frac{2R}{W}\right)^2-\left(\frac{2R}{W}\right)^4}{2K_T^{\infty}}. \quad (2.37)$$

Using the exact orthotropic FWCF corrected by Tan's magnification factor:

$$\hat{\bar{\sigma}}_g = \frac{1}{K_T^{\infty} F_w^*} = \frac{\frac{1}{M}-\frac{2R}{W}}{K_T^{\infty}} + \frac{1}{K_T^{\infty}(\alpha-\beta)}\left\{\frac{\beta}{1-\alpha}\left[1-(1-\alpha)\left(\frac{2R}{W}M\right)-\sqrt{1-(1-\alpha^2)\left(\frac{2R}{W}M\right)^2}\right]\right.$$
$$\left.-\frac{\alpha}{1-\beta}\left[1-(1-\beta)\left(\frac{2R}{W}M\right)-\sqrt{1-(1-\beta^2)\left(\frac{2R}{W}M\right)^2}\right]\right\}, \quad (2.38)$$

and with Tan's improved theory (orthotropic and corrected by M):

$$\hat{\sigma}_g = \frac{1}{K_T^{\infty} \tilde{F}_w^*} = \frac{1}{K_T^{\infty}}\left\{\frac{3(1-2R/W)}{2+(1-2R/W)^3}+\frac{(K_T^{\infty}-3)}{2}\left(\frac{2R}{W}\right)^6\left[1-\left(\frac{2R}{W}\right)^2\right]\right\}. \quad (2.39)$$

Finally, for Tan's improved theory in the isotropic case, which recovers Heywood's finite-width correction factor:

$$\hat{\bar{\sigma}}_g = \frac{1}{K_T^{\infty} F_w|_{Heyw.}} = \frac{1}{K_T^{\infty}}\left[\frac{3\left(1-\frac{2R}{W}\right)}{2+\left(1-\frac{2R}{W}\right)^3}\right]. \quad (2.40)$$

Adimensional net-section stress expressions

Using the exact anisotropic FWC factor derived from Lekhnitskii's solution:

$$\hat{\bar{\sigma}}_n = \frac{\frac{W}{\overline{W-2R}}}{K_T^{\infty} F_w} = \frac{1}{K_T^{\infty}} + \mathrm{Re}\left\langle \frac{\frac{W}{\overline{W-2R}}}{K_T^{\infty}(\mu_1-\mu_2)} \left\{ \frac{\mu_2}{1+i\mu_1}\left[1-(1+i\mu_1)\frac{2R}{W}-\sqrt{1-(1+\mu_1^2)\left(\frac{2R}{W}\right)^2}\right] \right.\right.$$
$$\left.\left. -\frac{\mu_1}{1+i\mu_2}\left[1-(1+i\mu_2)\frac{2R}{W}-\sqrt{1-(1+\mu_2^2)\left(\frac{2R}{W}\right)^2}\right] \right\} \right\rangle ; \quad (2.41)$$

for the purely orthotropic case, using the expressions of α, β reduces (2.41) to:

$$\hat{\bar{\sigma}}_n = \frac{\frac{W}{\overline{W-2R}}}{K_T^{\infty} F_w|_{orth.}} = \frac{1}{K_T^{\infty}} + \frac{\frac{W}{\overline{W-2R}}}{K_T^{\infty}(\alpha-\beta)} \left\{ \frac{\beta}{1-\alpha}\left[1-(1-\alpha)\frac{2R}{W}-\sqrt{1-(1-\alpha^2)\left(\frac{2R}{W}\right)^2}\right] \right.$$
$$\left. -\frac{\alpha}{1-\beta}\left[1-(1-\beta)\frac{2R}{W}-\sqrt{1-(1-\beta^2)\left(\frac{2R}{W}\right)^2}\right] \right\} . \quad (2.42)$$

With the FWC factor calculated using Tan's orthotropic approximation:

$$\hat{\bar{\sigma}}_n = \frac{\frac{W}{\overline{W-2R}}}{K_T^{\infty} \tilde{F}_w|_{orth.}} = \frac{1}{2K_T^{\infty}\left(1-\frac{2R}{W}\right)} \left\{ 2-\left(\frac{2R}{W}\right)^2-\left(\frac{2R}{W}\right)^4+(K_T^{\infty}-3)\left(\frac{2R}{W}\right)^6\left[1-\left(\frac{2R}{W}\right)^2\right] \right\} , \quad (2.43)$$

and particularized for the isotropic case:

$$\hat{\bar{\sigma}}_n = \frac{\frac{W}{\overline{W-2R}}}{K_T^{\infty} \tilde{F}_w|_{isot.}} = \frac{2-\left(\frac{2R}{W}\right)^2-\left(\frac{2R}{W}\right)^4}{2K_T^{\infty}\left(1-\frac{2R}{W}\right)} . \quad (2.44)$$

Finally, for Tan's improved theory in the isotropic case, which recovers Heywood's finite-width correction factor:

$$\hat{\bar{\sigma}}_g = \frac{\frac{W}{\overline{W-2R}}}{K_T^{\infty} F_w|_{Heyw.}} = \frac{1}{K_T^{\infty}}\left[\frac{3}{2+\left(1-\frac{2R}{W}\right)^3}\right] . \quad (2.45)$$

The transformation from gross-sectional to net-sectional stress in the cases where Tan's magnification factor is applied requires some discussion that will be done in the next section.

2.1.3 Notch sensitivity results and fit curves

2.1.3.1 Notch sensitivity curves comparison

When plotting the adimensional stress at failure (according to the maximum stress criterion at the edge of the hole) versus the diameter-to-width ratio of the specimen, the two models described, i.e., notch insensitivity (NI) and notch sensitivity (NS), result respectively in a straight line and a curve that become closer to each other the nearer the ratio is to 1. The stress plotted can be either that at the gross or the net sections of the specimen; the transformation from one to the other is done via the factor $(1 - 2R/W)$, so their relative shape is unchanged.

It will be observed that the experimental results of uniaxial tests of notched laminates fall in between those two lines, sometimes closer to one than to the other. This seems to indicate that the real failure is either dominated by one of the models or a combination of both, being the notch-insensitive one an upper bound and the notch-sensitive case a lower bound for the stress at fracture.

The former is a straight line for both the gross- and net-sectional stresses, so no further analysis can be done. The latter, as explained in the previous section, is the reciprocal of the stress concentration factor for the chosen stress, and depends on the related finite-width correction factor for a given laminate.

Figures 2-3 to 2-5 represent some of these curves, those of equations (2.4), (2.34), (2.36), (2.37), and (2.40) for the adimensional $\bar{\sigma}_g$, and equations (2.3), (2.41), (2.43), (2.44), and (2.45) for the adimensional $\bar{\sigma}_n$. The orthotropic laminates represented are the ones used in this thesis' experimental campaign (AS4/8552 CFR epoxy, $[0]_6$, $[90]_6$ and $[0/90]_{2s}$).

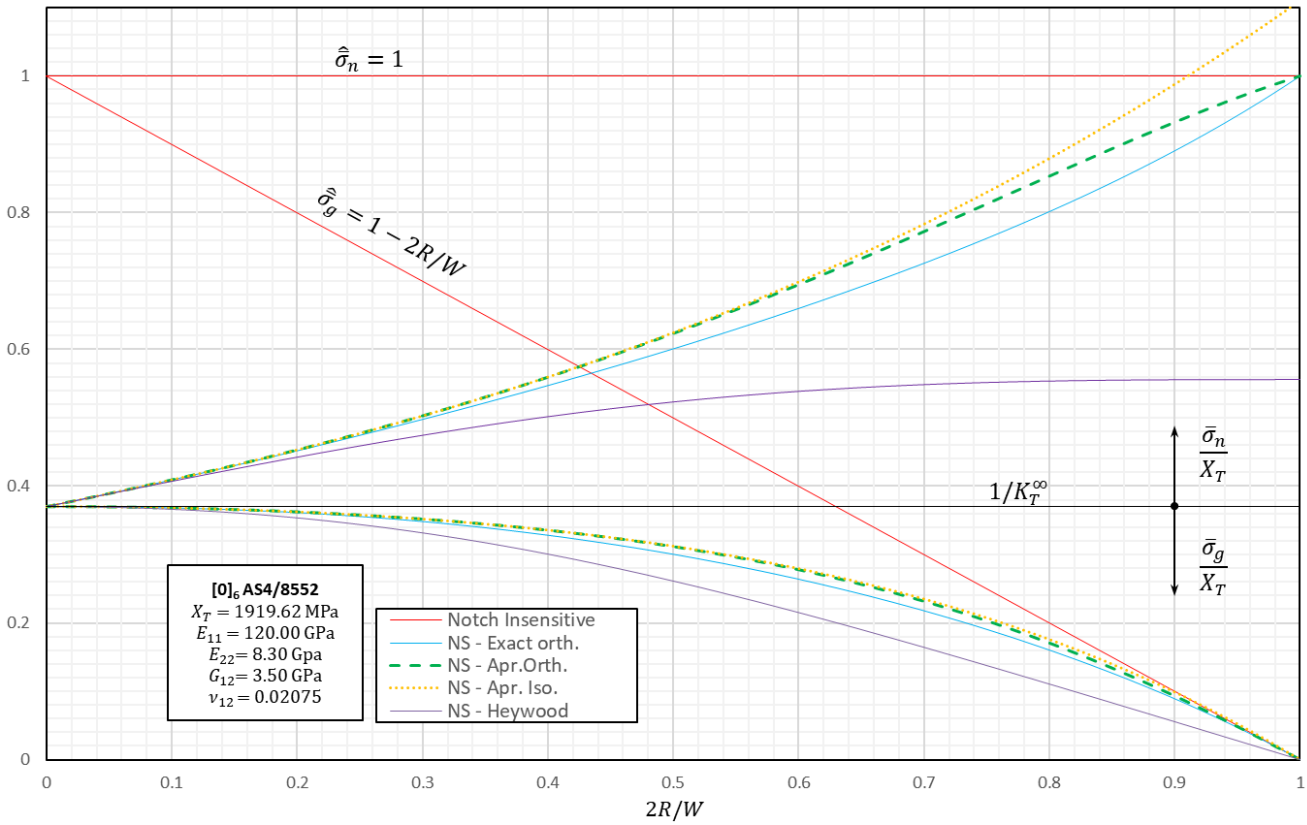

Figure 2-3. Notch sensitivity curves for the $[0]_6$ laminate.

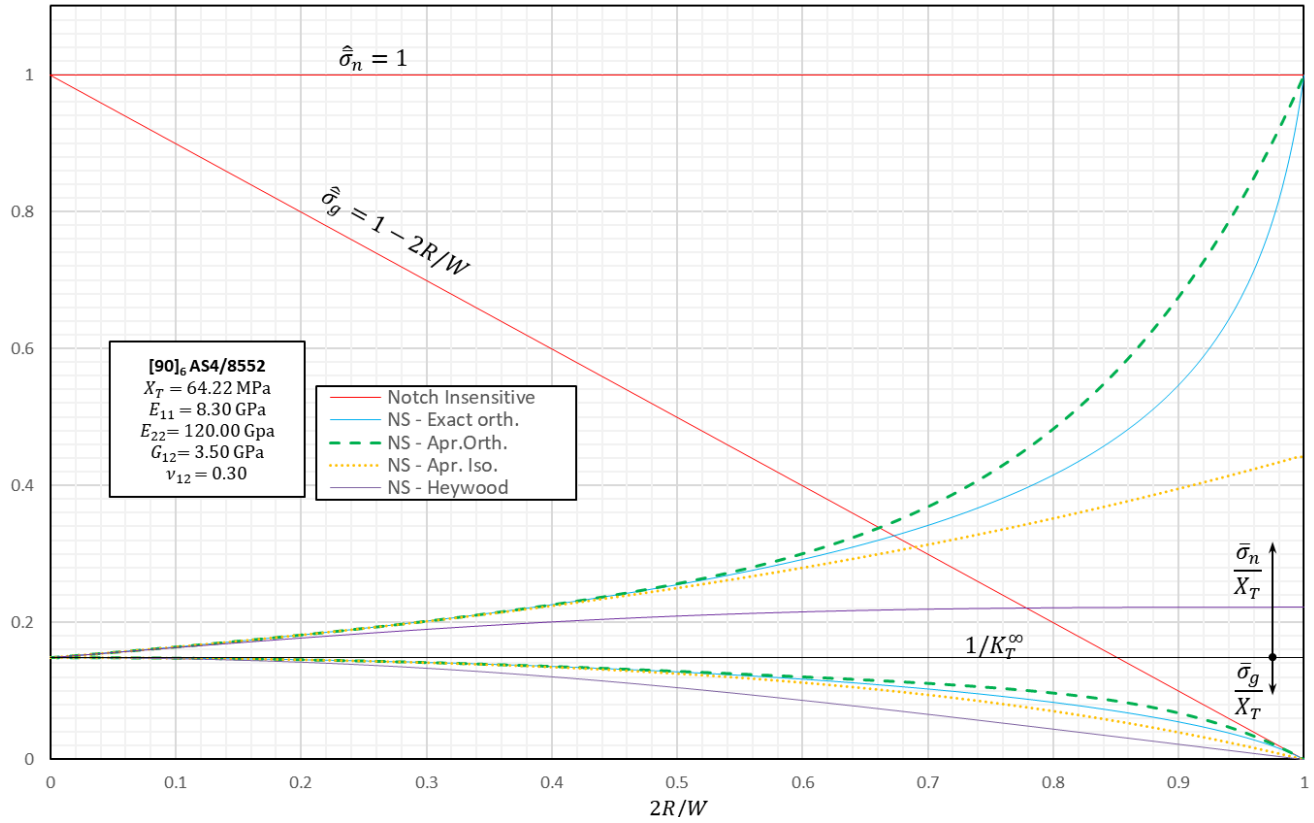

Figure 2-4. Notch sensitivity curves for the $[90]_6$ laminate.

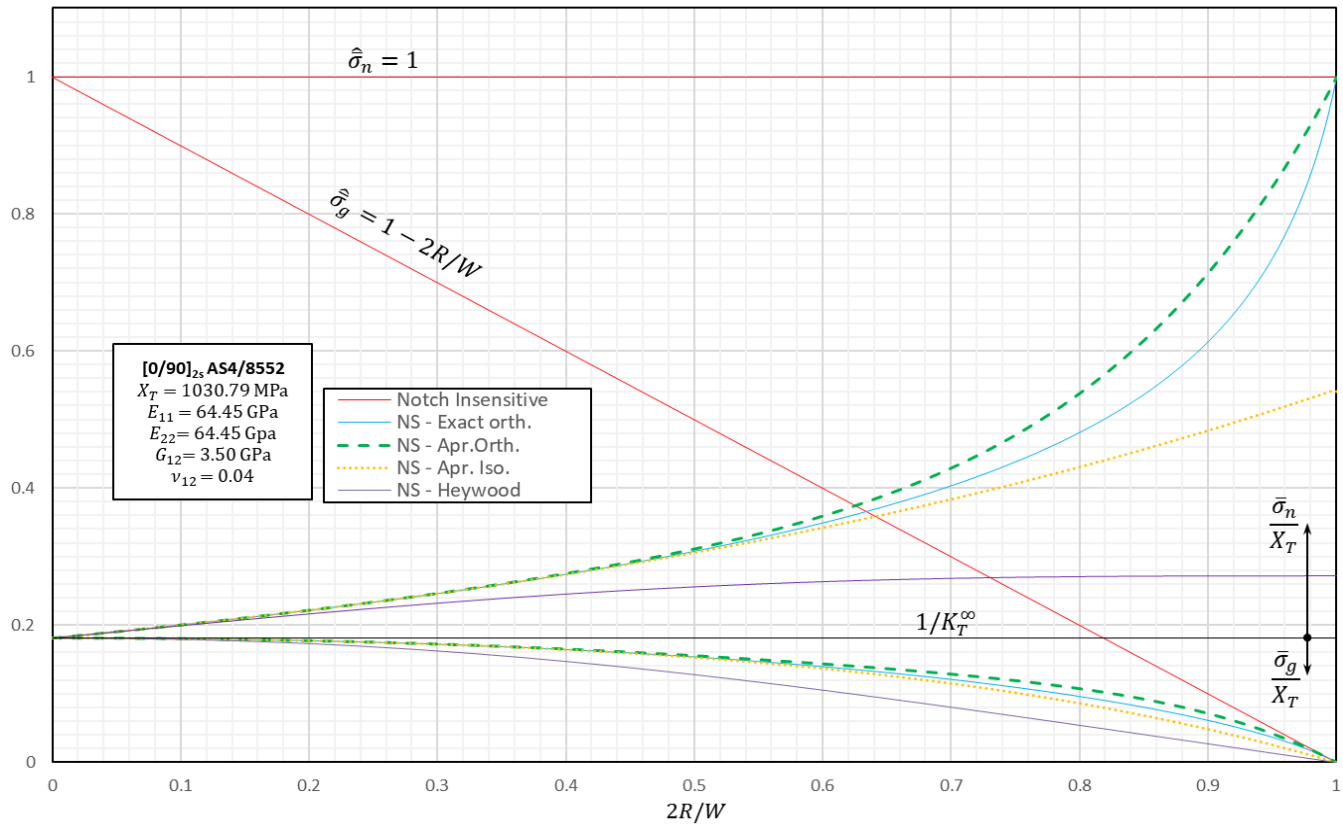

Figure 2-5. Notch sensitivity curves for the $[0/90]_{2s}$ laminate.

Except for the curves obtained using Heywood's FWC factor, the others are very close to each other in the gross-sectional stress representation. The higher differences between those lines occur for diameter-to-width ratios higher than 0.6, which are difficult to obtain in practice due to the very small net section. These differences are amplified in the net-sectional stress curves because they are divided by $1 - 2R/W$. Thus, and considering that the exact anisotropic FWCF is not an expression considerably more complex than the approximations, it seems reasonable to use the former as a way of avoiding possible rounding errors when computing these equations.

A commentary about this must be done: the use of this exact anisotropic FWCF has been performed in the graphics above via the calculation of the parameters α and β, dependent on the laminate's properties, from (2.8). As pointed out when these expressions were introduced, it is necessary to check that $\alpha, \beta \in \mathbb{R}$, which happens if

$$\frac{E_{11}}{G_{12}} - 2\nu_{12} - 2\sqrt{\frac{E_{11}}{E_{22}}} \geq 0\ ; \tag{2.46}$$

this inequality might not be true for certain laminates, such as the Graphite/Epoxy AS4/3502 material in an anisotropic-behaving $[\pm 45]_{4s}$ lay-up, as used by Tan in [40]; this behavior is due to the loading not being directed along the orthotropy axes. The author explains that, for this laminate, the maximum stress does not occur at the edge of the hole, but a little further away from it, so the failure criterion (2.30) does not hold up in this case. However, this offset maximum stress is indeed seen in Lekhnitskii's anisotropic solution with complex parameters, so the exact anisotropic FWCF could be used theoretically, but another failure model should be used, such as the Point Stress Criterion.

Also, for isotropic or quasi-isotropic laminates, the expression on the left-hand side of (2.46) should be nil, but due to rounding errors its value might be close to, but not exactly, zero; same thing happens with the complex parameters, which should be $\mu_1 = \mu_2 = i$ but could be different when directly computed from (2.8). This can lead to great computational errors later on, so an "isotropic tolerance" value must be introduced when coding these equations, so that if the term in (2.46) is sufficiently close to zero, the exact isotropic distribution, (2.22), and FWC factor, (2.25), will be used.

2.1.3.2 Tan's magnification factor suitability discussion

The curves for Tan's modified FWC factors have not been plotted yet because there is an argument to be made about its usage in this maximum stress criterion. The corrections introduced by the magnification factor M are effectively modifying either the radius of the hole or the width of the specimen:

$$R^* = RM \ \vee \ W^* = \frac{W}{M}\ . \tag{2.47}$$

When calculated, it is not specified whether the force resultant balance (2.19) between the gross and net sections is modified by this factor as well. In physical terms, this does not make much sense because it unlinks the real from the theoretical problem, specially considering that the modification changes for every value of the diameter-to-width ratio. The next graph shows the values of both M and the modified ratio $2R^*/W$:

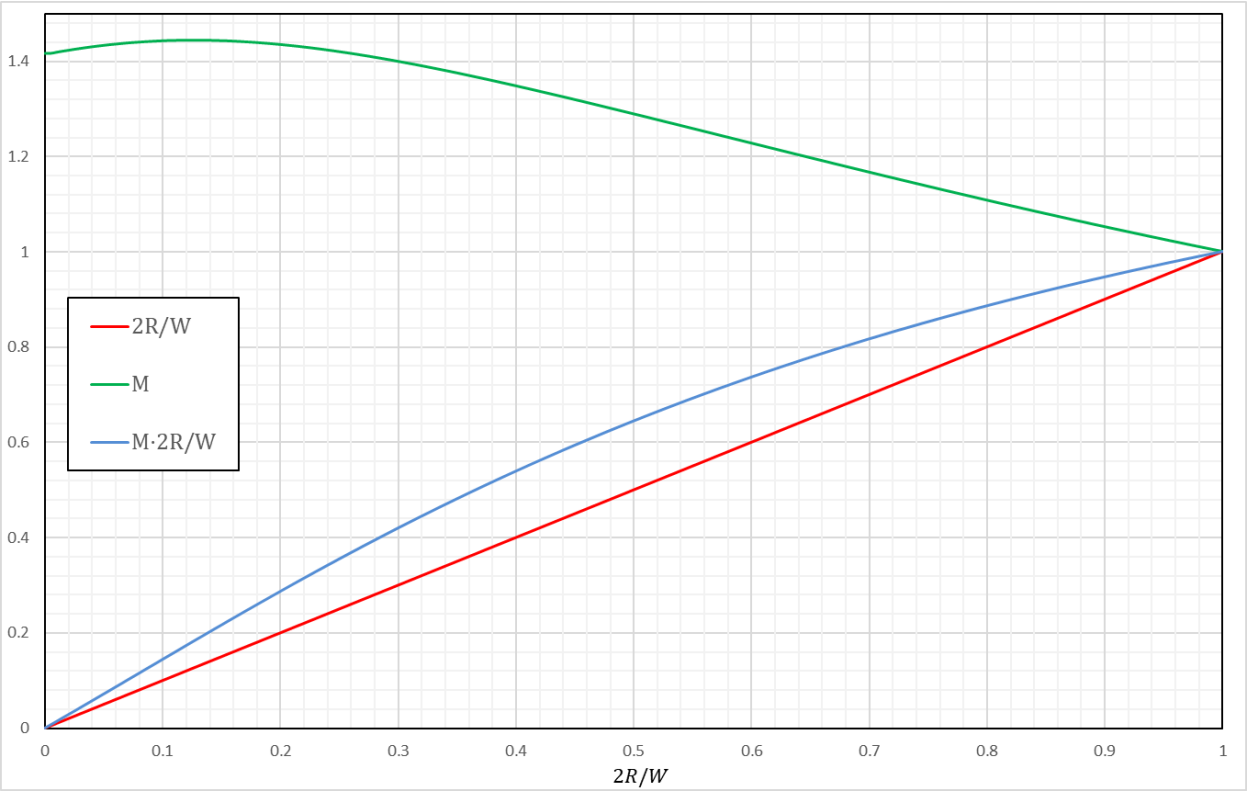

Figure 2-6. Tan's magnification factor and modified diameter-to-width ratios.

As it can be seen, when the diameter-to-width ratio is around 0.125, the magnification factor increases the radius of the hole by more than 40%. This reinforces the idea that the balance that relates σ_g and σ_n is no longer applicable under the real dimensions of the radius and the width. If one tries to apply this balance regardless, it can also be proven mathematically that an inconsistency is reached.

Let us begin from the definition of the net-section stress introduced in (2.18), and adimensionalize it with the variable $\gamma = x/R$ that has been presented before:

$$\sigma_n \coloneqq \frac{2}{W-2R}\int_R^{W/2} \sigma_y(x,0)\,\mathrm{d}x = \frac{1}{(W/2R)-1}\int_1^{W/2R} \sigma_y(\gamma,0)\,\mathrm{d}\gamma \ ; \tag{2.48}$$

introducing now the hypothesis (2.14) on which this analytical model is developed,

$$\sigma_n = \frac{1}{(W/2R)-1}\int_1^{W/2R} F_w \sigma_y^{\infty}(\gamma,0)\,\mathrm{d}\gamma \ . \tag{2.49}$$

The failure criterion, i.e., maximum stress at the edge of the hole, can be rewritten as (2.50) via the definitions of both the stress concentration factor for the finite plate (2.16) and the FWC factor (2.15); from it, F_w can be expressed as (2.51):

$$X_T = \bar{\sigma}_y(x=R,0) = K_T\bar{\sigma}_g = K_T^{\infty}F_w\bar{\sigma}_g \ , \tag{2.50}$$

$$F_w = \frac{X_T}{K_T^\infty \bar{\sigma}_g} \,. \tag{2.51}$$

Applying the criterion in this form to (2.49) and reordering yields

$$\frac{\bar{\sigma}_n}{X_T} = \frac{1/K_T^\infty}{(W/2R) - 1} \int_1^{W/2R} \frac{\bar{\sigma}_y^\infty(\gamma, 0)}{\bar{\sigma}_g} \, \mathrm{d}\gamma \,, \tag{2.52}$$

where the notation for adimensionality and fracture $\hat{\square}$ will be applied in what follows. In the limit $2R/W \to 1$, which is equivalent to $W/2R \to 1$, an indetermination of the type $0/0$ is reached in the second member of (2.52). Thus, L'Hôpital's rule w.r.t. $W/2R$ can be applied:

$$K_T^\infty \hat{\bar{\sigma}}_n|_{\frac{W}{2R} \to 1} = \lim_{\frac{W}{2R} \to 1} \left\{ \frac{\partial}{\partial \left(\frac{W}{2R} \right)} \left[\int_1^{W/2R} \hat{\bar{\sigma}}_y^\infty(\gamma, 0) \, \mathrm{d}\gamma \right] \right\} . \tag{2.53}$$

The derivative of the integral can be solved employing Leibniz's rule and remembering that $\hat{\bar{\sigma}}_y^\infty(\gamma, 0)$ only depends on the material's properties and γ:

$$K_T^\infty \hat{\bar{\sigma}}_n|_{\frac{W}{2R} \to 1} = \lim_{\frac{W}{2R} \to 1} \left[\hat{\bar{\sigma}}_y^\infty \left(\gamma = \frac{W}{2R}, 0 \right) \right] = \hat{\bar{\sigma}}_y^\infty(\gamma = 1, 0) \,, \tag{2.54}$$

which, from the very definition of the SCF for an infinite plate, (2.10), results in

$$\hat{\bar{\sigma}}_n|_{\frac{W}{2R} \to 1} = 1 \,. \tag{2.55}$$

This result is applicable whichever the form of the finite-width correction factor is. Thus, if the balance (2.19) is employed using the definition of σ_n from (2.48) and the FWCF modified by Tan through the magnification factor M, the adimensional failure criterion for the net section should also tend to 1 when the hole diameter approaches the width of the plate. It can be seen that this is not so by taking this limit in (2.33) and using either F_w^* from (2.28) or $\tilde{F}_w^*$ from (2.29) for the finite-width correction factor.

This last step requires the application of L'Hôpital's rule and some complicated derivation, so the incongruence of the use of this magnification factor in this context will be shown graphically, instead. Figures 2-7 to 2-9 show the adimensional net-section stress at failure for both the exact orthotropic and the approximate FWCF's, ones as originally obtained, and the others after applying the M factor. The expression of σ_n is that of (2.19), this is, without applying the corrected radius R^* or width W. It is worth recalling that it does not make sense to use the correction of M neither in the approximate isotropic nor the Heywood's FWC factors, since it was from the combination of these two expressions that the magnification factor itself was obtained.

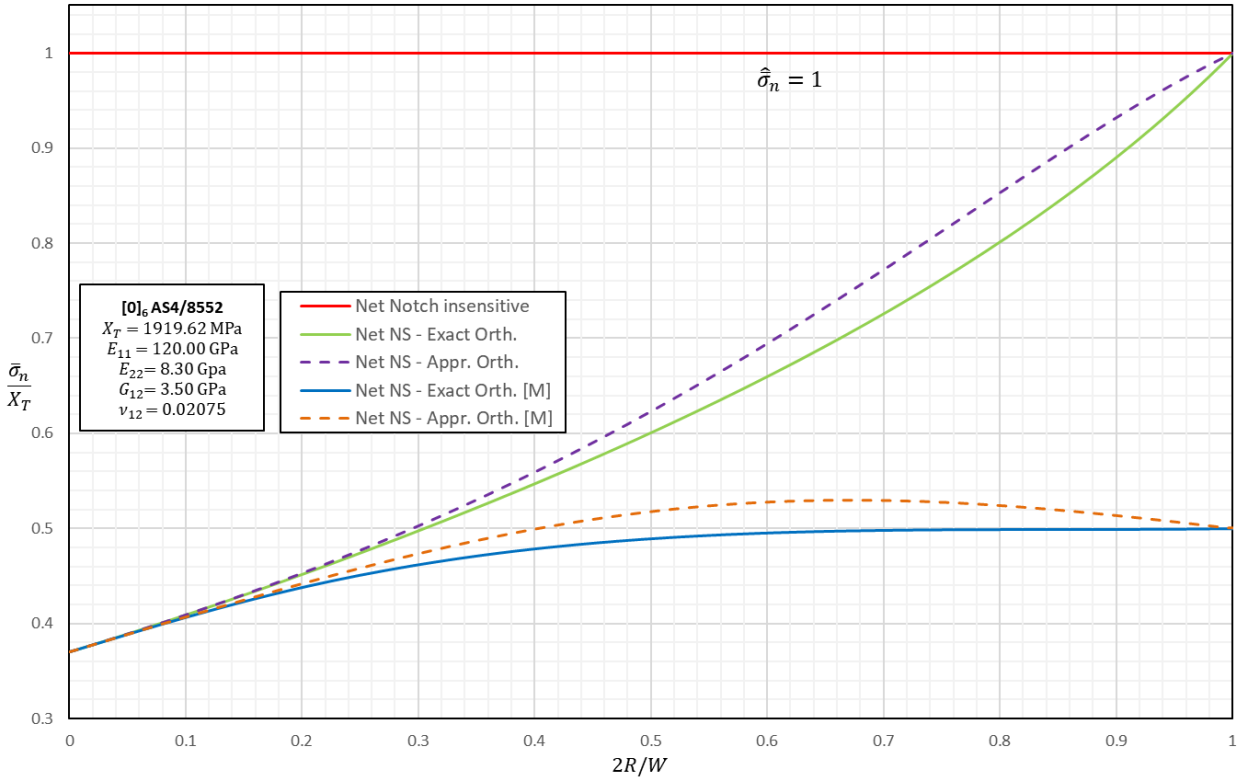

Figure 2-7. Comparison of the notch sensitivity curves for the net-section stress; laminate $[0]_6$.

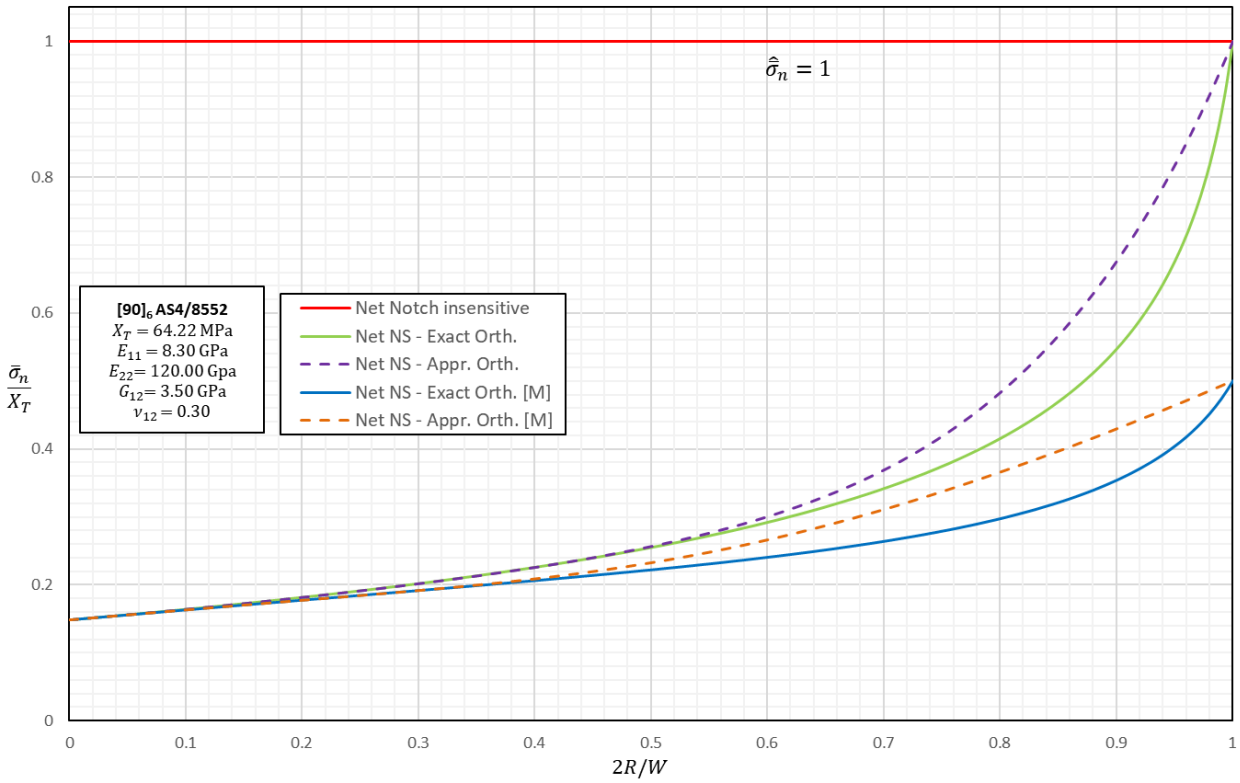

Figure 2-8. Comparison of the notch sensitivity curves for the net-section stress; laminate $[90]_6$.

It can be seen, as was shown in the previous graphs, that both the exact and the approximate orthotropic expressions of $\hat{\bar{\sigma}}_n$ do tend to 1 in the limit. When these expressions use the corrected ratio $2R^*/W$, their tendency is towards 0.5 in all three lay-ups examined, which leads to thinking that if the limit described above is calculated, it would probably result in ½ independently of material properties.

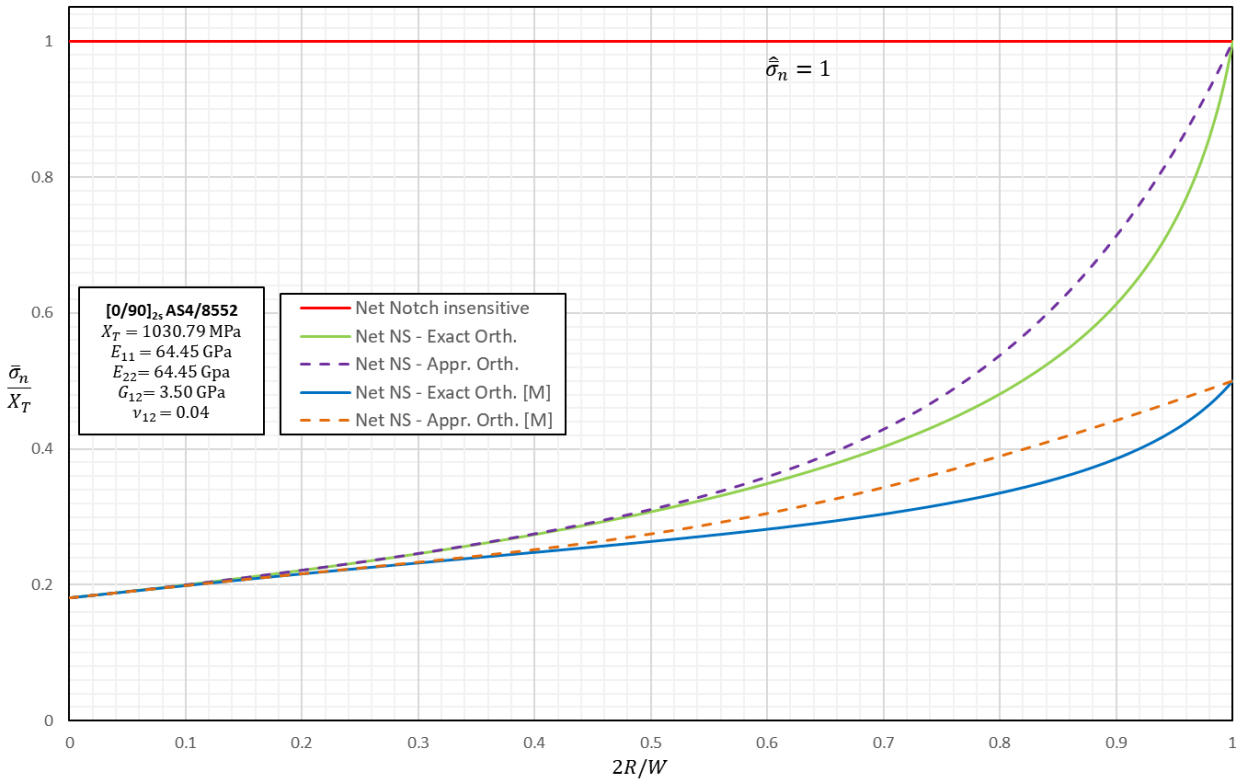

Figure 2-9. Comparison of the notch sensitivity curves for the net-section stress; laminate $[0/90]_{2s}$.

The expressions for the corrected FWCF's with M would indeed tend to 1 if the magnification factor was applied to the radius in the force balance and transformed it to R^*. However, this would also require the redefinition of the net-sectional stress to (2.56), which results in an expression not so easy to compute and that is unrelated to the actual, real problem studied.

$$\sigma_n^* := \frac{2}{W-2R^*}\int_{R^*}^{W/2}\sigma_y(x,0)\,\mathrm{d}x = \frac{W}{W-2R^*}\sigma_g\,. \tag{2.56}$$

2.1.3.3 Size effect fit curves

The careful analysis of the different finite-width correction factors performed in the last sections is useful for designing curves to fit experimental data by a minimum squares approach. These curves are intended to reflect the so-called size effect: the experimental observation that, for a given ratio $2R/W$, bigger holes result in a reduced tensile strength of the specimens tested.

When plotting the adimensional stress at failure versus the ratio using the diameters as a parameter, the size effect can be seen as a transformation from the notch-insensitivity line when the radius is small, to the notch-sensitivity curve the bigger this dimension gets. These desired fit curves can be expressed in the following form for both the gross and net section stresses:

$$\hat{\bar{\sigma}}|_{fit} = \hat{\bar{\sigma}}|_{NI}\left(\frac{\hat{\bar{\sigma}}|_{NS}}{\hat{\bar{\sigma}}|_{NI}}\right)^{f(2R)} , \tag{2.57}$$

with $f(2R)$ being a function that returns 0 when the diameter is nil, and 1 when the radius tends to infinity. A function that behaves like this is the arctangent, except that its tendency at the infinity of the diameter is to $\pi/2$ rather than to 1. Nevertheless, since it is used to fit experimental results, a coefficient must be added that can account for this value. Let us then define the fit curve

$$\hat{\bar{\sigma}}|_{fit} \coloneqq \hat{\bar{\sigma}}|_{NI}\left(\frac{\hat{\bar{\sigma}}|_{NS}}{\hat{\bar{\sigma}}|_{NI}}\right)^{m\arctan(2R)} , \tag{2.58}$$

with m being the coefficient that needs to be adjusted experimentally, and that is different for the gross and the net sections. This way, for small holes close to zero in diameter, the fit curve equation equals the notch insensitive line, and for growing diameters it transforms gradually to the notch sensitive curve.

Although in this thesis the exact anisotropic FWCF will be used, as an example, let us express (2.58) according to the gross-sectional stress and using the approximate orthotropic equation for the notch sensitive stress, (2.43):

$$\hat{\bar{\sigma}}|_{fit}^{\widetilde{orth.}} = \left(1-\frac{2R}{W}\right)\left\{\frac{2-\left(\frac{2R}{W}\right)^2-\left(\frac{2R}{W}\right)^4+(K_T^\infty-3)\left(\frac{2R}{W}\right)^6\left[1-\left(\frac{2R}{W}\right)^2\right]}{2K_T^\infty\left(1-\frac{2R}{W}\right)}\right\}^{m_g\arctan(2R)} . \tag{2.59}$$

2.2 Point Stress and Average Stress Criteria

The most widely used criteria for the design of notched composite laminates under uniaxial tensile loading are Whitney and Nuismer's Point Stress (PSC) and Average Stress Criteria (ASC) [50]. The first one applies the maximum stress criterion to a point in the x axis of the laminate at a distance d_0 from the edge of the hole. The ASC does a similar approach, but extending the maximum stress criterion to an area from the bottom of the opening up until a distance a_0. Both "characteristic distances" were originally said to be a material propertiy, but it has been proven that they also depend on the geometry of the tested laminate [60], [61].

Using the same model as in the section before, Figure 2-1, these criteria can be formally expressed as

$$\bar{\sigma}_y(R+d_0,0) = X_T , \tag{2.60}$$

$$\frac{1}{a_0}\int_R^{R+a_0}\bar{\sigma}_y(x,0)\,\mathrm{d}x = X_T , \tag{2.61}$$

where the distribution $\sigma_y(x,0)$ is to be chosen and X_T is the unnotched laminate's tensile strength. The original approach, dismissing the finite size effect, proposed a distribution based on Timoshenko's isotropic solution for an infinite plate [58]:

$$\sigma_y^\infty(\gamma,0) = \frac{\sigma_g}{2}[2+\gamma^{-2}+3\gamma^{-4}] , \qquad \gamma = \frac{x}{R} . \tag{2.22}$$

Lately, Tan's orthotropic approximation, described in section 2.1.2.3, equation (2.23), has been implemented including his finite-width correction and magnification factors [62]. However, as discussed in section 2.1.3.2, the use of the M factor does not make much sense without using the corrected radius R^*, which depends itself on the diameter-to-width ratio. Since the characteristic distances are also a function of the geometry, they too would have to be corrected. This is a conceptually complicated process that can be avoided by directly drawing on the exact anisotropic solution by Lekhnitskii, (2.5). It may look difficult to implement, but considering that most software nowadays, including Excel, can deal with imaginary numbers, there does not seem to be a reason not to use it, provided that the commentary at the end of section 2.1.3.1 is taken into account. This equation will be copied here again, and integrated so that it can be used as a reference:

$$\sigma_y^{\infty}(\gamma,0)=\sigma_g+\sigma_g\,\mathrm{Re}\left\{\frac{1}{\mu_1-\mu_2}\left[\frac{-\mu_2(1-i\mu_1)}{\sqrt{\gamma^2-1-\mu_1^2}\left(\gamma+\sqrt{\gamma^2-1-\mu_1^2}\right)}+\frac{\mu_1(1-i\mu_2)}{\sqrt{\gamma^2-1-\mu_2^2}\left(\gamma+\sqrt{\gamma^2-1-\mu_2^2}\right)}\right]\right\}, \tag{2.62}$$

$$\int\frac{\sigma_y^{\infty}(\gamma,0)}{\sigma_g}\,\mathrm{d}\gamma=\gamma+\mathrm{Re}\left\{\frac{1}{\mu_1-\mu_2}\left[\frac{\mu_2}{1+i\mu_1\left(\gamma+\sqrt{\gamma^2-1-\mu_1^2}\right)}-\frac{\mu_1}{1+i\mu_2\left(\gamma+\sqrt{\gamma^2-1-\mu_2^2}\right)}\right]\right\}+C\,, \tag{2.63}$$

where C is the integration constant. The solution of this integral has been used implicitly before in (2.19) to obtain the exact orthotropic FWCF. A simple replacement can be made to check this result, considering that, when substituting $\gamma=1$, the term $\sqrt{(\gamma^2-1-\mu_j^2)}$, with $j=1,2$, should retain the same sign as that of the complex parameter μ_j under the square root in the other substitution [57]; the same comment applies when solving to obtain (2.66).

Using the adimensional characteristic distances defined in (2.64), and introducing the finite width correction factor, the PSC and the ASC can be expressed in terms of the exact anisotropic stress distribution as (2.65), (2.66):

$$\hat{d}_0=\frac{d_0}{R},\qquad \hat{a}_0=\frac{a_0}{R}\,, \tag{2.64}$$

$$\bar{\sigma}_g\big|_{PSC}^{Anis.}=\frac{X_T}{F_w}\left\langle 1+\mathrm{Re}\left\{\frac{1}{\mu_1-\mu_2}\left[\frac{\dfrac{-\mu_2(1-i\mu_1)}{\sqrt{\hat{d}_0{}^2+2\hat{d}_0-\mu_1^2}}}{1+\hat{d}_0+\sqrt{\hat{d}_0{}^2+2\hat{d}_0-\mu_1^2}}+\frac{\dfrac{\mu_1(1-i\mu_2)}{\sqrt{\hat{d}_0{}^2+2\hat{d}_0-\mu_1^2}}}{1+\hat{d}_0+\sqrt{\hat{d}_0{}^2+2\hat{d}_0-\mu_2^2}}\right]\right\}^{-1}\right\rangle\,, \tag{2.65}$$

$$\bar{\sigma}_g\big|_{ASC}^{Anis.} = \frac{X_T \hat{a}_0}{F_w}\left\langle \hat{a}_0 + \mathrm{Re}\left\{ \frac{1}{\mu_1 - \mu_2}\left[\frac{\mu_2}{1+i\mu_1}\left(\frac{1}{1+\hat{a}_0+\sqrt{{\hat{a}_0}^2+2\hat{a}_0-\mu_1^2}} - \frac{1}{1-i\mu_1} \right) - \frac{\mu_1}{1+i\mu_2}\left(\frac{1}{1+\hat{a}_0+\sqrt{{\hat{a}_0}^2+2\hat{a}_0-\mu_2^2}} - \frac{1}{1-i\mu_2} \right) \right] \right\}^{-1} \right\rangle \quad , (2.66)$$

These equations use the anisotropic expression of the FWCF and will be called the "exact anisotropic PSC" (EA-PSC) and "exact anisotropic ASC" (EA-ASC), respectively. They will be compared to the typically used expressions of these criteria that employ the approximate orthotropic stress distribution $\tilde{\sigma}_y^{\infty}(\gamma, 0)$ from (2.23) and the corrected orthotropic FWC factor $\tilde{F}_w^*$ given in (2.29); these are written explicitly below as (2.67) and (2.68):

$$\bar{\sigma}_g\big|_{PSC} = \frac{2X_T}{\tilde{F}_w^*\left\{2+\left(1+\hat{d}_0\right)^{-2}+3\left(1+\hat{d}_0\right)^{-4}-(K_T^{\infty}-3)\left[5\left(1+\hat{d}_0\right)^{-6}-7\left(1+\hat{d}_0\right)^{-8}\right]\right\}} \; ; \quad (2.67)$$

$$\bar{\sigma}_g\big|_{ASC} = \frac{2X_T\hat{a}_0}{\tilde{F}_w^*\{2(1+\hat{a}_0)-(1+\hat{a}_0)^{-1}-(1+\hat{a}_0)^{-3}+(K_T^{\infty}-3)[(1+\hat{a}_0)^{-5}-(1+\hat{a}_0)^{-7}]\}} \; . \quad (2.68)$$

In both the anisotropic and the classical approaches, the characteristic distances must be estimated from experimental results. This will be done in the "Results" chapter.

2.3 Finite Fracture Mechanics approach

The Finite Fracture Mechanics (FFM) approach, in the context of notched laminates under tensile loading, proposes that both a stress and an energetic criteria must be fulfilled simultaneously for a crack to propagate and cause the failure of the laminate. This idea was originally proposed by Leguillon [63] using the point-stress criterion. The approach in this section is the one developed by Cornetti et al. [64], which alternatively uses the average-stress criterion.

This FFM proposal assumes that the crack propagates by finite steps, rather than continuously, so that the coupled energy-stress criterion described can be written as:

$$\begin{cases} \dfrac{1}{l}\displaystyle\int_R^{R+l} \sigma_y(x,0)\,\mathrm{d}x = X_T \ , \\ \dfrac{1}{l}\displaystyle\int_R^{R+l} K_I^2(a)\,\mathrm{d}a = K_{Ic}^2 \ , \end{cases} \quad (2.69)$$

where X_T and K_{Ic} are the tensile strength and the mode I fracture toughness of the unnotched laminate, respectively, and a is the usual crack length for the definition of the stress intensity factor (SIF)[5]. The distance l is the crack extension at failure, and is equivalent to the characteristic distance a_0 of the ASC. As stated by

[5] From the definition of (2.70) in [65], a is measured from the center of the plate, i.e., it includes the radius of the hole.

Cornetti at al., the system in (2.69) is a necessary and sufficient condition for fracture to propagate, and it can be physically interpreted as the fact that *fracture is energy driven but a sufficiently high stress field must act in order to trigger crack propagation* [64].

The notation for the dimension l differs from Cornetti's original Δ_{SE} and is taken from Camanho et al. [62], who solve this system in the context of tensile loading by dividing the energetic integral by the square of the stress one and substituting the expressions of $\sigma_y(x,0)$ and $K_I^2(a)$. For the stress distribution, they use Tan's orthotropic approximation corrected by the magnification factor M. As done in the previous section, in this thesis the exact anisotropic stress distribution (2.5) and FWCF (2.20) will be used, instead, to be compared later against Camanho's approach.

The stress intensity factor employed by Camanho et al. is that of two symmetric cracks emanating from a plate with a central circular hole; however, here too they use an isotropic approach from Newman [65], and only indicate that the orthotropy should be accounted for as in Bao et al. [66]. For maximum consistency with the stress distribution, and lacking an anisotropic expression for $K_I(a)$, the orthotropy factor from this last reference, (2.71), will be used in addition to the isotropic expression of the SIF:

$$K_I(a) = \sigma_g f_o f_w f_h \sqrt{\pi a}\,, \tag{2.70}$$

where f_o is the orthotropy factor previously mentioned, (2.71), f_w is the boundary-correction factor for the finite-width[6] SIF ,(2.72), f_h is the boundary-correction factor for the circular hole for two symmetrical cracks, (2.73), and $\lambda = a/R$.

$$f_o = 1 + 0.1(\rho-1) - 0.016(\rho-1)^2 + 0.002(\rho-1)^3\,, \qquad \rho = \frac{\sqrt{E_{11}E_{22}}}{2G_{12}} - \sqrt{\nu_{12}\nu_{21}}\,, \tag{2.71}$$

$$f_w = \sqrt{\sec\left(\frac{\pi R}{W}\right)\sec\left(\frac{\pi a}{W}\right)}\,, \tag{2.72}$$

$$f_h = f_{n=2}\sqrt{1-\lambda^{-1}}\,, \qquad f_{n=2} = 1 + 0.358\lambda^{-1} + 1.425\lambda^{-2} - 1.578\lambda^{-3} + 2.156\lambda^{-4}\,, \tag{2.73}$$

The solution method of SYS described by Camanho et al. results in the following non-linear equation for the length l:

$$\frac{\pi f_o^2 l \int_R^{R+l}(f_w f_h)^2 a\,\mathrm{d}a}{F_w^2\left[\int_R^{R+l}\frac{\sigma_y^\infty(x,0)}{\sigma_g}\,\mathrm{d}x\right]^2} = \left(\frac{K_{Ic}}{X_T}\right)^2\,. \tag{2.74}$$

For comparison, the explicit forms of (2.74) before solving numerically will be presented for both Camanho's and this thesis' approaches. In the former case, f_o is taken as the unit (isotropic approximation), the FWCF is that of equation (2.29), $\tilde{F}_w^*$, and the stress profile is Tan's approximation (2.23), $\tilde{\sigma}_y^\infty$:

[6] Not to be confused with the FWCF for stress concentration factors F_w.

$$\frac{\int_1^{1+\hat{l}} \lambda \sec\left(\frac{\pi R}{W}\lambda\right)[1-\lambda^{-1}][1+0.358\,\lambda^{-1}+1.425\,\lambda^{-2}-1.578\,\lambda^{-3}+2.156\,\lambda^{-4}]^2 \mathrm{d}\lambda}{\frac{\left(\frac{K_{Ic}}{X_T}\tilde{F}_w^*\right)^2}{4\pi l \sec\left(\frac{\pi R}{W}\right)}\left\{2\left(1+\hat{l}\right)-\left(1+\hat{l}\right)^{-1}-\left(1+\hat{l}\right)^{-3}+\left(K_T^{\infty}-3\right)\left[\left(1+\hat{l}\right)^{-5}-\left(1+\hat{l}\right)^{-7}\right]\right\}^2}=1\,, \quad (2.75)$$

where $\hat{l}=l/R$. Let us call the integral in the numerator $I(\hat{l})$; then, the expression of (2.74) using the anisotropic expression of both the stress distribution and the FWCF, plus Suo's orthotropy correction factor (2.71), is:

$$\frac{f_0 X_T}{F_w K_{Ic}}\sqrt{\pi \sec\left(\frac{\pi R}{W}\right) I(\hat{l})}=\hat{l}+\mathrm{Re}\left\{\frac{1}{\mu_1-\mu_2}\left[\frac{\mu_2}{1+i\mu_1}\left(\frac{1}{1+\hat{l}+\sqrt{\hat{l}^2+2\hat{l}-\mu_1^2}}-\frac{1}{1-i\mu_1}\right)\right.\right.$$
$$\left.\left.-\frac{\mu_1}{1+i\mu_2}\left(\frac{1}{1+\hat{l}+\sqrt{\hat{l}^2+2\hat{l}-\mu_2^2}}-\frac{1}{1-i\mu_2}\right)\right]\right\}\,, \quad (2.76)$$

3 RESULTS

Big results require big ambitions.

- Heraclitus -

The equations developed in the previous chapter are applied to the experimental results from the campaign done for this thesis. The notch sensitivity models only provide lower and upper bounds for fracture; the other methods do predict the gross-sectional stress at failure for specific configurations, so they can be compared directly to the specimens' values.

3.1 Experimental results data

In this section, the experimental results of the campaign performed in the context of this thesis will be presented graphically, to be then analyzed in the following sections. The notch insensitive (NI) and notch-sensitive (NS) curves will be plotted for each laminate and reference stress (either σ_g or σ_n) alongside the test data. The notch-sensitive curves are those for the exact anisotropic FWCF, (2.34), using the results of the unnotched specimens as the experimental laminate tensile strength, X_T.

The whole experimental campaign is described in detail in Appendix A. The data obtained from the testing machines was the ultimate tensile force of each specimen exerted by the grips, measured in Newtons. This force was then divided by the corresponding area to obtain the gross-sectional and net-sectional stresses. The radii and widths of the specimens can be examined in the tables 3-2 to 3-5 in the next section; the thicknesses of the specimens are available in the Excel file along with the results for each individual specimen. As a reference, the nominal ply thickness is 0.184 mm.

The following table presents the intact laminate properties, calculated from the classical theory of laminates considering the minimum theoretical values for the lamina; these were obtained from the corresponding AIPS for the Hexcel AS4/8552 CFRE unidirectional prepeg [67].

Min. values	E_{11} [GPa]	E_{22} [GPa]	G_{12} [GPa]	ν_{12} [-]	K_T^∞ [-]	Experimental X_T [MPa]
$[0]_6$	120.00	8.30	3.50	0.02	2.70	1919.62
$[90]_6$	64.45	64.45	3.50	0.04	5.51	64.22
$[0/90]_{2s}$	8.30	120.00	3.50	0.30	6.76	1030.79

Table 3-1. Mechanical properties of the laminates used in the experimental campaign.

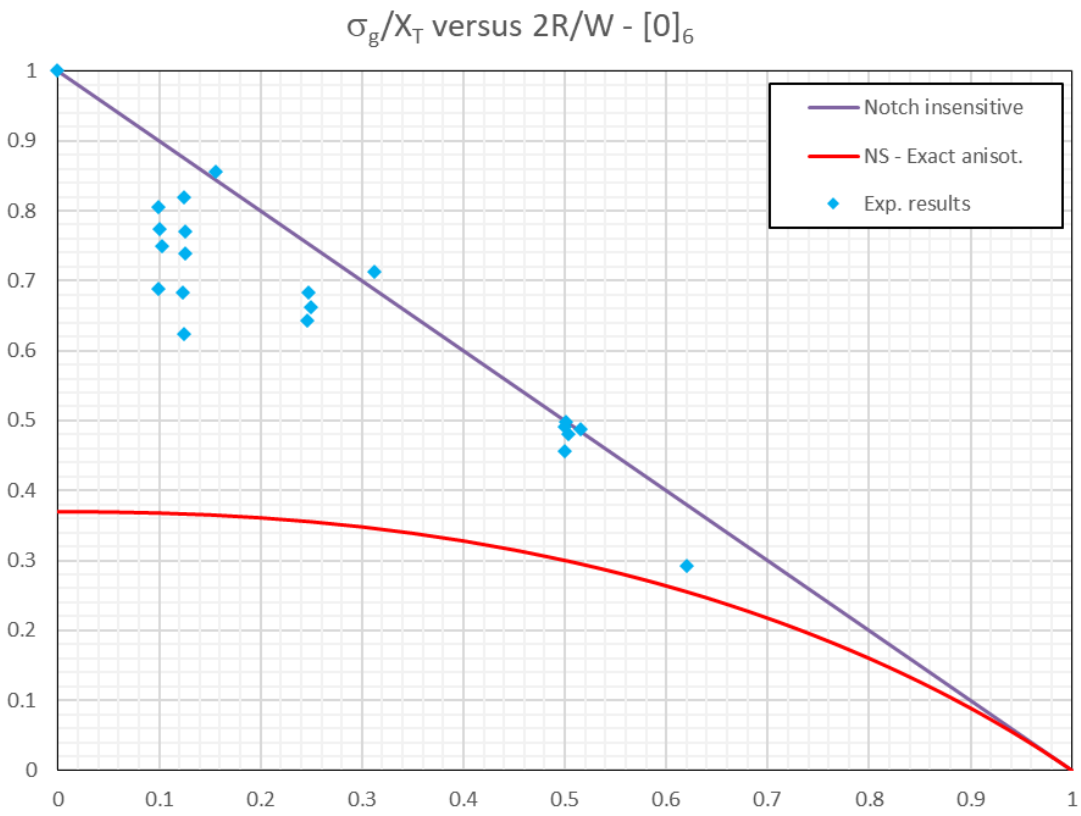

Figure 3-1

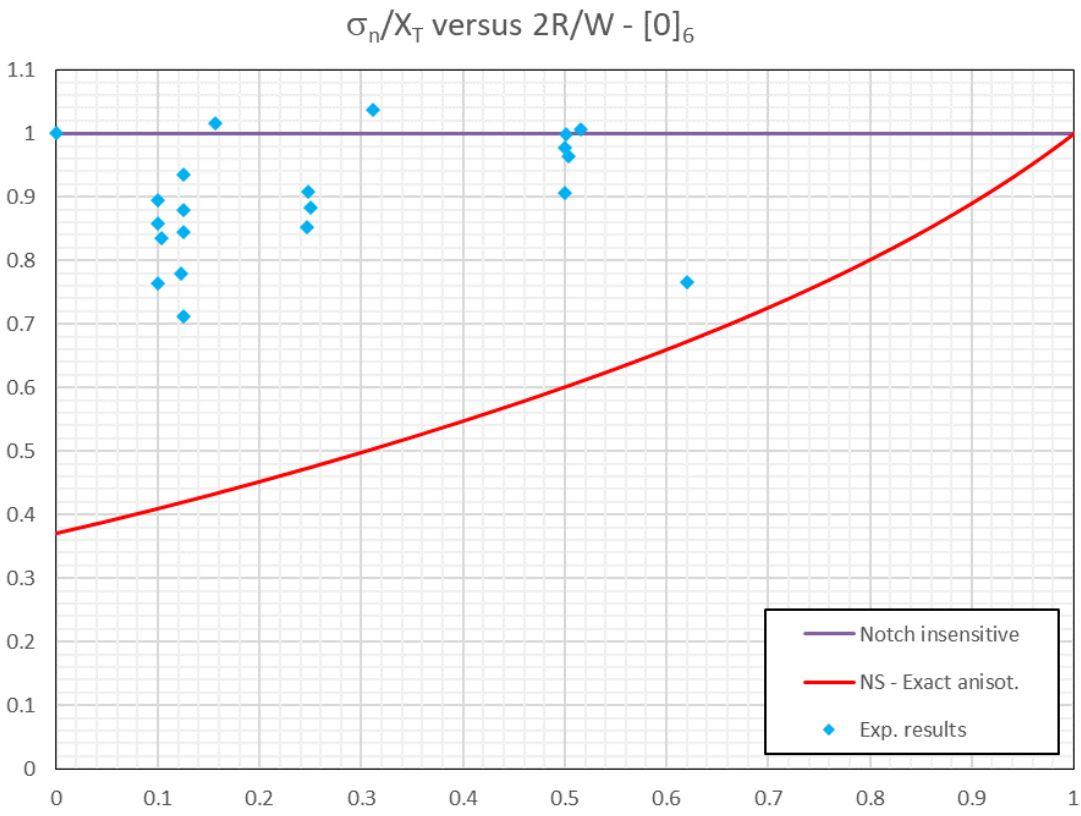

Figure 3-2

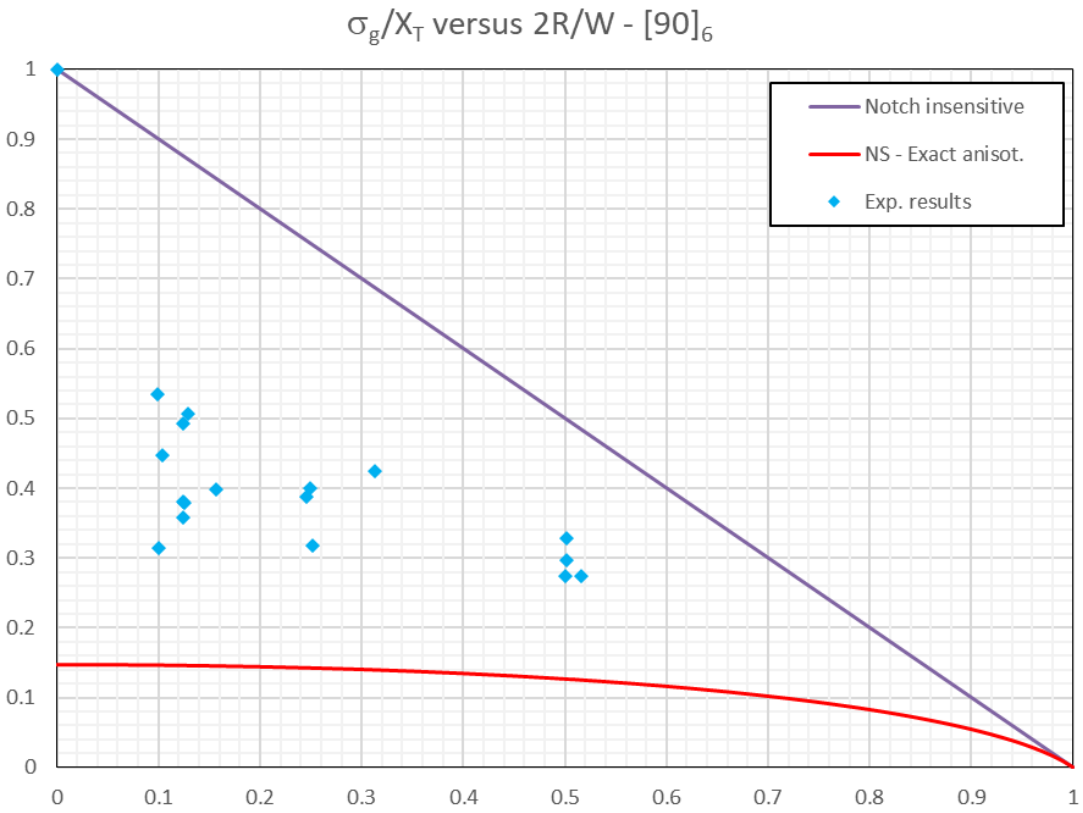

Figure 3-3

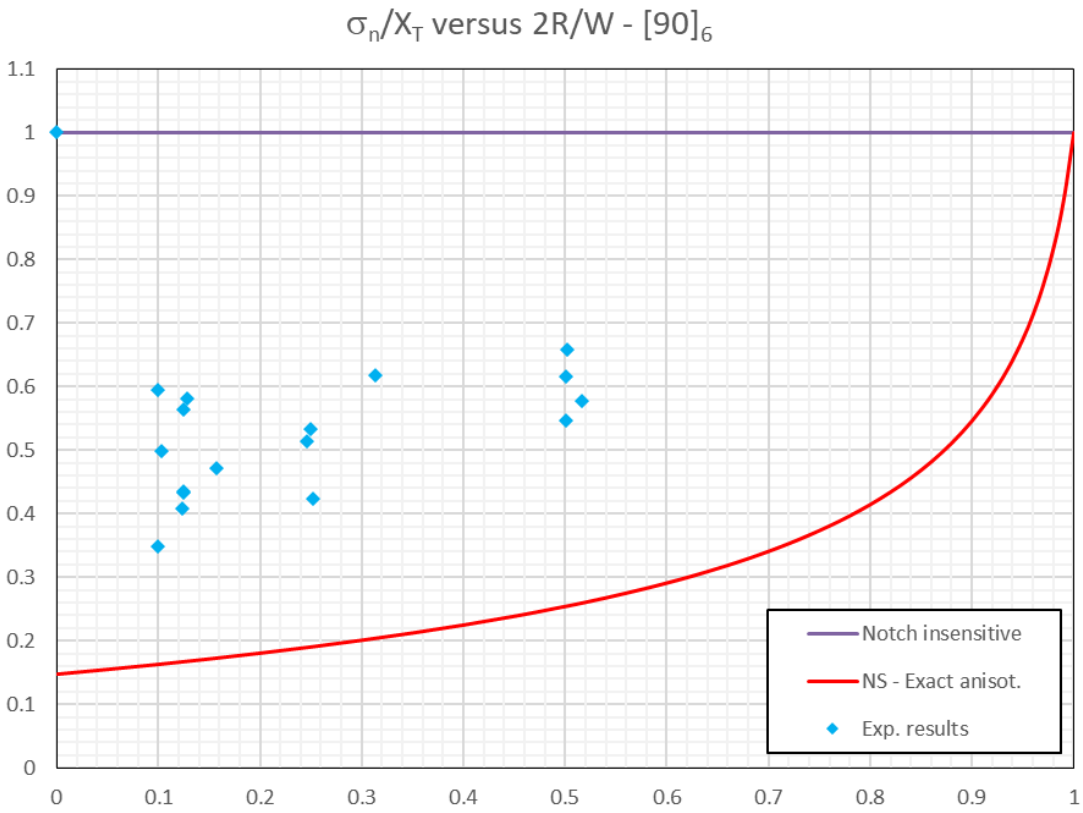

Figure 3-4

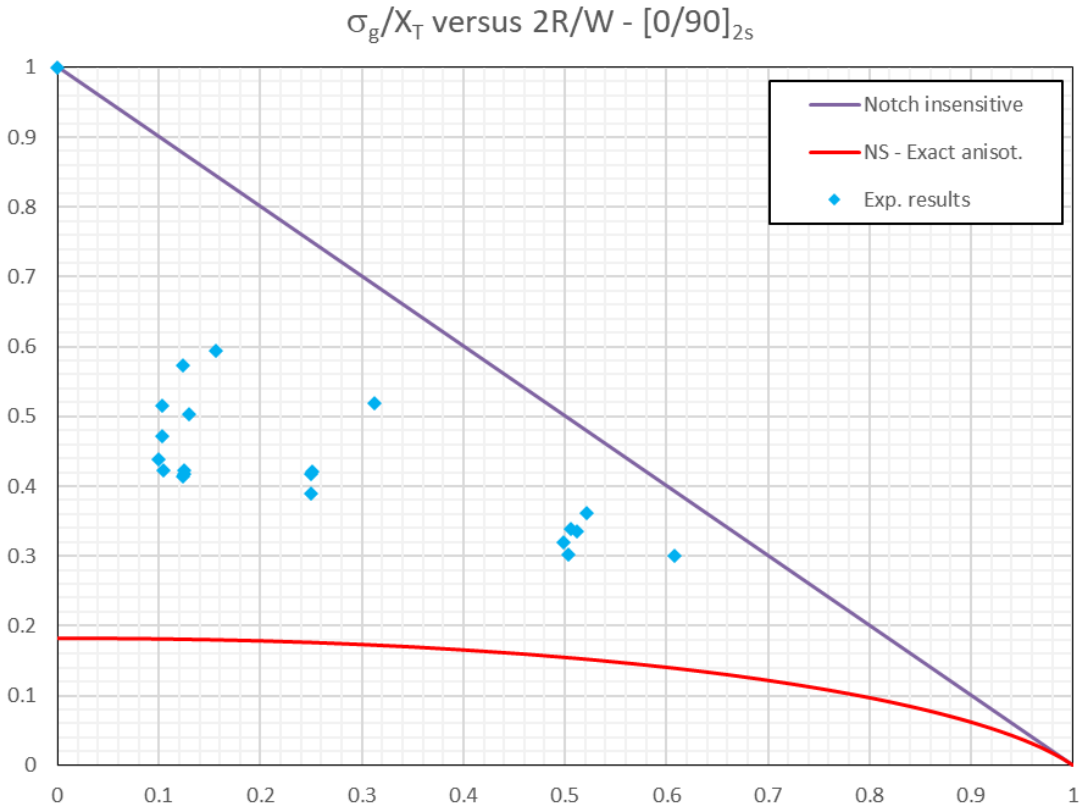

Figure 3-3

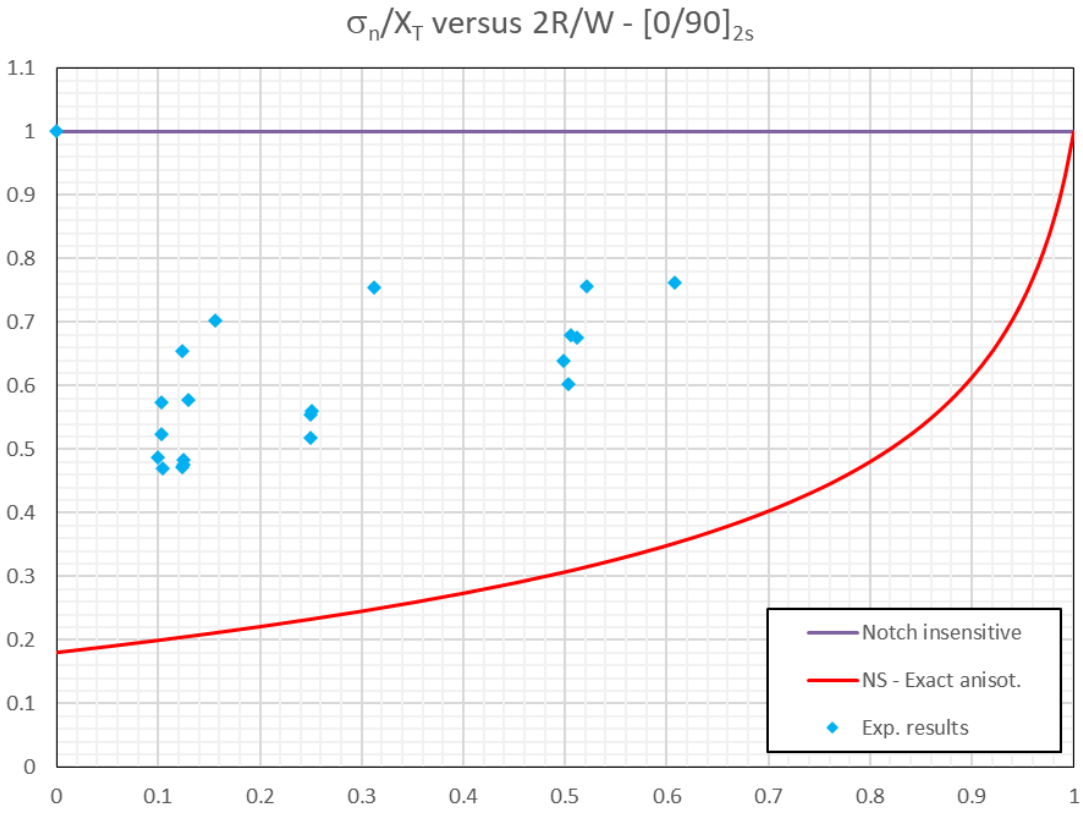

Figure 3-4

3.2 Size effect

The size effect in the tensile testing of notched laminates is the decrease in the ultimate strength with bigger hole radii, for a given width-to-diameter ratio. It was already observed by Waddoups [49] and by Whitney and Nuismer [50] when they introduced their PS and AS criteria.

From the results of the experimental campaign of this thesis, the size effect can be observed for the $[0/90]_{2s}$ configurations, but not so much for the others; it is somewhat observable for the $W/2R = 8$ values in the $[0]_6$ laminate. This can be seen in the graphs for the ultimate gross-sectional stress versus the hole radius that are presented in the following figures.

There also seems to be a change in the trend for the holes that are 8 mm in diameter. There's either a rise or a stabilization of the tensile strength, but not in all cases, such as the mentioned ratio for the $[0]_6$ lay-up. In the more regular $[0/90]_{2s}$ case, this change in the size effect for the 8 mm diameters is more accentuated for lower values of the width-to-diameter ratio, or equivalently, for higher values of $2R/W$. This might be caused due to a change in the failure mechanism, but no macroscopic hint of this effect could be observed from the tested specimens. It will be discussed further when the fit curves' results are presented.

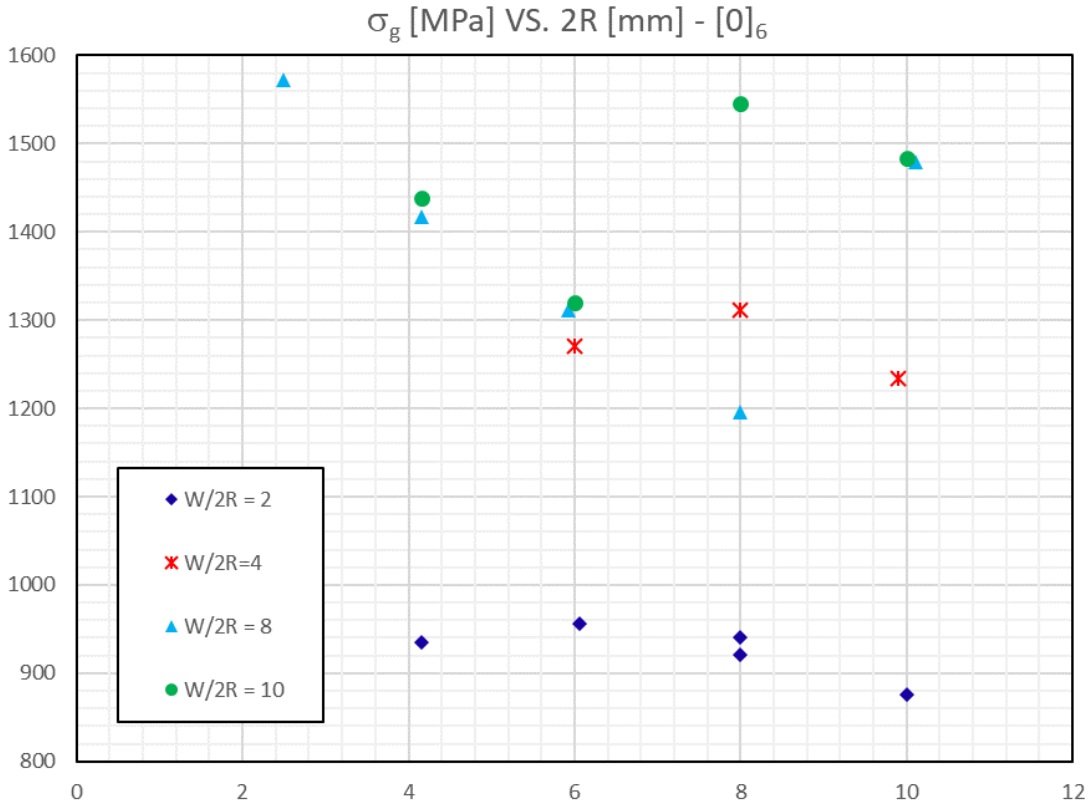

Figure 3-5

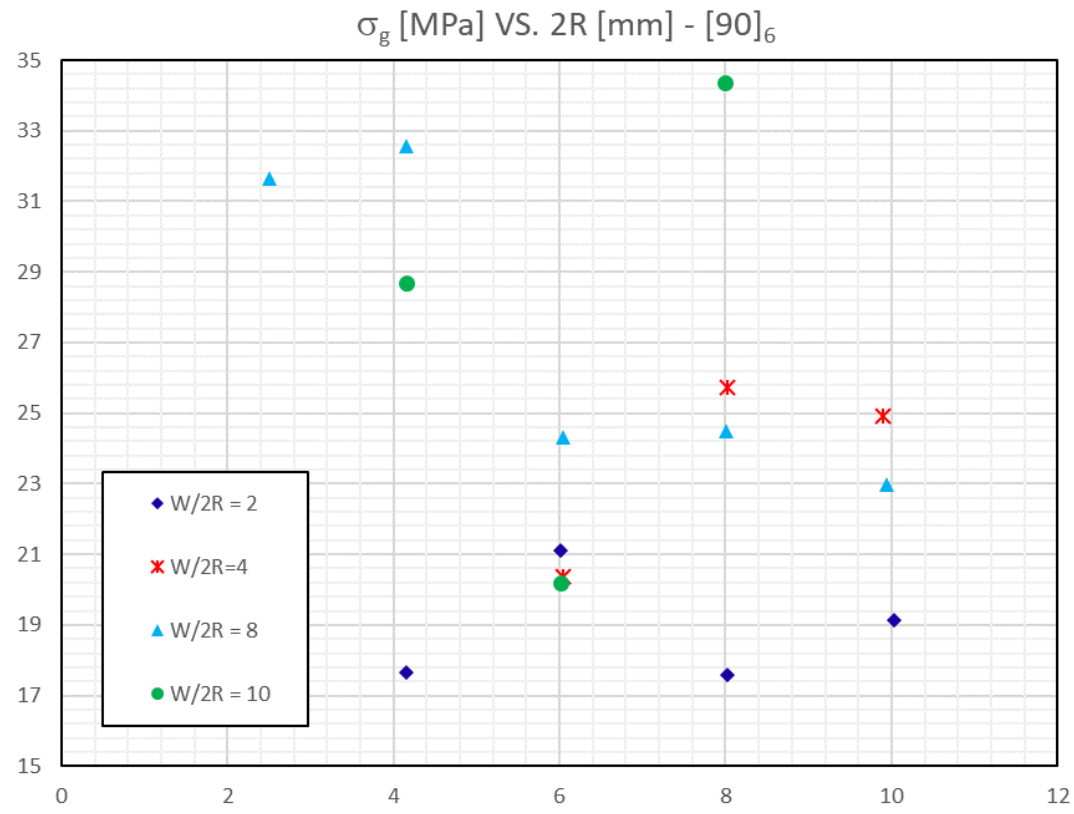

Figure 3-6

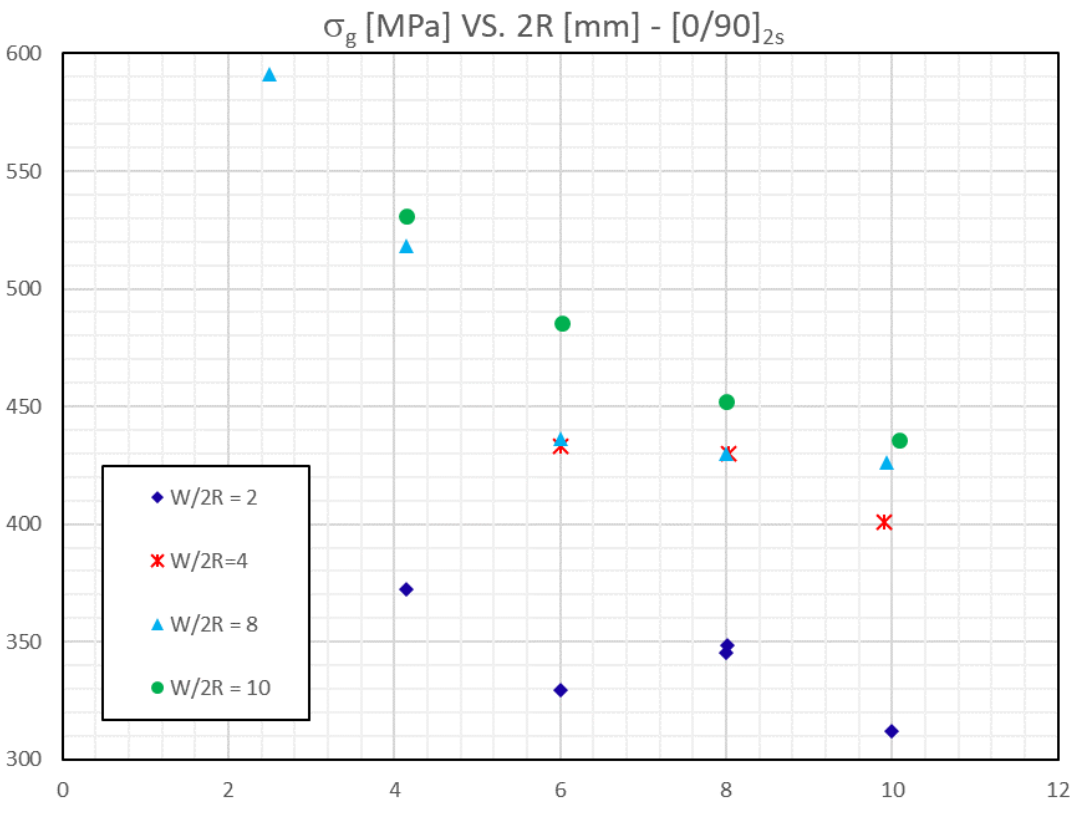

Figure 3-7

3.3 Notch-sensitivity percentage

As stated when the equations were developed, the notch-sensitive and notch-insensitive curves constitute a lower and an upper bound, respectively, for the stress at failure. The proximity to either of these curves indicates which failure mechanism controls the fracture. Thus, to quantify this dominance, a "notch sensitivity percentage" can be defined as a simple level-rule to for each value of the diameter-to-width ratio:

$$NI\% = \frac{\bar{\sigma}_{NI} - \bar{\sigma}_{exp.}}{\bar{\sigma}_{NI} - \bar{\sigma}_{NS}} \times 100\,, \qquad NS\% = \frac{\bar{\sigma}_{exp.} - \bar{\sigma}_{NS}}{\bar{\sigma}_{NI} - \bar{\sigma}_{NS}} \times 100\,. \tag{3.1}$$

The experimental results of this thesis' campaign are compared to these notch-sensitivity predictions in tables 3-2 to 3-4, one for each different lay-up configuration. It also compares the differences when using the approximate orthotropic (A.O.), (2.34), and the exact anisotropic (E.A.), (2.36), notch-sensitive equations. Table 3-1 gathers the minimum specified mechanical properties of these laminates; the material is made from a Hexcel AS4/8552 unidirectional prepeg roll.

Initially, every diameter-to-width ratio was designed to consider five values of $2R$; however, during the manufacturing process, some of these ratios were not achieved exactly due to limitiations in the minimum drilling diameter available and some cutting errors. Since the notch sensitivity percentage would be affected by a change in the value of the ratio, the real, exact one was kept instead of using the originally designed value.

2R/W	$\bar{\sigma}_g\big\vert_{NI}$ [MPa]	$\bar{\sigma}_g\big\vert_{NS}^{AO}$ [MPa]	$\bar{\sigma}_g\big\vert_{NS}^{EA}$ [MPa]	2R [mm]	W [mm]	$\bar{\sigma}_g^{exp}$ [MPa]	NI% (A.O.)	NI % (E.A.)	NS% (A.O.)	NS % (E.A.)
0.00	1919.62	710.44	710.44	0.00	14.96	1919.62	100.00	100.00	0.00	0.00
0.10	1727.66	706.86	706.67	4.15	40.09	1438.67	71.69	71.70	28.31	28.30
				6.00	60.12	1320.18	60.08	60.09	39.92	39.91
				8.00	80.18	1545.71	82.18	82.18	17.82	17.82
				9.99	100.01	1483.98	76.13	76.13	23.87	23.87
0.12	1689.27	705.25	704.88	2.50	20.08	1572.38	88.12	88.13	11.88	11.87
				5.92	48.27	1311.28	61.59	61.60	38.41	38.40
				8.00	64.13	1195.88	49.86	49.88	50.14	50.12
				9.98	80.44	1479.62	78.69	78.70	21.31	21.30
0.13	1670.07	704.34	703.84	4.15	33.06	1417.73	73.87	73.88	26.13	26.12
0.16	1612.48	701.12	700.10	2.50	16.00	1643.83	100*	100*	0*	0*
0.25	1439.72	686.83	682.65	6.00	24.01	1270.91	77.58	77.70	22.42	22.30
				7.99	32.20	1311.65	82.99	83.08	17.01	16.92
				9.90	40.16	1233.85	72.66	72.81	27.34	27.19
0.31	1324.54	672.94	665.34	2.50	8.00	1368.46	100*	100*	0*	0*
0.50	959.81	598.20	576.59	6.03	12.03	956.07	98.97	99.02	1.03	0.98
				8.00	16.06	941.13	94.83	95.13	5.17	4.87
				8.00	15.94	921.40	89.38	89.98	10.62	10.02
				9.97	20.07	875.80	76.77	78.08	23.23	21.92
0.52	921.42	586.89	563.98	4.15	8.04	935.32	100*	100*	0*	0*
0.62	729.46	517.71	490.49	2.50	4.04	560.69	20.30	29.38	79.70	70.62

Table 3-2

2R/W	$\bar{\sigma}_g\|_{NI}$ [MPa]	$\bar{\sigma}_g\|_{NS}^{AO}$ [MPa]	$\bar{\sigma}_g\|_{NS}^{EA}$ [MPa]	2R [mm]	W [mm]	$\bar{\sigma}_g^{exp}$ [MPa]	NI% (A.O.)	NI % (E.A.)	NS% (A.O.)	NS % (E.A.)
0.00	64.22	9.50	9.50	0.00	19.10	64.22	100.00	100.00	0.00	0.00
0.10	57.80	9.45	9.45	4.15	40.00	28.68	39.77	39.77	60.23	60.23
				6.01	60.12	20.18	22.19	22.19	77.81	77.81
				8.00	80.07	34.36	51.52	51.52	48.48	48.48
0.12	56.51	9.43	9.43	2.50	20.06	31.66	47.22	47.22	52.78	52.78
				8.02	64.17	24.48	31.97	31.97	68.03	68.03
				9.93	80.07	22.97	28.76	28.76	71.24	71.24
0.13	55.87	9.41	9.41	4.15	32.23	32.56	49.83	49.83	50.17	50.17
				6.03	48.21	16.22	14.66	14.66	85.34	85.34
0.16	53.94	9.37	9.37	2.50	15.98	25.59	36.39	36.39	63.61	63.61
0.25	48.17	9.18	9.19	6.03	24.06	20.37	28.70	28.68	71.30	71.32
				8.01	32.10	25.73	42.45	42.43	57.55	57.57
				9.90	40.18	24.91	40.34	40.33	59.66	59.67
0.31	44.31	9.01	9.02	2.50	7.99	27.23	51.61	51.60	48.39	48.40
0.50	32.11	8.22	8.17	6.01	12.00	14.07	24.49	24.64	75.51	75.36
				8.01	16.04	17.60	39.26	39.39	60.74	60.61
0.52	30.83	8.12	8.05	4.15	7.93	17.66	42.01	42.19	57.99	57.81
				8.00	15.32	17.61	41.79	41.97	58.21	58.03
				10.02	19.47	19.12	48.44	48.60	51.56	51.40

Table 3-3

2R/W	$\bar{\sigma}_g\|_{NI}$ [MPa]	$\bar{\sigma}_g\|_{NS}^{AO}$ [MPa]	$\bar{\sigma}_g\|_{NS}^{EA}$ [MPa]	2R [mm]	W [mm]	$\bar{\sigma}_g^{exp}$ [MPa]	NI% (A.O.)	NI % (E.A.)	NS% (A.O.)	NS % (E.A.)
0.00	1030.79	187.11	187.11	0.00	15.04	1030.79	100.00	100.00	0.00	0.00
0.10	927.71	186.17	186.16	4.15	40.14	530.80	46.47	46.48	53.53	53.52
				6.01	59.40	485.47	40.36	40.36	59.64	59.64
				8.01	80.20	451.97	35.84	35.85	64.16	64.15
				9.98	99.19	435.84	33.67	33.67	66.33	66.33
0.12	907.10	185.74	185.73	2.50	20.15	591.47	56.25	56.25	43.75	43.75
				6.01	48.20	436.24	34.73	34.73	65.27	65.27
				8.00	64.10	429.89	33.85	33.85	66.15	66.15
				9.91	80.16	426.52	33.38	33.38	66.62	66.62
0.13	896.79	185.50	185.49	4.15	32.06	518.39	46.80	46.80	53.20	53.20
0.16	865.86	184.66	184.63	2.50	16.01	612.12	62.75	62.75	37.25	37.25
0.25	773.09	180.95	180.82	6.01	24.01	433.14	42.59	42.60	57.41	57.40
				8.01	32.13	430.00	42.06	42.07	57.94	57.93
				9.90	39.84	401.13	37.18	37.20	62.82	62.80
0.31	711.25	177.44	177.18	2.50	7.98	534.57	66.90	66.92	33.10	33.08
0.50	515.40	160.62	158.85	6.00	12.00	329.36	47.56	47.82	52.44	52.18
				8.00	15.85	345.21	52.03	52.27	47.97	47.73
				8.01	15.93	348.44	52.94	53.17	47.06	46.83
				9.97	19.99	311.82	42.62	42.90	57.38	57.10
0.52	494.78	158.36	156.22	4.15	7.98	390.44	68.99	69.18	31.01	30.82
0.60	412.32	148.31	144.17	2.50	4.13	310.03	61.26	61.85	38.74	38.15

Table 3-4

In the case of the $[0]_6$ laminate, some of the results are slightly above the predicted value, so they have been adjusted to a 100% value of the NI percentage; this is indicated by an asterisk. It can also be observed that for this laminate, these NI percentages are above 60% in general, except some outlying cases. This seems to point to a notch-insensitive dominated failure.

For the $[90]_6$ lay-up, the NI percentages range from about 20% to almost 50%, which indicates a higher relative notch sensitivity tan the $[0]_6$ laminate. This might be due to the stress distribution along the net section having a smoother, more homogenous path along which to regularize the same way that the notch-sensitive curve does, whereas for the fibers at 0º, this path is "blocked" by the perpendicular fibers and keeps relatively constant along this section.

The $[0/90]_{2s}$ configuration shows a mixture of these two effects: its NI percentage varies from around 34% to 67%, somewhere in between the two previous laminates, but seemingly closer to the one with the fibers perpendicular to the loading direction. Probably, the laminae at 0º contribute to the notch insensitivity and the laminae at 90º to the notch sensitivity, and since the mid-plane contains two 90º plies together, its effect might be amplified along this path.

With respect to the differences between Tan's approximate orthotropic and Lekhnitskii's exact anisotropic stress distributions, it is seen that the first one provides a slightly higher prediction for the notch-sensitive curves than the latter, particularly for $2R/W$ values higher tan 0.5. Since the NS curve acts as a lower limit for failure, it seems more appropriate to use it in this context, but more experiments in the upper range of the diameter-to-width ratio should be performed to make sure that it does not overestimate the real failure stress values.

3.4 Fit curves' results

Using the equation for experimentally-fitted curves (2.58) with the exact anisotropic FWC factor, along with the test data, it can be checked that the experimental curves of constant diameter in the stress-versus-ratio graphs do have a shape similar to the proposed transformation from the notch-insensitive to the notch-sensitive curve from lower to higher diameters. In fact, the obtained exponents that better fit the results do actually show not only the size effect for the whole range of diameter-to-width ratios for a given lay-up, but also the notch-sensitivity effect for different laminates that was pointed out in the notch-sensitivity percentage section.

These exponents for both the adimensional gross- and net-sectional stresses are shown for the three lay-up configurations in tables 3-5(a) to 3-5(c); it also gathers the sums of the squared differences of the adimensional stresses that have been used as a minimization objective. However, and for clarity, only the fit curves for the $[0/90]_{2s}$ laminate will be plotted here, since it is the one that shows better the size effect, as stated in section 3.2.

In the next figures, 3-10 and 3-11, the fit curves are graphed along the experimental data for the $[0/90]_{2s}$ laminates to show their good agreement with both the gross-section and the net-section stresses; the second graph's fit demonstrates the suitability of the net-sectional FWCF chosen. As was indicated in the size effect section, the stresses stop decreasing for a diameter of 8 mm, so it can be noted that this curve is very similar to that of a constant diameter of 6 mm. In tables 3-5(a) to 3-5(c) it can be seen that the error of this curve is higher than those for the rest, so it is possible that this dissipation of the size-effect for this diameter is just a statistical deviation of the data.

2R [mm]	m_g^0	$\sum_{[0]_6} \chi_g^2$	m_n^0	$\sum_{[0]_6} \chi_n^2$
2.5	0.03579169	0.01070725	0.07285488	0.05476343
4.15	0.2196452	0.00220993	0.19329662	0.00843575
6	0.28261751	0.00652525	0.25045253	0.01761741
8	0.22050297	0.01916722	0.19441682	0.03028151
10	0.18164223	0.0007138	0.18765194	0.00109278

Table 3-5(a)

2R [mm]	m_g^{90}	$\sum_{[90]_6} \chi_g^2$	m_n^{90}	$\sum_{[90]_6} \chi_n^2$
2.5	0.46726015	0.00484874	0.4614608	0.00742305
4.15	0.4143408	0.00320167	0.42482628	0.00510633
6	0.55739528	0.00890597	0.52105424	0.02499905
8	0.41034333	0.01146611	0.42456321	0.01614049
10	0.47567346	0.0028868	0.44814031	0.00716445

2R [mm]	$m_g^{0/90}$	$\sum_{[0/90]_{2s}} \chi_g^2$	$m_n^{0/90}$	$\sum_{[0/90]_{2s}} \chi_n^2$
2.5	0.31526861	0.05476343	0.3138569	0.00278947
4.15	0.39657804	0.00843575	0.37505637	0.00551
6	0.46699333	0.01761741	0.45999501	0.00217106
8	0.46125251	0.03028151	0.43679122	0.00972718
10	0.49363851	0.00109278	0.48963348	0.00063837

Tables 3-5(b) and (c)

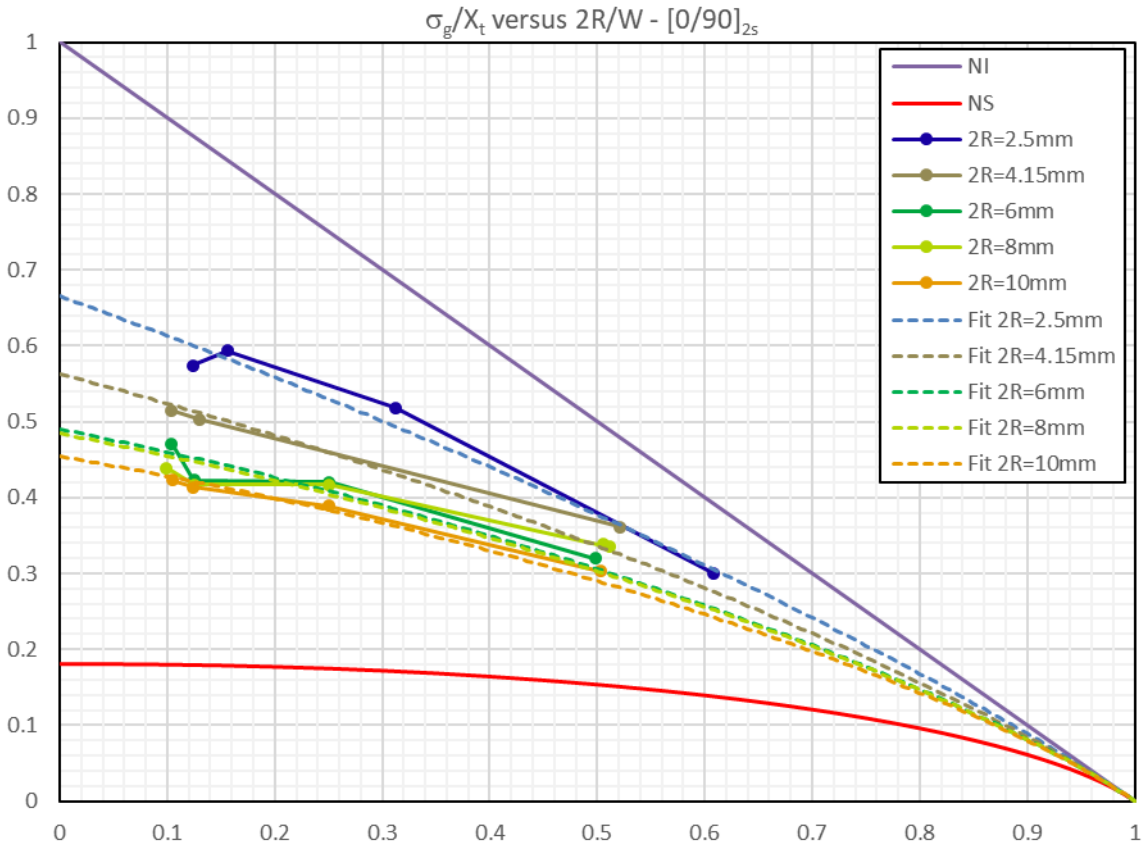

Figure 3-8

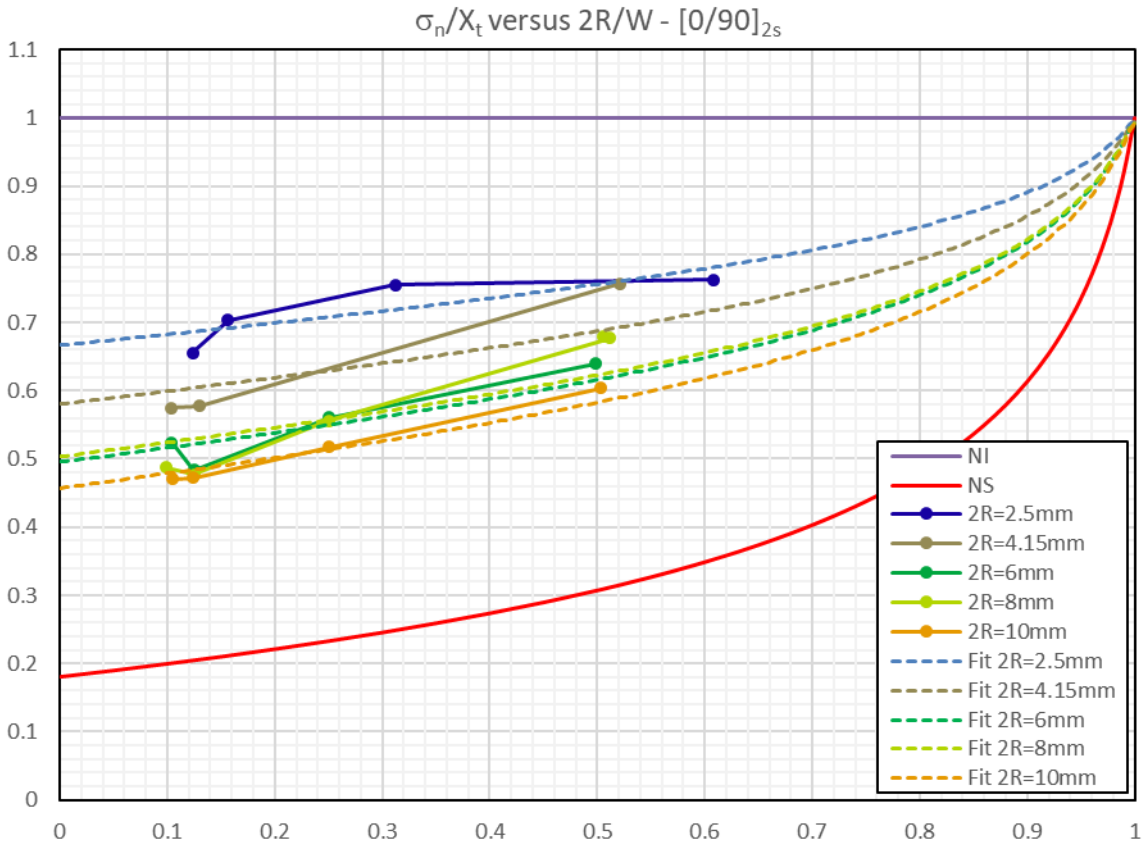

Figure 3-9

3.5 Point Stress and Average Stress criteria results

The two criteria developed by Whitney and Nuismer using both the corrected-through-M approximate orthotropic (AOM), as used by Camanho, and the exact anisotropic (EA) stress distribution are compared to the experimental results of the campaign.

These models make use of the characteristic distances, d_0 and a_0, which have to be obtained from a previous test in another notched specimen. Since they have been proved to depend bot on the laminate properties and the geometry [61], but with a stronger dependency on the diameter-to-width ratio than on the radius of the hole, the characteristic distance obtained from one test will only be used for those other specimens with the same ratio. In order to see the variation in choosing a different radius value to estimate the failure stresses of the rest of the specimens, several double-entry tables are presented for each lay-up and $2R/W$. These are tables 3-6 to 3-29.

For each laminate and ratio, the four or five test specimens with varying radii are listed in the rows[7], indicating their experimental gross-section stress at failure $\bar{\sigma}_g^{exp}$. In the columns, these same specimens are the ones used for the estimation of the characteristic distances of the rest, so the diagonals contain the corresponding distance adimensionalized by the radius of the reference specimen, $\hat{d}_0$ and $\hat{a}_0$. They are then used in the calculations of the rest of the column. For clarity, only the errors relative to the experimental stresses are listed. Also, each prediction is presented in each cell of the table using one the two models described above (AOM or EA).

[7] Some of the specimens that resulted in a different ratio than originally designed have been included along the others with their initial ratio. These have been marked with an asterisk in both the row and the column.

The first thing that can be noted from these error tables is that the PSC (for the three types of laminates) overestimates the experimental results of those specimens with a smaller diameter than that of the specimen used for calibration, and underestimates it for the ones with a bigger diameter than the calibrating one: this is noticeable in the signs of the errors on one side and the other of the diagonal. For the majority of the predictions, unacceptably high errors are reached, but with that in mind, some cases do provide good estimations that require some comments.

Another interesting conclusion that can be drawn from these tables is that, in most cases, the exact anisotropic model provides a smaller relative error than Tan's corrected, approximate orthotropic one. There are some exceptions, and the higher number of them can be found in the ASC for the $[0]_6$ laminates, specially for the highest diameter-to-width ratio of 0.5. However, except for this last case, the EA model provides a higher error than the AOM one mostly for those that are greater than 5%; when the precision of the AOM model is below that value, the EA approach results in a smaller relative error.

PSC for the $[0]_6$ laminates

The point stress criterion for the laminates with fibers parallel to the loading direction show, in most of the cases, an increase in the precision for higher values of $2R/W$. However, when the calibration diameter is small (or has a different real value of the ratio, as denoted by the asterisk), the predictions are generally too inaccurate.

The predictions for the ratio of 0.125 are very good using the exact anisotropic model if the specimens with the higher diameter are not considered. In the other cases, the maximum error for a given calibration specimen is in between 10% and 15% in general.

PSC for $[0]_6$ - 2R/W = 0.1			Errors [%] using the specimen with 2R=			
2R [mm]	$\overline{\sigma}_g^{exp}$ [MPa]	Model	4.15	6.00	8.00	9.99
4.15	1438.67	AOM	$\hat{d}_0 = 0.78$	3.62	22.05	23.23
		EA	$\hat{d}_0 = 0.77$	1.37	21.07	21.90
6.00	1320.18	AOM	-4.05	$\hat{d}_0 = 0.61$	25.37	27.34
		EA	-1.48	$\hat{d}_0 = 0.56$	24.36	25.57
8.00	1545.71	AOM	-26.21	-23.08	$\hat{d}_0 = 0.99$	2.14
		EA	-22.49	-21.32	$\hat{d}_0 = 1.03$	1.19
9.99	1483.98	AOM	-28.88	-26.03	-2.47	$\hat{d}_0 = 0.86$
		EA	-24.16	-23.05	-1.31	$\hat{d}_0 = 0.87$

Table 3-6

PSC for $[0]_6$ - 2R/W = 0.125			Errors [%] using the specimen with 2R=				
2R [mm]	$\bar{\sigma}_g^{exp}$ [MPa]	Model	2.50	4.15*	5.92	8.00	9.98
2.50	1572.38	AOM	$\hat{d}_0 = 1.09$	3.59	6.22	7.17	16.69
		EA	$\hat{d}_0 = 1.13$	1.74	3.18	2.77	16.67
4.15*	1417.73	AOM	-5.00	$\hat{d}_0 = 0.76$	4.04	5.59	24.47
		EA	-2.17	$\hat{d}_0 = 0.74$	1.86	1.31	23.34
5.92	1311.28	AOM	-9.60	-4.44	$\hat{d}_0 = 0.60$	1.77	28.01
		EA	-4.23	-1.97	$\hat{d}_0 = 0.55$	-0.58	26.35
8.00	1195.88	AOM	-11.01	-6.16	-1.80	$\hat{d}_0 = 0.47$	31.50
		EA	-3.65	-1.40	0.59	$\hat{d}_0 = 0.40$	30.35
9.98	1479.62	AOM	-33.06	-29.73	-26.66	-25.37	$\hat{d}_0 = 0.87$
		EA	-26.73	-25.08	-23.62	-24.05	$\hat{d}_0 = 0.87$

Table 3-7

PSC for $[0]_6$ - 2R/W = 0.25			Errors [%] using the specimen with 2R=			
2R [mm]	$\bar{\sigma}_g^{exp}$ [MPa]	Model	2.50*	6.00	7.99	9.90
2.50*	1368.46	AOM	$\hat{d}_0 = 0.95$	11.71	17.27	17.67
		EA	$\hat{d}_0 = 0.80$	12.16	19.71	19.63
6.00	1270.91	AOM	-16.45	$\hat{d}_0 = 0.65$	12.72	13.86
		EA	-13.36	$\hat{d}_0 = 0.55$	11.35	11.22
7.99	1311.65	AOM	-26.52	-12.52	$\hat{d}_0 = 0.71$	1.22
		EA	-22.27	-10.65	$\hat{d}_0 = 0.62$	-0.12
9.90	1233.85	AOM	-26.76	-13.89	-1.30	$\hat{d}_0 = 0.60$
		EA	-21.66	-10.56	0.12	$\hat{d}_0 = 0.50$

Table 3-8

PSC for $[0]_6$ - 2R/W = 0.50			Errors [%] using the specimen with 2R=				
2R [mm]	$\bar{\sigma}_g^{exp}$ [MPa]	Model	4.15*	6.03	8.00	8.00	9.97
4.15*	935.32	AOM	$\hat{d}_0 = 0.66$	12.15	18.73	17.59	19.14
		EA	$\hat{d}_0 = 0.36$	11.87	18.78	16.79	17.22
6.03	956.07	AOM	-12.23	$\hat{d}_0 = 0.65$	7.70	6.30	8.21
		EA	-10.19	$\hat{d}_0 = 0.37$	6.33	4.47	4.88
8.00	941.13	AOM	-18.95	-7.77	$\hat{d}_0 = 0.62$	-1.46	0.54
		EA	-14.66	-5.75	$\hat{d}_0 = 0.35$	-1.70	-1.34
8.00	921.40	AOM	-17.75	-6.40	1.48	$\hat{d}_0 = 0.59$	2.03
		EA	-13.18	-4.11	1.73	$\hat{d}_0 = 0.33$	0.37
9.97	875.80	AOM	-18.77	-8.29	-0.56	-2.05	$\hat{d}_0 = 0.50$
		EA	-12.56	-4.22	1.29	-0.35	$\hat{d}_0 = 0.27$

Table 3-9

PSC for the $[90]_6$ laminates

These laminates are very poorly predicted using the point stress criterion with either of the stress models, so not many useful comments can be made about these cases. The only noticeable data is the reduced values of the adimensional characteristic distances compared to the other laminates, which seem to confirm that this distance is under the size effect as well.

PSC for $[90]_6$ - 2R/W = 0.1			Errors [%] using spec. with 2R=		
2R [mm]	$\bar{\sigma}_g^{exp}$ [MPa]	Model	4.15	6.01	8.00
4.15	28.68	AOM	$\hat{d}_0 = 0.17$	-8.77	75.17
		EA	$\hat{d}_0 = 0.15$	-18.17	53.36
6.01	20.18	AOM	8.28	$\hat{d}_0 = 0.11$	108.15
		EA	21.42	$\hat{d}_0 = 0.06$	90.78
8.00	34.36	AOM	-46.91	-50.32	$\hat{d}_0 = 0.22$
		EA	-36.70	-47.38	$\hat{d}_0 = 0.23$

Table 3-10

PSC for $[90]_6$ - 2R/W = 0.125			Errors [%] using the specimen with 2R=				
2R [mm]	$\bar{\sigma}_g^{exp}$ [MPa]	Model	2.50	4.15*	6.03	8.02	9.93
2.50	31.66	AOM	$\hat{d}_0 = 0.20$	44.43	-8.71	61.50	66.39
		EA	$\hat{d}_0 = 0.19$	25.87	-28.28	25.22	28.12
4.15*	32.56	AOM	-33.48	$\hat{d}_0 = 0.21$	-38.46	23.02	33.05
		EA	-21.67	$\hat{d}_0 = 0.20$	-43.06	-0.58	2.01
6.03	16.22	AOM	6.29	50.97	$\hat{d}_0 = 0.07$	87.60	106.63
		EA	34.51	71.43	$\hat{d}_0 = 0.04$	70.42	74.97
8.02	24.48	AOM	-38.71	-17.88	-41.63	$\hat{d}_0 = 0.14$	9.87
		EA	-20.50	0.59	-39.55	$\hat{d}_0 = 0.10$	2.65
9.93	22.97	AOM	-40.00	-23.01	-42.39	-8.29	$\hat{d}_0 = 0.13$
		EA	-21.87	-1.97	-39.43	-2.53	$\hat{d}_0 = 0.09$

Table 3-11

PSC for $[90]_6$ - 2R/W = 0.25			Errors [%] using the specimen with 2R=			
2R [mm]	$\overline{\sigma}_g^{exp}$ [MPa]	Model	2.50*	6.03	8.01	9.90
2.50*	27.23	AOM	$\hat{d}_0 = 0.18$	37.76	76.88	81.43
		EA	$\hat{d}_0 = 0.15$	6.27	48.32	55.26
6.03	20.37	AOM	-22.94	$\hat{d}_0 = 0.12$	57.15	77.69
		EA	-5.53	$\hat{d}_0 = 0.07$	42.54	50.85
8.01	25.73	AOM	-46.42	-33.68	$\hat{d}_0 = 0.16$	13.78
		EA	-32.83	-29.16	$\hat{d}_0 = 0.12$	5.88
9.90	24.91	AOM	-48.79	-38.67	-11.59	$\hat{d}_0 = 0.16$
		EA	-35.59	-32.28	-5.52	$\hat{d}_0 = 0.11$

Table 3-12

PSC for $[90]_6$ - 2R/W = 0.50			Errors [%] using the specimen with 2R=			
2R [mm]	$\overline{\sigma}_g^{exp}$ [MPa]	Model	4.15*	6.01	8.01	10.02
4.15*	17.66	AOM	$\hat{d}_0 = 0.13$	-1.22	60.31	101.48
		EA	$\hat{d}_0 = 0.07$	-10.52	28.70	56.17
6.01	14.07	AOM	0.99	$\hat{d}_0 = 0.09$	54.25	102.83
		EA	10.63	$\hat{d}_0 = 0.04$	40.48	70.40
8.01	17.60	AOM	-30.17	-30.72	$\hat{d}_0 = 0.12$	30.25
		EA	-20.04	-27.03	$\hat{d}_0 = 0.07$	20.66
10.02	19.12	AOM	-42.14	-42.52	-21.39	$\hat{d}_0 = 0.14$
		EA	-32.34	-37.75	-16.57	$\hat{d}_0 = 0.08$

Table 3-13

PSC for the $[0/90]_{2s}$ laminates

It can be seen that the errors for this laminate are lower than those for the $[0]_6$ one. Using calibration specimens with a diameter in the intermediate range provides similar maximum error values in between 10% and 15% for a given calibration and the EA model. This is a considerable improvement of the approximate stress model, which returns maximum errors of around 30% in some cases.

PSC for $[0/90]_{2s}$ - 2R/W = 0.1			Errors [%] using the specimen with 2R=			
2R [mm]	$\bar{\sigma}_g^{exp}$ [MPa]	Model	4.15	6.01	8.01	9.98
4.15	530.80	AOM	$\hat{d}_0 = 0.22$	13.64	23.97	33.04
		EA	$\hat{d}_0 = 0.21$	5.31	9.36	14.48
6.01	485.47	AOM	-12.54	$\hat{d}_0 = 0.19$	10.76	21.50
		EA	-5.14	$\hat{d}_0 = 0.17$	3.97	9.08
8.01	451.97	AOM	-20.09	-9.56	$\hat{d}_0 = 0.17$	10.20
		EA	-8.69	-3.81	$\hat{d}_0 = 0.14$	4.95
9.98	435.84	AOM	-25.78	-17.05	-8.93	$\hat{d}_0 = 0.16$
		EA	-12.77	-8.23	-4.66	$\hat{d}_0 = 0.12$

Table 3-14

PSC for $[0/90]_{2s}$ - 2R/W = 0.125			Errors [%] using the specimen with 2R=				
2R [mm]	$\bar{\sigma}_g^{exp}$ [MPa]	Model	2.50	4.15*	6.01	8.00	9.91
2.50	591.47	AOM	$\hat{d}_0 = 0.26$	15.21	19.31	30.27	36.69
		EA	$\hat{d}_0 = 0.28$	5.81	2.84	12.12	19.41
4.15*	518.39	AOM	-15.76	$\hat{d}_0 = 0.21$	5.11	21.53	33.44
		EA	-5.86	$\hat{d}_0 = 0.20$	-3.02	6.57	14.48
6.01	436.24	AOM	-18.74	-4.84	$\hat{d}_0 = 0.16$	17.19	31.89
		EA	-2.90	3.12	$\hat{d}_0 = 0.13$	10.00	18.47
8.00	429.89	AOM	-28.21	-17.68	-13.92	$\hat{d}_0 = 0.15$	12.89
		EA	-11.48	-6.15	-8.92	$\hat{d}_0 = 0.12$	7.69
9.91	426.52	AOM	-33.72	-25.33	-22.31	-10.92	$\hat{d}_0 = 0.15$
		EA	-17.39	-12.60	-15.10	-7.03	$\hat{d}_0 = 0.12$

Table 3-15

PSC for $[0/90]_{2s}$ - 2R/W = 0.25			Errors [%] using the specimen with 2R=			
2R [mm]	$\bar{\sigma}_g^{exp}$ [MPa]	Model	2.50*	6.01	8.01	9.90
2.50*	534.57	AOM	$\hat{d}_0 = 0.26$	23.57	34.10	37.02
		EA	$\hat{d}_0 = 0.24$	10.42	21.04	22.18
6.01	433.14	AOM	-22.89	$\hat{d}_0 = 0.17$	18.05	24.79
		EA	-9.78	$\hat{d}_0 = 0.13$	10.85	12.09
8.01	430.00	AOM	-32.32	-14.89	$\hat{d}_0 = 0.17$	5.96
		EA	-18.19	-9.65	$\hat{d}_0 = 0.13$	1.11
9.90	401.13	AOM	-33.43	-18.55	-5.42	$\hat{d}_0 = 0.15$
		EA	-18.54	-10.40	-1.08	$\hat{d}_0 = 0.11$

Table 3-16

PSC for $[0/90]_{2s}$ - 2R/W = 0.50			Errors [%] using the specimen with 2R=				
2R [mm]	$\bar{\sigma}_g^{exp}$ [MPa]	Model	4.15*	6.00	8.00	8.01	9.97
4.15*	390.44	AOM	$\hat{d}_0 = 0.21$	3.17	26.61	27.41	28.90
		EA	$\hat{d}_0 = 0.15$	-4.65	12.24	13.18	9.30
6.00	329.36	AOM	-3.03	$\hat{d}_0 = 0.15$	25.38	26.38	28.25
		EA	4.72	$\hat{d}_0 = 0.09$	17.40	18.40	14.33
8.00	345.21	AOM	-21.57	-19.38	$\hat{d}_0 = 0.17$	0.81	2.34
		EA	-10.46	-14.30	$\hat{d}_0 = 0.10$	0.83	-2.56
8.01	348.44	AOM	-22.19	-20.02	-0.80	$\hat{d}_0 = 0.17$	1.52
		EA	-11.19	-15.00	-0.82	$\hat{d}_0 = 0.11$	-3.35
9.97	311.82	AOM	-21.58	-19.64	-2.17	-1.42	$\hat{d}_0 = 0.14$
		EA	-7.78	-11.53	2.53	3.35	$\hat{d}_0 = 0.08$

Table 3-17

ASC for the $[0]_6$ laminates

It is worth noting the big differences between the adimensional characteristic distances that each of the models provide for the ASC applied to the $[0]_6$ laminates; this difference is not seen in the other lay-up configurations. Some of the error values are strikingly low in certain cases, such as the ones for $2R/W = 0.125$ without considering the specimens with the 10-mm diameter: for the EA model, the errors are lower than around 1%. This is similar to the accuracy of the PSC for this same value of the ratio, but wheter these results are an indication of something characteristic of these criteria or a statistical exception is not clear and would require a more specific analysis.

ASC for $[0]_6$ - 2R/W = 0.1			Errors [%] using the specimen with 2R=			
2R [mm]	$\bar{\sigma}_g^{exp}$ [MPa]	Model	4.15	6.00	8.00	9.99
4.15	1438.67	AOM	$\hat{a}_0 = 2.68$	-0.30	17.26	17.20
		EA	$\hat{a}_0 = 5.23$	0.01	17.61	17.63
6.00	1320.18	AOM	0.36	$\hat{a}_0 = 1.82$	22.33	22.24
		EA	-0.01	$\hat{a}_0 = 3.62$	22.49	22.51
8.00	1545.71	AOM	-20.32	-20.62	$\hat{a}_0 = 3.91$	-0.09
		EA	-20.95	-20.94	$\hat{a}_0 = 7.56$	0.03
9.99	1483.98	AOM	-21.79	-22.10	0.10	$\hat{a}_0 = 3.11$
		EA	-22.81	-22.80	-0.03	$\hat{a}_0 = 6.07$

Table 3-18

ASC for $[0]_6$ - 2R/W = 0.125			Errors [%] using the specimen with 2R=				
2R [mm]	$\bar{\sigma}_g^{exp}$ [MPa]	Model	2.50	4.15*	5.92	8.00	9.98
2.50	1572.38	AOM	$\hat{a}_0 = 4.52$	-0.94	-0.78	-1.65	11.54
		EA	$\hat{a}_0 = 8.55$	-0.63	-0.21	-0.79	12.22
4.15*	1417.73	AOM	1.28	$\hat{a}_0 = 2.56$	0.22	-0.95	18.45
		EA	0.86	$\hat{a}_0 = 4.95$	0.57	-0.22	19.02
5.92	1311.28	AOM	1.23	-0.26	$\hat{a}_0 = 1.82$	-1.35	22.86
		EA	0.34	-0.67	$\hat{a}_0 = 3.56$	-0.93	23.22
8.00	1195.88	AOM	2.83	1.20	1.48	$\hat{a}_0 = 1.27$	28.66
		EA	1.41	0.29	1.04	$\hat{a}_0 = 2.54$	28.87
9.98	1479.62	AOM	-21.63	-22.91	-22.69	-23.84	$\hat{a}_0 = 3.16$
		EA	-23.15	-24.05	-23.45	-24.28	$\hat{a}_0 = 6.07$

Table 3-19

ASC for $[0]_6$ - 2R/W = 0.25			Errors [%] using the specimen with 2R=			
2R [mm]	$\bar{\sigma}_g^{exp}$ [MPa]	Model	2.50*	6.00	7.99	9.90
2.50*	1368.46	AOM	$\hat{a}_0 = 3.65$	4.68	10.31	9.71
		EA	$\hat{a}_0 = 5.51$	8.42	14.73	14.36
6.00	1270.91	AOM	-6.84	$\hat{a}_0 = 2.03$	9.40	8.33
		EA	-11.49	$\hat{a}_0 = 3.57$	10.07	9.43
7.99	1311.65	AOM	-16.23	-9.62	$\hat{a}_0 = 2.31$	-1.13
		EA	-21.33	-10.26	$\hat{a}_0 = 4.04$	-0.66
9.90	1233.85	AOM	-15.90	-9.10	1.24	$\hat{a}_0 = 1.78$
		EA	-21.76	-10.32	0.73	$\hat{a}_0 = 3.17$

Table 3-20

ASC for $[0]_6$ - 2R/W = 0.50			Errors [%] using the specimen with 2R=				
2R [mm]	$\bar{\sigma}_g^{exp}$ [MPa]	Model	4.15*	6.03	8.00	8.00	9.97
4.15*	935.32	AOM	$\hat{a}_0 = 2.07$	7.92	11.90	10.70	10.44
		EA	$\hat{a}_0 = 2.31$	11.54	17.76	16.14	17.17
6.03	956.07	AOM	-8.44	$\hat{a}_0 = 2.03$	4.47	3.11	2.81
		EA	-11.26	$\hat{a}_0 = 2.36$	6.40	4.71	5.78
8.00	941.13	AOM	-13.29	-4.74	$\hat{a}_0 = 1.86$	-1.46	-1.78
		EA	-17.28	-6.41	$\hat{a}_0 = 2.21$	-1.70	-0.62
8.00	921.40	AOM	-12.01	-3.33	1.48	$\hat{a}_0 = 1.75$	-0.32
		EA	-15.84	-4.79	1.73	$\hat{a}_0 = 2.09$	1.10
9.97	875.80	AOM	-12.02	-3.16	1.92	0.34	$\hat{a}_0 = 1.39$
		EA	-16.95	-5.99	0.65	-1.13	$\hat{a}_0 = 1.74$

Table 3-21

ASC for the $[90]_6$ laminates

Again, most of the errors for this laminate are too high to consider the ASC as valid for this configuration.

ASC for $[90]_6$ - 2R/W = 0.1			Errors [%] using spec. with 2R=		
2R [mm]	$\bar{\sigma}_g^{exp}$ [MPa]	Model	4.15	6.01	8.00
4.15	28.68	AOM	$\hat{a}_0 = 0.55$	-15.33	48.34
		EA	$\hat{a}_0 = 0.67$	-19.93	46.26
6.01	20.18	AOM	18.74	$\hat{a}_0 = 0.27$	88.63
		EA	24.66	$\hat{a}_0 = 0.25$	86.58
8.00	34.36	AOM	-39.61	-48.75	$\hat{a}_0 = 0.84$
		EA	-33.86	-46.69	$\hat{a}_0 = 1.14$

Table 3-22

ASC for $[90]_6$ - 2R/W = 0.125			Errors [%] using the specimen with 2R=				
2R [mm]	$\bar{\sigma}_g^{exp}$ [MPa]	Model	2.50	4.15*	6.03	8.02	9.93
2.50	31.66	AOM	$\hat{a}_0 = 0.69$	23.57	-21.73	25.07	28.39
		EA	$\hat{a}_0 = 0.90$	21.15	-31.25	15.47	16.71
4.15*	32.56	AOM	-23.27	$\hat{a}_0 = 0.74$	-41.00	1.58	5.09
		EA	-18.63	$\hat{a}_0 = 0.98$	-43.84	-5.17	-4.04
6.03	16.22	AOM	27.78	70.27	$\hat{a}_0 = 0.17$	73.41	80.49
		EA	43.06	76.48	$\hat{a}_0 = 0.13$	67.05	69.09
8.02	24.48	AOM	-26.26	-1.92	-40.75	$\hat{a}_0 = 0.40$	4.40
		EA	-14.26	5.69	-39.18	$\hat{a}_0 = 0.43$	1.23
9.93	22.97	AOM	-28.56	-6.13	-41.24	-4.28	$\hat{a}_0 = 0.35$
		EA	-15.11	4.39	-38.96	-1.20	$\hat{a}_0 = 0.36$

Table 3-23

ASC for $[90]_6$ - 2R/W = 0.25			Errors [%] using the specimen with 2R=			
2R [mm]	$\overline{\sigma}_g^{exp}$ [MPa]	Model	2.50*	6.03	8.01	9.90
2.50*	27.23	AOM	$\hat{a}_0 = 0.61$	9.32	41.02	46.47
		EA	$\hat{a}_0 = 0.66$	0.20	36.87	41.71
6.03	20.37	AOM	-9.81	$\hat{a}_0 = 0.31$	43.77	52.55
		EA	-0.20	$\hat{a}_0 = 0.28$	39.62	45.51
8.01	25.73	AOM	-37.41	-31.11	$\hat{a}_0 = 0.49$	6.87
		EA	-28.30	-28.16	$\hat{a}_0 = 0.54$	4.30
9.90	24.91	AOM	-40.77	-35.34	-6.76	$\hat{a}_0 = 0.46$
		EA	-30.91	-30.78	-4.14	$\hat{a}_0 = 0.49$

Table 3-24

ASC for $[90]_6$ - 2R/W = 0.50			Errors [%] using the specimen with 2R=			
2R [mm]	$\overline{\sigma}_g^{exp}$ [MPa]	Model	4.15*	6.01	8.01	10.02
4.15*	17.66	AOM	$\hat{a}_0 = 0.34$	-6.41	34.48	58.67
		EA	$\hat{a}_0 = 0.27$	-11.75	23.45	46.93
6.01	14.07	AOM	6.35	$\hat{a}_0 = 0.21$	44.34	75.00
		EA	12.55	$\hat{a}_0 = 0.13$	38.16	64.65
8.01	17.60	AOM	-25.31	-29.29	$\hat{a}_0 = 0.32$	22.77
		EA	-17.94	-26.59	$\hat{a}_0 = 0.25$	18.95
10.02	19.12	AOM	-37.97	-40.90	-18.66	$\hat{a}_0 = 0.39$
		EA	-30.30	-37.26	-15.67	$\hat{a}_0 = 0.33$

Table 3-25

ASC for the $[0/90]_{2s}$ laminates

Similarly to the point stress criterion, the best predictions of the ASC using the exact anisotropic model are obtained for this laminate. However, these results are better that the ones for the PSC when considering the specimens with the highest diameter values. These maximum errors are still around 15%, but some of the predictions are considerably good enough to require a more detailed study with the EA model, which in contrast provides maximum errors of around 19%.

ASC for $[0/90]_{2s}$ - 2R/W = 0.1			Errors [%] using the specimen with 2R=			
2R [mm]	$\bar{\sigma}_g^{exp}$ [MPa]	Model	4.15	6.01	8.01	9.98
4.15	530.80	AOM	$\hat{a}_0 = 0.73$	5.03	9.09	13.95
		EA	$\hat{a}_0 = 0.73$	3.24	5.69	9.46
6.01	485.47	AOM	-5.35	$\hat{a}_0 = 0.57$	4.40	9.75
		EA	-3.25	$\hat{a}_0 = 0.56$	2.47	6.33
8.01	451.97	AOM	-9.82	-4.48	$\hat{a}_0 = 0.48$	5.56
		EA	-5.63	-2.44	$\hat{a}_0 = 0.45$	3.83
9.98	435.84	AOM	-14.80	-9.76	-5.44	$\hat{a}_0 = 0.44$
		EA	-9.07	-6.03	-3.69	$\hat{a}_0 = 0.41$

Table 3-26

ASC for $[0/90]_{2s}$ - 2R/W = 0.125			Errors [%] using the specimen with 2R=				
2R [mm]	$\bar{\sigma}_g^{exp}$ [MPa]	Model	2.50	4.15*	6.01	8.00	9.91
2.50	591.47	AOM	$\hat{a}_0 = 1.01$	4.39	2.26	10.31	16.37
		EA	$\hat{a}_0 = 1.04$	2.87	-1.68	5.75	11.61
4.15*	518.39	AOM	-5.05	$\hat{a}_0 = 0.69$	-2.47	6.95	14.23
		EA	-3.04	$\hat{a}_0 = 0.69$	-4.79	3.09	9.54
6.01	436.24	AOM	-2.87	2.78	$\hat{a}_0 = 0.45$	10.79	19.41
		EA	1.87	5.13	$\hat{a}_0 = 0.41$	8.48	15.57
8.00	429.89	AOM	-12.67	-7.52	-10.07	$\hat{a}_0 = 0.43$	8.37
		EA	-6.08	-3.09	-7.78	$\hat{a}_0 = 0.39$	6.60
9.91	426.52	AOM	-19.44	-14.82	-17.12	-7.90	$\hat{a}_0 = 0.42$
		EA	-11.79	-9.03	-13.36	-6.16	$\hat{a}_0 = 0.38$

Table 3-27

ASC for $[0/90]_{2s}$ - 2R/W = 0.25			Errors [%] using the specimen with 2R=			
2R [mm]	$\overline{\sigma}_g^{exp}$ [MPa]	Model	2.50*	6.01	8.01	9.90
2.50*	534.57	AOM	$\hat{a}_0 = 0.99$	6.53	15.04	16.40
		EA	$\hat{a}_0 = 0.88$	5.53	14.12	14.25
6.01	433.14	AOM	-8.00	$\hat{a}_0 = 0.50$	11.21	13.07
		EA	-5.65	$\hat{a}_0 = 0.43$	9.28	9.42
8.01	430.00	AOM	-17.88	-10.62	$\hat{a}_0 = 0.49$	1.81
		EA	-13.59	-8.49	$\hat{a}_0 = 0.42$	0.13
9.90	401.13	AOM	-19.33	-12.36	-1.83	$\hat{a}_0 = 0.42$
		EA	-13.51	-8.52	-0.13	$\hat{a}_0 = 0.35$

Table 3-28

ASC for $[0/90]_{2s}$ - 2R/W = 0.50			Errors [%] using the specimen with 2R=				
2R [mm]	$\overline{\sigma}_g^{exp}$ [MPa]	Model	4.15*	6.00	8.00	8.01	9.97
4.15*	390.44	AOM	$\hat{a}_0 = 0.69$	-4.08	11.43	12.15	10.03
		EA	$\hat{a}_0 = 0.49$	-6.18	8.73	9.61	5.05
6.00	329.36	AOM	4.64	$\hat{a}_0 = 0.43$	18.16	19.02	16.47
		EA	6.51	$\hat{a}_0 = 0.28$	15.87	16.83	11.90
8.00	345.21	AOM	-11.98	-15.94	$\hat{a}_0 = 0.48$	0.78	-1.53
		EA	-7.96	-13.42	$\hat{a}_0 = 0.33$	0.82	-3.39
8.01	348.44	AOM	-12.67	-16.60	-0.78	$\hat{a}_0 = 0.49$	-2.30
		EA	-8.70	-14.13	-0.81	$\hat{a}_0 = 0.34$	-4.17
9.97	311.82	AOM	-10.63	-14.55	1.59	2.41	$\hat{a}_0 = 0.37$
		EA	-4.61	-10.09	3.43	4.27	$\hat{a}_0 = 0.24$

Table 3-29

4 CONCLUSIONS

Study the past if you would divine the future.

- Confucius -

The methods commonly employed to estimate the ultimate tensile strength of a notched laminate make use of approximations of the stress distribution along the net section of the specimen, which are based on Tan's improved theory from [57]. This theory is based on the exact isotropic solution for the infinite plate, and on the hypothesis (2.14). However, most of the applications of this approximation in the literature make use of quasi-isotropic lay-ups, which obviously do not show great deviations from the approximation.

When trying to predict the strength of orthotropic laminates loaded along one of their orthotropy axes, this approximation can be questioned since the justification for its use is based on the good agreement with experimental results of the stress concentration factor, but not the desired ultimate tensile strength.

For this reason, the usage of the exact anisotropic solution from Lekhnitskii's theory has been compared to Tan's approximation for three failure criteria: the maximum stress at the edge of the hole, the point stress criterion and the average stress criterion.

In the case of the maximum stress criterion, the predictions can be bound by an upper and a lower limit depending on the stress distribution along the net section that is implemented. It has been proven in section 2.1.3.2 that the use of the improved theory with the magnification factor M is inconsistent with the model's hypotheses. However, when using the notch-sensitive model as a lower limit for failure, both Tan's original orthotropic approximation (without the magnification factor) and the exact anisotropic solution provide similar results; the more noticeable differences are found for values of the diameter-to-width ratio of the specimen higher than 0.6, which are difficult to obtain in practice.

Using the exact anisotropic solution, experimentally-fitted curves can be obtained as described in section 2.1.3.3 and shown in section 3.4. These curves have been obtained from the large experimental campaign of this thesis, and are not suitable for other materials and configurations, but they do provide an experimental value of the exponent m that seems to account for both the hole radius' size effect and the notch sensitivity of different lay-up sequences.

The point stress and average stress criteria results, discussed in section 3.5, show that in general the errors obtained from their predictions are too high to be dismissed, at least for the orthotropic laminates studied here. In fact, the difference between E_{11} and E_{22} might have a certain effect on these errors: the predictions are worse for the $[0]_6$ and $[90]_6$ laminates when compared to those for the $[0/90]_{2s}$ lay-up. Nevertheless, in most of the cases the exact anisotropic solution applied to these criteria provides smaller relative errors when compared to the experimental results. Again, for isotropic and quasi-isotropic laminates, where it is noticeable that the mentioned elastic moduli are the same, Tan's improved theory might provide sufficiently good results, but it seems more reasonable to use a theory that would encompass most cases and not just a range of them.

4.1 Future work

From the conclusions of this thesis, there stem several topics that would be interesting to study in more profundity. These are some of the present author's suggestions, but the conclusions themselves remain open and welcome to analysis and criticism. Particularly, the experimental results used here should not be taken as totally accurate descriptions of the real values since the drilling process was not controlled via X-rays like most of the literature does.

The proposed future lines of work are:

- An experimental validation of the hypothesis in (2.14): according to Tan, this assumption is checked via a Finite Element Method, but it seems reasonable to find a variation of the finite-width correction factor along the net section. If found, this dependency can be included in all the model studied here.
- A careful analysis of the exponents of the proposed fit curves for different lay-up configurations, which might be a quantifying value of both the size effect and the notch sensitivity.
- A similar approach with the exact anisotropic solutions for different loading conditions, if available, such as biaxial loading, shear stress, etc.
- The repetition of the methodologies applied in this thesis to different materials and lay-ups, including elliptical notches, the consideration of which is already performed in both Lekhnitskii's and Tan's works.
- The usage of the exact anisotropic solution in the Finite Fracture Mechanics method, along with a possible orthotropic proposal for the stress intensity factor of the energetic approach. This work could not be performed in this thesis due to the shape of the SIF assumed for this problem.

All the pictures, graphs, documents and codes used for this thesis are available for download at the following direction: https://figshare.com/s/44b161e1141a6f12ffd0.

If the link does not work or any of the files is missing, the author can be contacted at the following email (for SPAM-filtering purposes, replace the terms in brackets with the author's name and surnames as written in the cover, but all lowercase and without accents): [name].[surnme1].[surnme2]@gmail.com

Appendix A. EXPERIMENTS DESCRIPTION

The proper method for inquiring after the properties of things is to deduce them from experiments.

- Sir Isaac Newton -

This appendix will describe in detail the fabrication process followed to obtain the test specimens used in this thesis for the sake of reproducibility and as a sort of unofficial example-based manual for future students and researchers who lack experience in the field of composite materials manufacturing. The testing methods will not be described in profundity because they were done by the common standards.

A. 1 The first step: Planification

Before getting into the fabrication process itself, it is very important to design the test campaign according to the results that want to be obtained. For the unexperienced, it is a difficult process, but will eventually save time and even greater difficulties later on.

In this project's case, our objective was to validate experimentally existing tensile failure criterions for open-hole composite specimens by covering a range of $2R/W$ and $2R$ values as wide as possible. To achieve that, a test matrix such as Table A-1 was designed:

D [mm] W/2R	SPECIMENS WIDTHS [mm]				
	2	**4.15**	**6**	**8**	**10**
2	4	8.3	12	16	20
4	8	16.6	24	32	40
8	16	33.2	48	64	80
10	20	41.5	60	80	100

Table A-1. Original distribution of test specimens' dimensions.

The diameter of 4.15 mm was chosen because it is a standard drill diameter, but it makes its corresponding specimens have widths with decimal values difficult to achieve in practice. To make manufacturing easier, these widths were rounded down using a factor of 0.15 times the $W/2R$ value; according to equation (A.1), the error after this rounding is an acceptable 3.6%:

$$\frac{\frac{W'}{2R}}{\frac{W}{2R}} = \frac{\frac{W - 0.15\frac{W}{2R}}{2R}}{\frac{W}{2R}} = \left(\frac{W}{2R} - 0.15\frac{W}{(2R)^2}\right)\frac{2R}{W} = 1 - \frac{0.15}{2R} = 1 - \frac{0.15}{4.15} = 0.963855422\,, \qquad (A.1)$$

and those widths are transformed as gathered in Table A-2:

W [mm]	8.3	16.6	33.2	41.5
W' [mm]	8	16	32	40

Table A-2. Corrected widths for homogenization.

Secondly, the lengths of the specimens were needed. Since this parameter was not to be studied, there was a certain freedom in its choosing. Thus, other aspects were taken into consideration: tabbing and fabrication.

The decision to use tabs was adopted to avoid any possible damage to the specimens, even though the norm did not mandate it [68]–[70]. However, a more careful analysis could have been done to determine if tabbing was necessary for all the specimens with their configurations, which could have saved some manufacturing time. The analysis that was actually performed required first the knowledge of the specimens' thickness, which depended on the lay-up configuration.

To avoid an excessive workload, the initial lay-ups chosen were simple: $[0°]_{10}$, $[90°]_{10}$ and $[0°/90°]_{3s}$. According to the material specifications [67], the cured ply thickness is of 0.184 mm, and this would result in specimens of around 2 mm thick. However, after reading several articles and finding one, a project by another student using the same material [71], where tab failure occurred, it was decided to reduce the number of laminae to the final configurations of $[0°]_6$, $[90°]_6$ and $[0°/90°]_{2s}$. This way, the thickness would be kept as a constant parameter, it would not pose a problem for tabbing, and the manufacturing would be faster.

Knowing the theoretical thickness value, t, a preliminary calculation for tab strength was performed thanks to Professor Cañas, assuming a standard tab length of either 50 mm or 100 mm (those of the grips available in the laboratory). With these geometries, the material tensile strength X_t, and the adhesive shear strength [72], it was possible to compare the maximum strength of the adhesive, equation (A.2), to the maximum tensile strength for each configuration in the most demanding case, i.e., that of 0° laminae assuming a notch-insensitive failure, equation (A.3(:

$$\sigma_{adh,max} = 4\,\tau_{adh} L_{tab} W\,, \qquad (A.2)$$

$$\sigma_{n,max} = X_t (W - 2R) t\,. \qquad (A.3)$$

It was proven that $\sigma_{adh,max}$ was higher than $\sigma_{n,max}$ for every configuration in Table A-1. These calculations were put in tables for each diameter value, similar to Table A-2. L_{gauge} is the length of the specimen's gauge section, that is, the one between tabs; these lengths were chosen from 50 mm to 300 mm in increments of 50 mm in order to make manufacturing easier, but always maintaining a minimum L/W ratio of 3.

$2R = 10$	Dimensions in mm, loads in MPa						
$\frac{W}{2R}$	W	$W - 2R$	L_{tab}	L_{gauge}	$\sigma_{adh,max}$	$\sigma_{n,max}$	Valid?
2	20	10	50	100	50000	20424	OK
4	40	30	50	150	100000	61272	OK
8	80	70	100	250	400000	142968	OK
10	100	90	100	300	500000	183816	OK

Table A-3. Tab resistance check for all the configurations corresponding to a diameter of 10 mm.

After all L_{gauge} values were chosen, the final step of the planification process was to sum all the specimens' widths and lengths, adding some extra millimeters to each coupon to account for the circular saw's thickness, and obtain the final dimensions of the panels to be manufactured. It is worth noting that every configuration would be made three times to obtain statistically significant values. Also, the extra dimensions to the edges of the panels was added to fit both width and length to multiples of 15 mm, given that the unidirectional tape width was 150 mm and there were ten laminae in each direction for every configuration (e.g., six laminae in direction 0º for the $[0]_6$ panels plus four more for the $[0/90]_{2s}$ ones); this way the waste of material was minimized and the manufacturing would be easier. The planning is summarized in the two following tables; Table A-4 is derived from Table A-1 and lists all configurations' widths and lengths (including the circular saw's extra width) with a color code to group configurations in the same panel, and the second one sums all those dimensions (multiplied by three specimens for each one) and adjusts them to the multiples of 15 as explained before:

W/2R \ D [mm]	WIDTHS AND LENGTHS [mm]				
	2	**4.15**	**6**	**8**	**10**
2	7 150	11 150	16 150	20 150	23 200
4	11 150	21 200	29 200	37 250	45 250
8	21 200	37 200	53 300	69 300	85 450
10	23 200	45 250	65 300	85 450	105 500

Table A-4. Widths and lengths of each configuration for a given lay-up sequence.

Panel number	**P1**	**P2**	**P3**	**P4**	**P5**	**P6**
Sum of specimen's widths (x3) [mm]	195	462	391	571	510	315
Total width [mm] (next mult. of 15)	210	465	405	585	525	330
Original panel length [mm]	150	200	250	300	450	500
Total length [mm] (next mult. of 15)	165	225	270	315	465	525

Table A-5. Panels' dimensions after adding all margins.

Note that, regarding panels dimensions, *length* refers to the 0º direction of the panel and *width* to the 90º direction. Also, the tables above are for each lay-up, so there are three panels for each of these dimensions' combinations, e.g., P1-$[0]_6$, P1-$[0/90]_{2s}$ and P1-$[90]_6$, each one of size 210x165 mm.

A. 2 Manufacturing

After the planning is complete, it is time to start the manufacturing process itself. In this thesis' case, the fabrication was done in the Elasticity and Strength of Materials Group's (*GERM* in Spanish) Laboratory at the University of Seville. This Laboratory has been accredited by several organisms and companies, such as Bombardier, Boeing, or the former EADS-CASA, now Airbus, to perform mechanical tests [73]. Most of the fabrication was performed in its clean room that controls for temperature and has an extraction system for airborne particles.

Firstly, all the laminae needed to create the panels were cut from the unidirectional tape of *Hexcel Composites*' Hexply AS4/8552-RC34-AW194 carbon fiber reinforced epoxy prepeg. The number to be cut was precisely the integer that results from dividing the panels' dimensions by 15. This way, to manufacture the three panels P6, 22 pieces of 525 mm long were needed for the laminae at 0º, and 35 of them with a length of 330 mm for the 90º laminae; both had the standard roll width of 150 mm. The result can be seen in Figure A-1:

Figure A-1. All the laminae cut from the unidirectional tape ready to be piled.

After that, those laminae were cut again to adjust to the designed panels' dimensions. Thanks to having chosen them multiples of 15, all the leftover material that remained from one panel was reused in another. Then, the manual lay-up process started, lamina by lamina, and removing possible air bubbles with a soft spatula as the one seen in Figure A-2:

Figure A-2. Panel's laminae lay-up process.

The white paper that can be see discarded under the table is the prepeg release film, that was removed just before the next lamina was to be laid and remained on both faces of the final panel until before curing to avoid contamination. Once all the panels had been laid-up, and taking care of keeping the ones that are not to be used yet as per the storage instructions [67], the next stage was creating the vacuum bags.

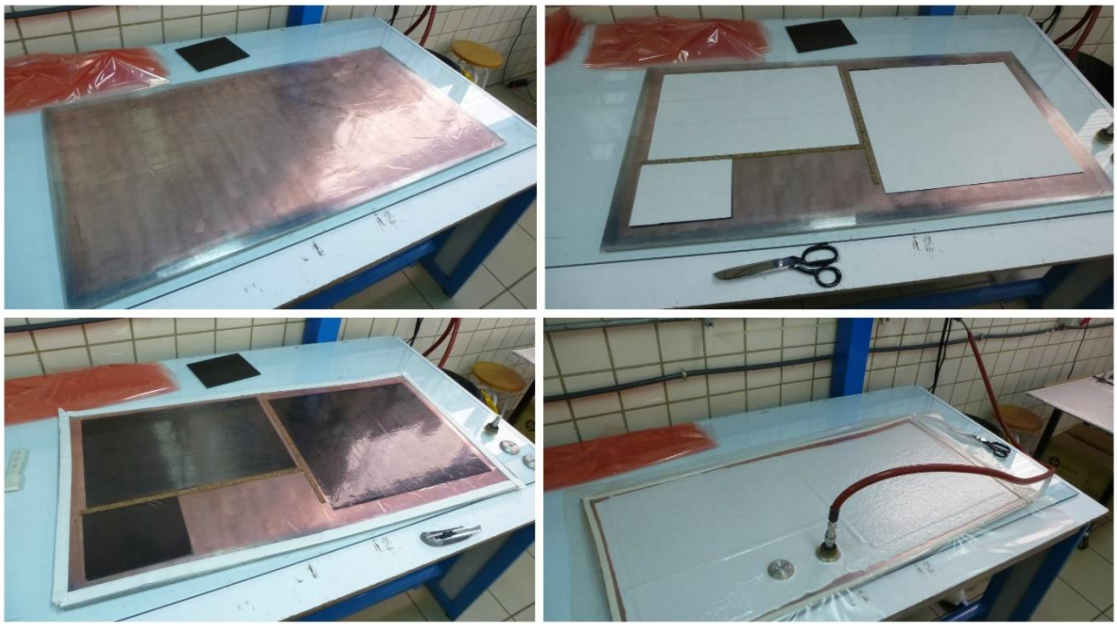

Figure A-3. Vacuum bag fabrication procedure. a) top left, b) top right, c) bottom left, d) bottom right.

The process, as summarized in the pictures of Figure A-3, is the following:

a) Take an aluminum plate and cover it with a sheet of Teflon.
b) Distribute the panels on the release Teflon film to maximize the used area; use a cork separator if the panels are too close to each other to avoid them getting joined by the flowing resin. Leave some space for the vacuum fittings.

c) Remove the white release film on both sides of the panels, place the panels again on the plate and cover them with another Teflon film. Take a vacuum bag sealant tape (also known as chromate) and place it around the edges of the aluminum plate without it touching the Teflon sheets or other elements. This sealant tape placement is critical to avoid leakages during the curing process.
d) Cover the upper Teflon film with a piece of breather fabric and position the two vacuum fittings' bottom parts onto the breather. Remove the chromate release film carefully and place a sheet of vacuum bagging film over the whole arrangement. Make sure there are no leaks by connecting one of the vacuum fittings' connector to the base that has remained inside the bag, and then connecting it to a vacuum pump to create an initial negative pressure and check for possible leaks by listening for air flow and using a vacuum gauge on the other fitting (see Figure A-4). If there are any leaks, use a spatula to press down the vacuum bagging film onto the bag sealant tape.

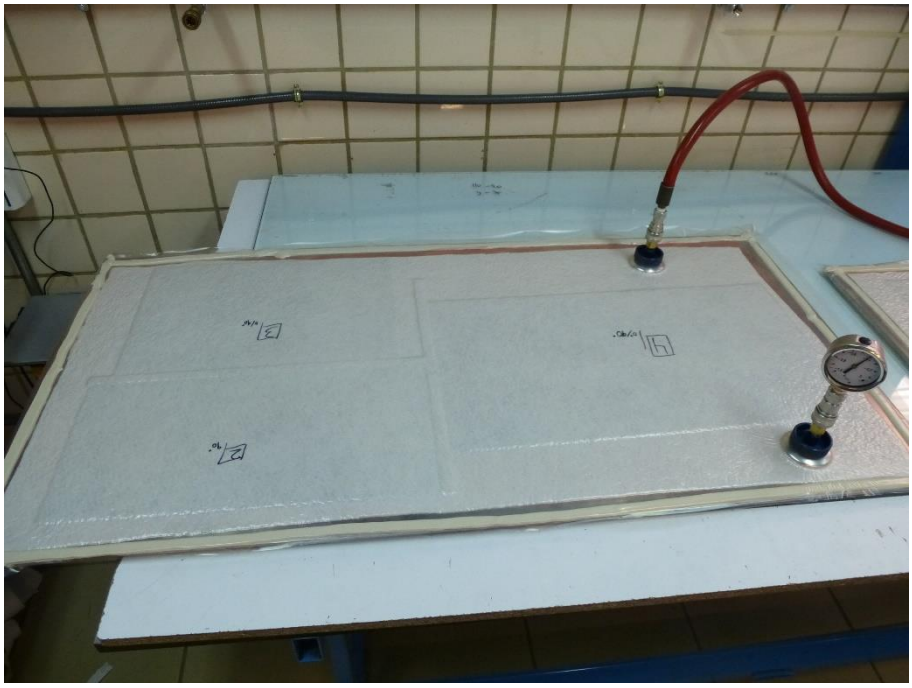

Figure A-4. Final state of the vacuum bag, checking for possible leaks using a vacuum gauge.

Leave this vacuum on for some minutes to allow for the panels to be compacted. Do not forget to carefully write down which panel is which with a marker pen on the bag.

This process was done for the maximum number of panels able to fit at one time in the autoclave, i.e., three aluminum plates with three panels each. Then, the curing stage was done according to the norm [67], which states:

- *Vacuum bag: Apply vacuum pressure (inside the bag) between 0.65 bars to 0.75 bars (490 mm Hg to 560 mm Hg).*
- *Autoclave pressure: 3.5 bars to 7.2 bars.*
- *Heating rate: 0.2 ºC/min to 3.5 ºC/min.*
- *Curing time and temperature: 120 min to 135 min at (185 ± 5) ºC or 120 to 210 min at (185 ± 5) ºC.*
- *Cooling rate: 0. 2 ºC/min to 3.5 ºC/min.*

Figure A-5. Autoclave and panels after curing.

After all the panels were cured and the rough edges cut and adjusted to their design size using the diamond circular saw, the next phase was tabbing. The tabs were cut from fiberglass panels that are manufactured in the Laboratory, and were to be positioned in the ±45º directions. First, they were polished and the rectangular tabs were sketched on them, then to be cut as seen in Figure A-6:

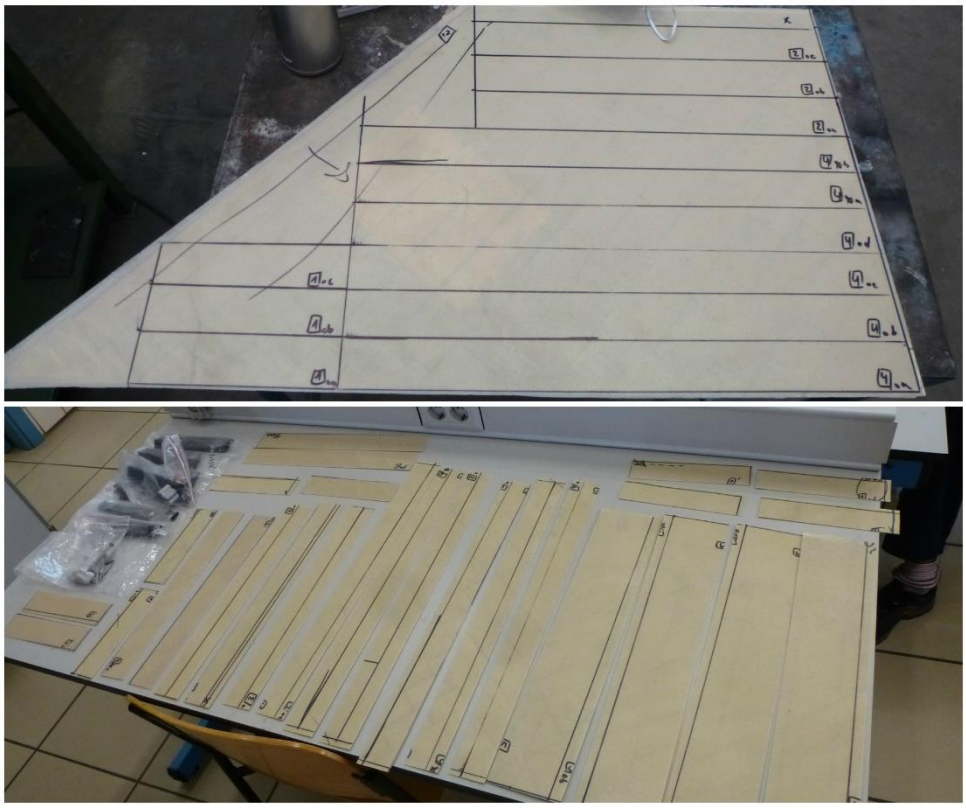

Figure A-6. *Above*: Fiberglass panel ready to be cut; *Below*: All tabs already cut.

The bigger dimension of the tabs was adjusted to each panel's width, and the smaller one was either 50 mm or 100 mm, as initially designed in the planning phase. Once cut, they were cleaned to eliminate any impurities between the surface and the adhesive. The panels' tab area was also polished and cleaned before adding the adhesive. This adhesive was an epoxy structural one with a polyester mat carrier, reference code Z-15429 [72]. Its mechanical properties are as listed in Table A-6:

PROPERTY	VALUE
Areal weight [g/m2]	300 ± 30
Volatile content [%]	1.5 max.
Tensile shear strength at 23ºC [MPa]	24 individual min. / 30 average min.
Bell-Peel at 23ºC [N]	180 indiv. min. / 225 aver. min.

Table A-6. Mechanical properties of the adhesive Z-15429 used for tabbing.

When all the polishing and cleaning is done, the adhesive is added to the tabs, then the tabs are positioned on the panel and gripped to keep them fixed, controlling that the gauge section length is the designed one. Finally, some high-temperature tape is placed around the edges of the tabs (to easily peel off the exceeding adhesive that might flow onto the panel) and also joining them along the length of the panel to avoid that the tabs move when cured. This is summarized in the pictures in Figure A-7:

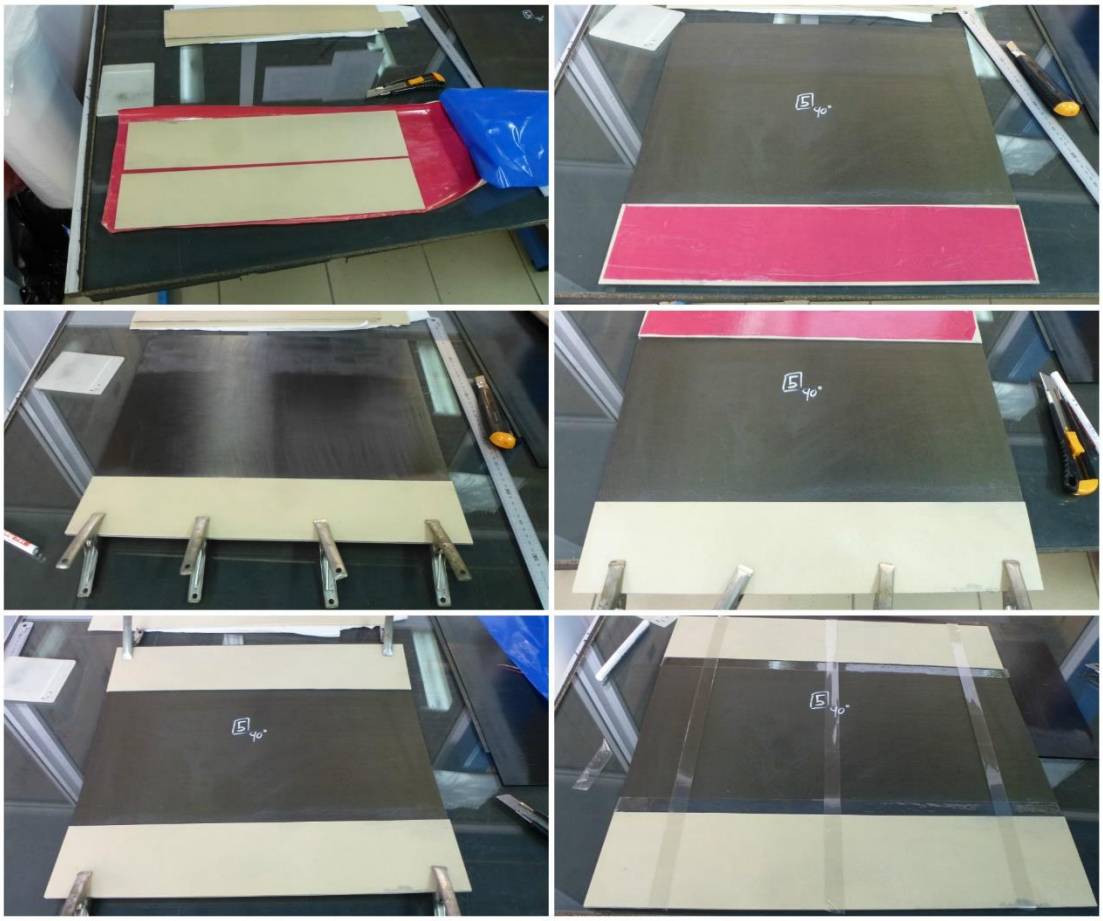

Figure A-7. Panel tabbing process.

Next, another set of vacuum bags had to be fabricated to cure the adhesive according to its specifications [72]:

- *Cure: 60 minutes at 120-145ºC and 0.24 ± 0.03 MPa or 90 min at 107-120ºC and 0.24 ± 0.03 MPa.*

These vacuum bags were done the same way as when the panels were cured, but this time no aluminum plates were needed since all the elements were already flat and solid. Instead, the vacuum bag film was folded upon itself and sealed with the chromate, as seen in Figure A-8:

Figure A-8. Second vacuum bag for the curing of the tabbing adhesive.

After the curing of the adhesive, the panels were ready to be cut using the diamond circular saw, Figure A-9:

Figure A-9. Panels after the curing of the adhesive in the autoclave.

The cutting was done for all the panels, checking with a caliper that the widths of the obtained specimens were the ones desired, and correcting the saw's caliper if any inaccuracies were found. The most important part of this process was marking every specimen with its reference code; in this thesis, the format used for this purpose has been [PanelNo.]-[LayUp]-[Width]-[Config.Letter], so the example *P1-0/90-16-b* means that the specimen comes from panel number 1, whose length is given in Table A-5, with the lay-up configuration of $[0/90]_{2s}$, a width of 16 mm, and, that for that given configuration, it is the specimen "b" out of the possible "a, b, c" equal ones repeated for statistical significance. In Figure A-10, the diagonal lines marked on the tabs were done for traceability in case the labels were wrongly written.

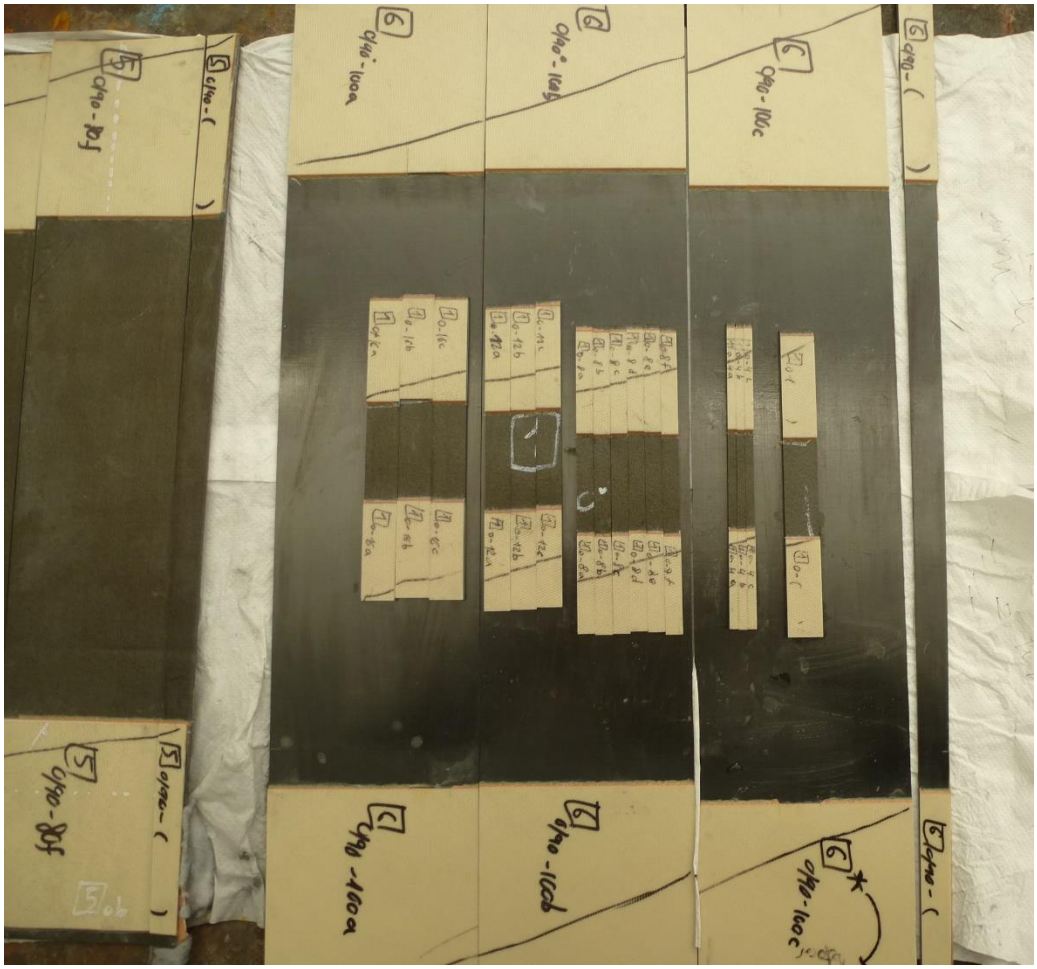

Figure A-10. Coupons obtained after cutting panels P1-0º and P6-0/90º.

The last step of the manufacturing process was drilling the holes. This was done according to the relevant AIPS (Airbus Process Specification), [74]. Firstly, the centers of the specimens were marked using a vertical caliper with a hardened tip. The holes were then drilled using an *Erlo* TF-30 drilling machine with reamers of the appropriate diameters as shown in the next picture:

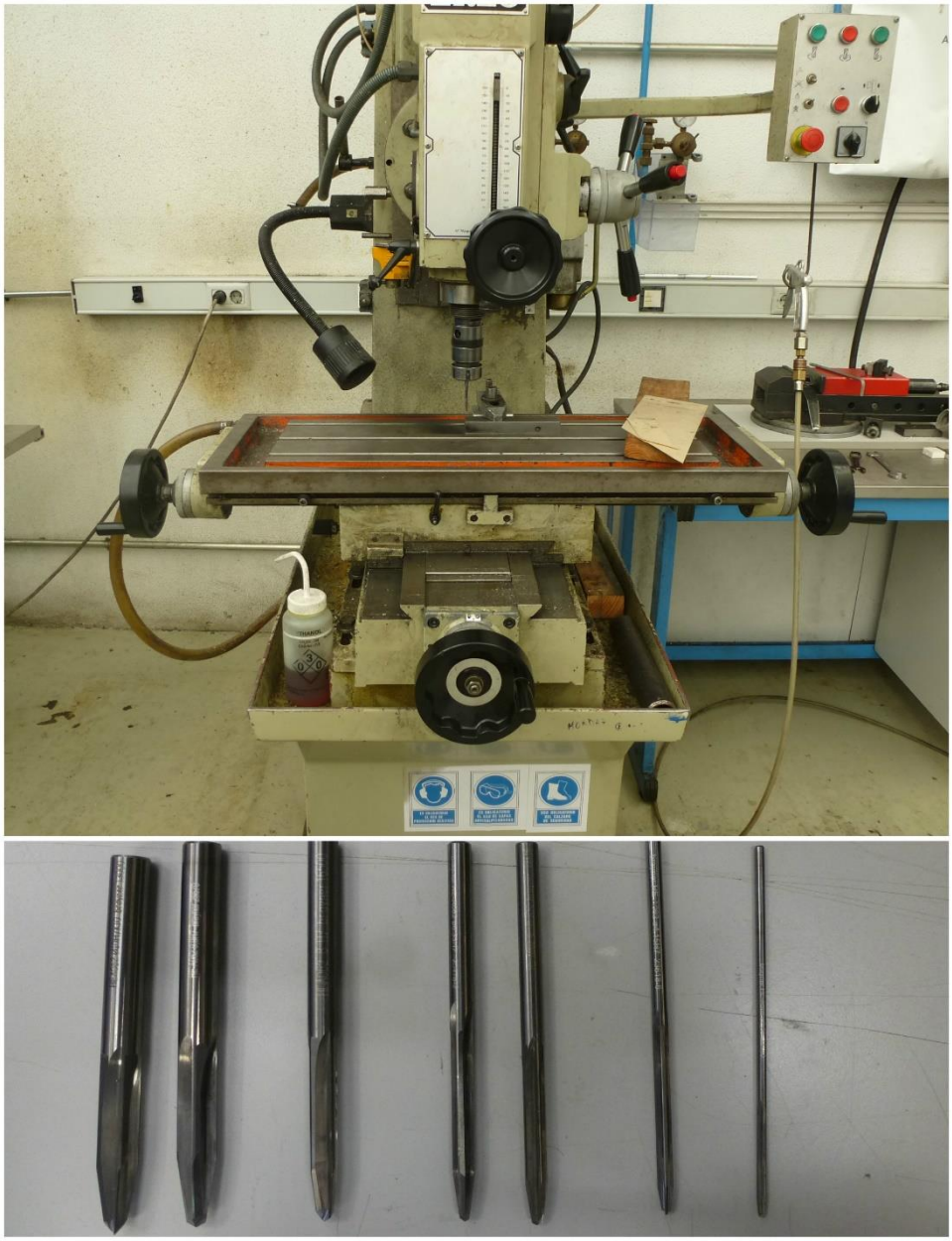

Figure A-11. Drilling machine and reamers used during the drilling stage.

To avoid delamination and the relative movement of the specimen, a configuration as shown in Figure A-12 was prepared for every specimen using spare parts of tabbing fiberglass (over both faces of the specimen), a metal prism that served as a reference, and a clamp. Also, following the recommendations for drilling holes in composites [74], the drill speed was chosen as the highest when feasible and the feed as low as possible.

It was not possible to find a reamer 2 mm in diameter, so instead a 2.5 mm one was used. This affected the diameter-to-width ratios of some specimens, that ended up being a little higher than initially designed.

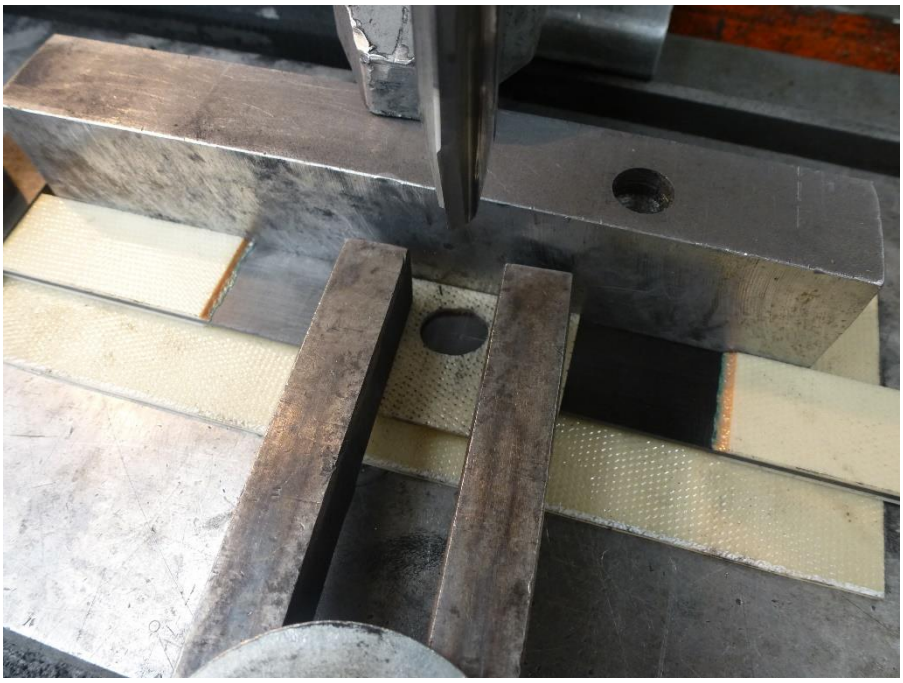

Figure A-12. Setup with clamps and spare fiberglass to avoid delamination.

Once the holes had been drilled, all the dimensions of the finished coupons were measured one more time and collected in an Excel table called *Final specimens dimensions*, that should be available for the reader along with this project's files. The totality of this campaign's specimens, 180 of them, can be appreciated in Figure A-13, where one can see the broad range of widths, lengths and diameters that have been covered in this project.

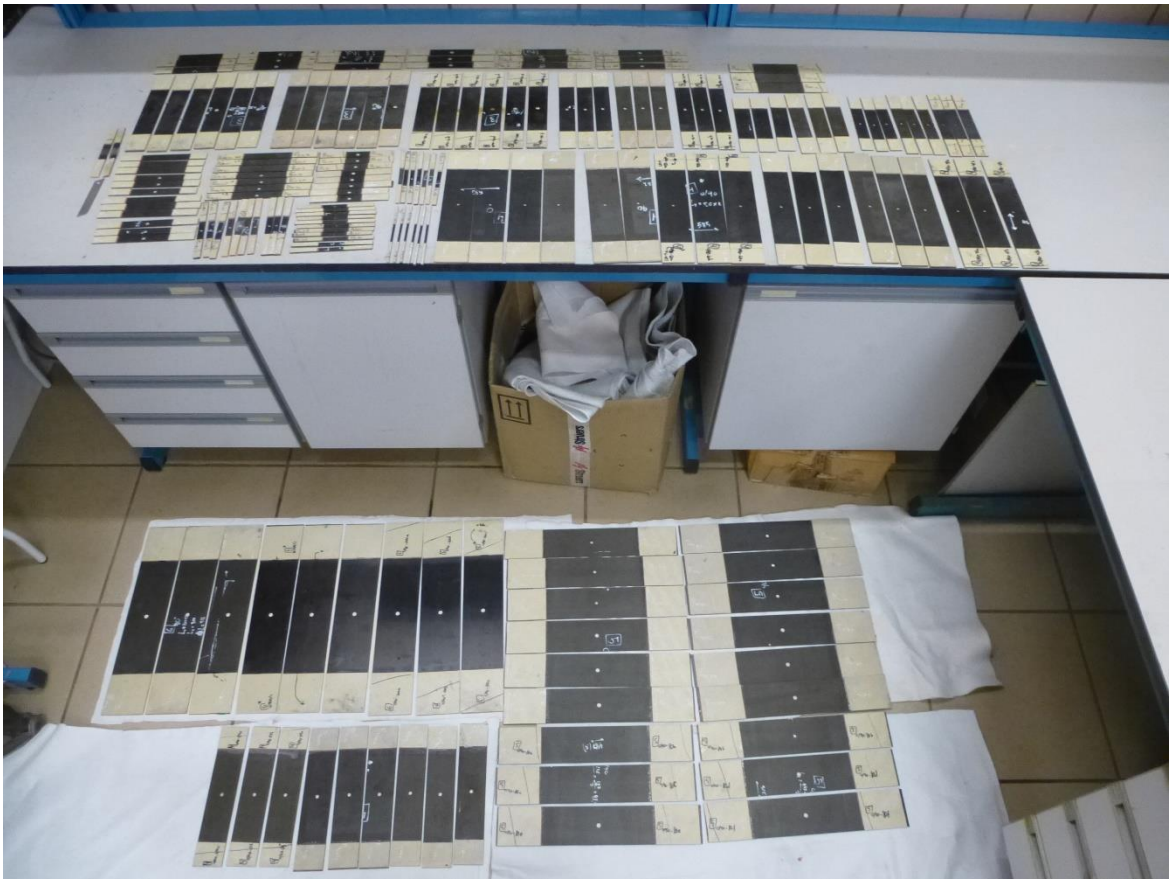

Figure A-13. Complete set of test specimens for this thesis.

A. 3 Testing

All the months-long preparation described above was performed in order to get to this final stage of the thesis: the tensile testing of the specimens up to total failure in order to know how their strength varies with respect to geometric variables.

Again, this was done in the GERM's Laboratory using two types of tensile testing machines: for most of the specimens, i.e., the ones less than 50 mm wide, the Instron mechanical machine was used, and the results obtained through the *LabVIEW* environment under a .csv format that were later plotted; the biggest coupons (those of a width larger than 50 mm) had to be tested in a machine with wider grips, a hydraulic Instron model, that also returned .csv files for the tests but generated the graphs as well. All these data, and the pictures of the broken specimens after testing, are stored in the folder called *PFC_data*, that should also be available with the rest of the files of this thesis; the results are ordered in subfolders, each with the code name of the specific specimen tested, as explained before. The outcomes of the tests and their analysis are shown in the "Results" chapter.

All testing was performed following the industry standards [68]–[70]. Special care was taken to ensure the coupons were centered and straight when clamped. The test speed ranged from 0.5 mm/min up to 2.5 mm/min, depending on the size of the specimen. Whenever possible, the slowest speed was chosen; the higher speeds were used due to some tests taking too long to finish and the time availability of the machines.

A selection of broken coupons' pictures is shown. Most of the $[0]_6$ specimens failed in an explosive way, as seen in A-14. Some of the smaller ones were not so catastrophic; see A-15. The $[0/90]_{2s}$ tests resulted in quasi-symmetrical fractures along the midline of the gauge section, A-16. Some of them, however, presented important delamination. There are no pictures of the $[90]_6$ specimens because all of them failed in a similar way to the $[0/90]_{2s}$ ones but without any delamination or relevant issues to be documented.

Figure A-14. Explosive failure of P3-0º-40-b.

Figure A-15. Non-explosive failure of P1-0º-12-a.

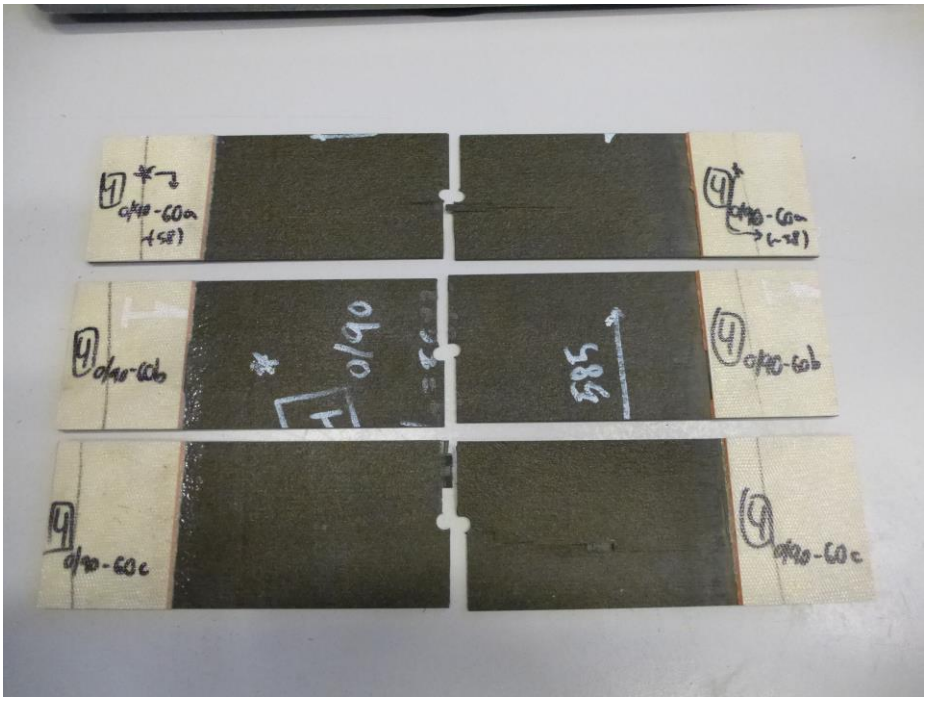

Figure A-16. Broken specimens P4-0/90º-60-a,b,c.

REFERENCES

[1] L. S. Arias and L. Vanegas, "Falla de los materiales compuestos laminados," *Sci. Tech.*, no. 25, pp. 113–118, 2004.

[2] E. J. Barbero and D. H. Cortes, "A mechanistic model for transverse damage initiation, evolution, and stiffness reduction in laminated composites," *Compos. Part B Eng.*, vol. 41, no. 2, pp. 124–132, 2010.

[3] A. Miravete, "Optimisation of composite structures design." Woodhead Publishing Limited, 1996.

[4] M. Molinier, *Análisis de los criterios de falla aplicados a los laminados compuestos*. Universidad de Buenos Aires.

[5] A. C. Orifici, I. Herszberg, and R. S. Thomson, "Review of methodologies for composite material modelling incorporating failure," *Compos. Struct.*, vol. 86, no. 1–3, pp. 194–210, 2008.

[6] S. Pagès, J. Costa, J. A. Mayugo, and N. Blanco, "Tratamiento de la fatiga en el diseño estructural con materiales compuestos," in *VIII Congreso Nacional de Propiedades Mecánicas de Sólidos*, 2002, pp. 831–839.

[7] A. Shojaei, G. Li, P. J. Tan, and J. Fish, "Dynamic delamination in laminated fiber reinforced composites: A continuum damage mechanics approach," *Int. J. Solids Struct.*, vol. 71, pp. 262–276, 2015.

[8] M. J. Swindeman, E. V Iarve, R. A. Brockman, D. H. Mollenhauer, and S. R. Hallett, "Strength Prediction in Open Hole Composite Laminates by Using Discrete Damage Modeling," *AIAA J.*, vol. 51, no. 4, pp. 936–945, 2013.

[9] L. Noels, "Computational & Multiscale Mechanics of Materials," *University of Liège*. [Online]. Available: http://www.ltas-cm3.ulg.ac.be/FractureMechanics/?p=overview_P3. [Accessed: 08-Jun-2017].

[10] L. S. Sutherland, R. A. Shenoi, and S. M. Lewis, "Size and scale effects in composites: I. Literature review," *Compos. Sci. Technol.*, vol. 59, no. 2, pp. 209–220, 1999.

[11] L. S. Sutherland, R. A. Shenoi, and S. M. Lewis, "Size and scale effects in composites: II. Unidirectional laminates," *Compos. Sci. Technol.*, vol. 59, no. 2, pp. 221–233, 1999.

[12] L. S. Sutherland, R. A. Shenoi, and S. M. Lewis, "Size and scale effects in composites: III. Woven-roving laminates," *Compos. Sci. Technol.*, vol. 59, no. 2, pp. 235–251, 1999.

[13] K. L. Reifsnider *et al.*, "Survey of Failure and Post-Failure Theories of Laminated Fiber-Renforced Composites," *J. Compos. Technol. Res.*, vol. 8, no. 4, p. 138, 1986.

[14] D. W. Sleight, "Progressive Failure Analysis Methodology for Laminated Composite Structures," 1999.

[15] S. W. Tsai, *Strength characteristics of composite materials*. Springfield,VA: National Aeronautics and Space Administration, 1965.

[16] S. W. Tsai and E. M. Wu, "A General Theory of Strength for Anisotropic Materials," *J. Compos. Mater.*, vol. 5, no. 1, pp. 58–80, 1971.

[17] O. Hoffman, "The Brittle Strength of Orthotropic Materials," *J. Compos. Mater.*, vol. 1, no. 2, pp. 200–206, Apr. 1967.

[18] Z. Hashin and A. Rotem, "A Fatigue Failure Criterion for Fiber Reinforced Materials," *J. Compos. Mater.*, vol. 7, no. 4, pp. 448–464, 1973.

[19] F.-K. Chang and K.-Y. Chang, "A Progressive Damage Model for Laminated Composites Containing Stress Concentrations," *J. Compos. Mater.*, vol. 21, no. 9, pp. 834–855, 1987.

[20] J. Hou, P. Petrinic, C. Ruiz, and S. R. Hallett, "Prediction of impact damage in composite plates," *Compos. Sci. Technol.*, no. 60, pp. 273–281, 2000.

[21] A. Puck and H. Schürmann, "Failure analysis of FRP laminates by means of physically based phenomenological models," *Compos. Sci. Technol.*, no. 58, pp. 1045–1067, 1998.

[22] L. N. McCartney, "Energy-based prediction of progressive ply cracking and strength of general symmetric laminates using an homogenisation method," *Compos. Part A Appl. Sci. Manuf.*, vol. 36, no. 2, pp. 119–128, 2005.

[23] L. N. McCartney, "Energy-based prediction of failure in general symmetric laminates," *Eng. Fract. Mech.*, vol. 72, no. 6, pp. 909–930, 2005.

[24] E. J. Barbero, *Finite Element Analysis of Composite Materials*. Boca Raton, FL: CRC Press, 2008.

[25] E. J. Barbero, G. Sgambitterra, A. Adumitroaie, and X. Martinez, "A discrete constitutive model for transverse and shear damage of symmetric laminates with arbitrary stacking sequence," *Compos. Struct.*, vol. 93, no. 2, pp. 1021–1030, 2011.

[26] F. K. Wittel, J. Schulte-Fischedick, F. Kun, B.-H. Kröplin, and M. Frieß, "Discrete element simulation of transverse cracking during the pyrolysis of carbon fibre reinforced plastics to carbon/carbon composites," *Comput. Mater. Sci.*, vol. 28, no. 1, pp. 1–15, 2003.

[27] F. K. Wittel, F. Kun, B.-H. Kröplin, and H. J. Herrmann, "A study of transverse ply cracking using a discrete element method," *Comput. Mater. Sci.*, vol. 28, no. 3–4, pp. 608–619, 2003.

[28] Y. Sheng, D. Yang, Y. Tan, and J. Ye, "Microstructure effects on transverse cracking in composite laminae by DEM," *Compos. Sci. Technol.*, vol. 70, no. 14, pp. 2093–2101, 2010.

[29] H. C. Biscaia, R. Micaelo, J. Teixeira, and C. Chastre, "Numerical analysis of FRP anchorage zones with variable width," *Compos. Part B Eng.*, vol. 67, pp. 410–426, 2014.

[30] D. Yang, Y. Sheng, J. Ye, and Y. Tan, "Discrete element modeling of the microbond test of fiber reinforced composite," *Comput. Mater. Sci.*, vol. 49, no. 2, pp. 253–259, 2010.

[31] X. Yang, Y. Xia, and Q. Zhou, "Influence of stress softening on energy-absorption capability of polymeric foams," *Mater. Des.*, vol. 32, no. 3, pp. 1167–1176, 2011.

[32] L. Maheo, F. Dau, D. Andre, J.-L. Charles, and I. Iordanoff, "A promising way to model cracks in composite using Discrete Element Method," *Compos. Part B Eng.*, vol. 71, pp. 193–202, 2015.

[33] F. Pierron, B. Green, M. R. Wisnom, and S. R. Hallett, "Full-field assessment of the damage process of laminated composite open-hole tensile specimens. Part II: Experimental results," *Compos. Part A Appl. Sci. Manuf.*, vol. 38, no. 11, pp. 2321–2332, 2007.

[34] B. G. Green, M. R. Wisnom, and S. R. Hallett, "An experimental investigation into the tensile strength scaling of notched composites," *Compos. Part A Appl. Sci. Manuf.*, vol. 38, no. 3, pp. 867–878, 2007.

[35] M. A. Caminero, M. Lopez-Pedrosa, C. Pinna, and C. Soutis, "Damage monitoring and analysis of composite laminates with an open hole and adhesively bonded repairs using digital image correlation," *Compos. Part B Eng.*, vol. 53, pp. 76–91, 2013.

[36] G. N. Savin, *Stress distribution around holes*. NASA TT-F-607, 1970.

[37] R. E. Peterson, *Stress concentration factors; charts and relations useful in making strength calculations for machine parts and structural elements,*. Wiley, 1974.

[38] S. C. Tan, "Laminated Composites Containing an Elliptical Opening. I. Approximate Stress Analyses and Fracture Models," *J. Compos. Mater.*, vol. 21, no. 10, pp. 925–948, Jan. 1987.

[39] S. C. Tan, "Laminated Composites Containing an Elliptical Opening. II. Experiment and Model Modification," *J. Compos. Mater.*, vol. 21, no. 10, pp. 949–968, Jan. 1987.

[40] S. C. Tan, *Stress Concentrations in Laminated Composites*. Lancaster, PA: Technomic, 1994.

[41] M. Sánchez and N. Troyani, "Factor teórico de concentración de esfuerzos en piezas cortas de materiales anisótropos," *Mecánica Comput.*, no. 22, pp. 2135–2144, 2003.

[42] S. Maiz, R. Rossi, P. Laura, and D. Bambill, "Efectos de la Ortotropía sobre el Factor de Concentración de Tensiones," *Mecánica Comput.*, no. 23, pp. 673–692, 2004.

[43] J. W. Weeton, *Engineered Materials Handbook, Volume 1: Composites*. Metals Park, OH: ASM International, 1997.

[44] B. Y. Chen, T. E. Tay, P. M. Baiz, and S. T. Pinho, "Numerical analysis of size effects on open-hole tensile composite laminates," *Compos. Part A Appl. Sci. Manuf.*, vol. 47, no. 1, pp. 52–62, 2013.

[45] C. J. Liu, A. H. J. Nijhof, L. J. Ernst, and R. Marissen, "A New Ultimate Strength Model of Notched Composite Laminates — Including the Effects of Matrix Failure," *J. Compos. Mater.*, vol. 44, no. 11, pp. 1335–1349, 2010.

[46] P. P. Camanho, P. Maimí, and C. G. Dávila, "Prediction of size effects in notched laminates using continuum damage mechanics," *Compos. Sci. Technol.*, vol. 67, no. 13, pp. 2715–2727, 2007.

[47] G. H. Erçin, P. P. Camanho, J. Xavier, G. Catalanotti, S. Mahdi, and P. Linde, "Size effects on the tensile and compressive failure of notched composite laminates," *Compos. Struct.*, vol. 96, pp. 736–744, 2013.

[48] R. M. O'Higgins, M. A. McCarthy, and C. T. McCarthy, "Comparison of open hole tension characteristics of high strength glass and carbon fibre-reinforced composite materials," *Compos. Sci. Technol.*, vol. 68, no. 13, pp. 2770–2778, 2008.

[49] M. E. Waddoups, J. R. Eisenmann, and B. E. Kaminski, "Macroscopic Fracture Mechanics of Advanced Composite Materials," *J. Compos. Mater.*, vol. 5, no. 4, pp. 446–454, 1971.

[50] J. M. Whitney and R. Nuismer, "Stress fracture criteria for laminated composites containing stress concentrations," *J. Compos. Mater.*, vol. 8, no. 8, pp. 253–265, 1974.

[51] R. Nuismer and J. Whitney, "Uniaxial Failure of Composite Laminates Containing Stress Concentrations," in *Fracture Mechanics of Composites*, 100 Barr Harbor Drive, PO Box C700, West Conshohocken, PA 19428-2959: ASTM International, 1975, pp. 117–126.

[52] P. Lagace, "Notch Sensitivity and Stacking Sequence of Laminated Composites," in *Composite Materials: Testing and Design (Seventh Conference)*, 100 Barr Harbor Drive, PO Box C700, West Conshohocken, PA 19428-2959: ASTM International, 1986, pp. 161-161–16.

[53] P. N. Dominguez, R. D. Santos, S. I. Robles, and N. F. Ortega, "Concentración de tensiones en piezas de materiales compuestos," *Mecánica Comput.*, vol. XXV, pp. 537–548, 2006.

[54] C. E. Harris and D. H. Morris, "Role of Delamination and Damage Development on the Strength of Thick Notched Laminates," *Delamination and Debonding of Materials*. ASTM International, p. 424.

[55] F. Folgado Carmona, "Factor de escala y geometría en la resistencia a tracción de laminados con agujero de materiales compuestos," University of Seville, 2015.

[56] S. Lekhnitskii, S. W. Tsai, and T. Cheron, "Anisotropic plates." p. 546, 1968.

[57] S. C. Tan, "Finite-Width Correction Factors for Anisotropic Plate Containing a Central Opening," *J. Compos. Mater.*, vol. 22, no. 11, pp. 1080–1097, Jan. 1988.

[58] S. P. Timoshenko and J. N. Goodier, *Theory of Elasticity*. New Yor, NY: McGraw-Hill, 1951.

[59] A. J. Durelli, V. J. Parks, and H. C. Feng, "Stresses Around an Elliptical Hole in a Finite Plate Subjected to Axial Loading," *J. Appl. Mech.*, vol. 33, no. 1, p. 192, 1966.

[60] P. K. Govindan Potti, B. Nageswara Rao, and V. K. Srivastava, "Notched strength of carbon fibre/epoxy composite laminates with a circular hole," *Forsch. im Ingenieurwes.*, vol. 65, no. 10, pp. 295–300, 2000.

[61] C. G. D. P.P. Camanho, P. Maimí, "A design methodology for mechanically fastened joints in laminated composite materials," *Compos. Sci. Technol.*, no. 66, pp. 145–154, 2006.

[62] P. P. Camanho, G. H. Erçin, G. Catalanotti, S. Mahdi, and P. Linde, "A finite fracture mechanics model for the prediction of the open-hole strength of composite laminates," *Compos. Part A Appl. Sci. Manuf.*, vol. 43, no. 8, pp. 1219–1225, 2012.

[63] D. Leguillon, "Strength or toughness? A criterion for crack onset at a notch," *Eur. J. Mech. A/Solids*, vol. 21, no. 1, pp. 61–72, 2002.

[64] P. Cornetti, N. Pugno, A. Carpinteri, and D. Taylor, "Finite fracture mechanics: A coupled stress and

energy failure criterion," *Eng. Fract. Mech.*, vol. 73, no. 14, pp. 2021–2033, 2006.

[65] J. C. Newman, "A nonlinear fracture mechanics approach to the growth of small cracks," *Behav. Short Crack Airframe Components, AGARD Conf. Proc.*, vol. 5, pp. 1–26, 1983.

[66] G. Bao, S. Ho, Z. Suo, and B. Fan, "The role of material orthotropy in fracture specimens for composites," *Int. J. Solids Struct.*, vol. 29, no. 9, pp. 1105–1116, 1992.

[67] Airbus, "Hexply AS4/8552 - Airbus IPS05-01-001-03." Airbus S.A.S. Engineering Directorate, Blagnac, France, 2000.

[68] ECN - European Committee for Standarization, "Tensile test parallel to the fiber direction - Norm UNE-EN 2561." AENOR, Brussels, 1995.

[69] ECN - European Committee for Standarization, "Tensile test perpendicular to the fiber direction - Norm UNE-EN 2597." AENOR, Brussels, 1998.

[70] Airbus, "Determination of Plain, Open Hole and Filled Hole Tensile Strenght - AITM 1-0007." Airbus S.A.S. Engineering Directorate, Blagnac, France, 2004.

[71] F. Delmotte, "Caracterización a fatiga de compuestos de fibra de carbono unidireccional a 0° y 15°," University of Seville, 2013.

[72] A. de la Cruz and L. M. García, "Adhesive Z-15429 Documentation." CASA, Getafe, 1999.

[73] GERM, "Elasticity and Materials Strength Laboratory (LERM)," 2016. [Online]. Available: http://www.germus.es/lerm/#1453454381552-c28db8af-4486. [Accessed: 09-Jun-2017].

[74] Airbus, "Preparation of Holes in Plastic and Mixed (Plastic/Metal) Assemblies for Fastening - AIPS01-02-005." Airbus S.A.S. Engineering Directorate, Blagnac, France, 2016.

Citation Style used: IEEE.